Structural Control Strategies for Load Reduction of Floating Wind Turbines

Yulin Si

Structural Control Strategies for Load Reduction of Floating Wind Turbines

University of Agder

Faculty of Engineering and Science
2015

Doctoral Dissertation by the University of Agder 109
ISBN: 978-82-7117-795-9
ISSN: 1504-9272

Printed in the Printing Office, University of Agder
Kristiansand

PREFACE

This thesis contains the research results that I obtained during my PhD study at the University of Agder from 2012 to 2015. All of the presented work was conducted under the supervision of Professor Hamid Reza Karimi from University of Agder and Professor Huijun Gao from Harbin Institute of Technology.
This work has been partially supported by Norwegian Centre for Offshore Wind Energy (NORCOWE) under grant 193821/S60 from Research Council of Norway (RCN).

ACKNOWLEDGMENTS

These past 3 years during my stay in Grimstad has been the most memorable period in my life. I was changed a lot, especially my taste, not only in food and drink, but also in good and bad, gain and loss. I am going to miss the fun, the quietness, and the kindness in this lovely place.

First of all, I would like to express my sincere appreciation to my principle supervisor Prof. Hamid Reza Karimi. I am very impressed by his enthusiasm in scientific research works. He arranged regular meetings with me to exchange ideas on my work. Every time I had questions or progress, he would send me his feedback in a very short time. Also, he has very broad view on academic research, and I was provided with many good opportunities, such as attending international conferences and workshops, and discussing with many other outstanding researchers around the world. All his help benefits a lot on my PhD work and lays great foundation for my future career development.

Secondly, I would like to thank my co-supervisor Prof. Huijun Gao in China. He is a well-recognized scientist with many highly cited publications in internationally renowned journals. It is because of his guidance that I know going for an overseas study is what I want in my life. Although we didn't discuss too much details about my PhD work due to the long distance, he helped me a lot with his understanding on research directions and methods. He leads me to a broad road on research.

Thirdly, I want to give my sincere thanks to Dr. Jason Jonkman from

National Renewable Energy Laboratory. In the forum he organized, I found plenty of professional and useful information on wind turbine modelling and simulation. I have received many instant and detailed answers from him regarding the questions I raised in the forum, and I appreciate that a lot. I also owe thanks to Dr. Francisco Palacios from Universitat Politcnica de Catalunya in Spain. We have had many inspiring discussions, and I learned a lot from him on how to conduct research in a professional and fun way.

Fourthly, I am very lucky to be one of the faculty members in the Unversity of Agder. Much of my stress on the work was relieved in the coffee corner, the gym, and the quiz time, and I miss a lot the social environment they have created. Although many, I am still going to write down their names. They are Knut, Magnus, Øyvind, Tore, Jesper, Jannik, Morten, Witold, Zuolong, Pål, Martin, Charly, Indika, Lei, Huihui, Ilya, Åse Linn, Magnus Hegland, Emma, Kjell Gunnar, Geir, Michael, Rein Terje.

Last but not least, I would like to thank my parents and fiancée Shujie for their constant support and understanding. They kept encouraging and loving me, especially at the hardest time during my PhD. The thesis is not possible without them.

Yulin Si
Taiyuan, China
June 2015

ABSTRACT

Offshore wind energy has attracted great worldwide attention in recent years, while strong potentials have been found in deep sea areas in many places, such as the coastal lines of the United States, north Europe, and east Asia. According to extensive experiences in offshore industry, floating foundation for wind turbines is considered as an economical and applicable solution. So far, plenty of numerical investigations have been conducted by world-wide research institutions, and different kinds of prototype programs have also been launched, including OC3-Hywind, MIT/NREL TLP, ITI Barge, and Principle Power WindFloat, etc.

One big challenge for floating windmills different from fixed bottom installations is the extra platform motion, which will heavily increase the load on turbine structure due to the high inertial and gravitational forces or even cause the failure of turbine control strategy. Special mechanical design or advanced control technique is required to improve wind turbine reliability, and effective load reduction methods are needed for the design of floating wind turbines. Among different approaches for load mitigation, structural control has offered a direct solution to dynamically compensate the vibrations of turbine structures and reduce their loads.

This dissertation is mainly about the numerical investigations of different structural control ideas for load reduction of floating wind turbines. The state-of-the-art wind turbine simulator FAST-SC (customized for structural

control analysis) is used in the simulation analysis, and different scenarios, including the below rated, rated, and parked situations, are considered respectively. Papers A and B are dealing with the parameter optimization problem of a spar-type floating wind turbine equipped with tuned mass dampers (TMDs). The passive structural control devices can either be installed inside the platform (Paper A) or along the nacelle (Paper B). Different performance indices and parameter optimization methods are adopted for TMD parameter determination, including frequency analysis, exhaustive search, and intelligent algorithms. Particularly, a mathematical model for wind turbine surge-heave-pitch motion is established based on the D'Alembert's principle of inertial forces. Paper C investigates the idea of installing tuned liquid column dampers (TLCDs) in floating wind turbines for load reduction, and the code FAST-SC-TLCD is implemented based on FAST-SC for fully coupled high-fidelity wind turbine simulation with semi-active structural control channel. Optimal parameters are computed by using genetic algorithm based on the established model, while how to tune the head loss coefficient remains to be investigated. Paper D proposes a gain scheduling H_2/H_∞ active structural control deign for a hybrid mass damper (HMD) installed at the tower top of a floating wind turbine. The wind turbine dynamic model is improved in this work based on polynomial curve fitting approach, and different steady-state points are derived. The state feedback controller is designed by solving linear matrix inequalities (LMIs). However, full-state feedback controller is technically impossible to implement due to lack of sensors, while the observer-based control design could be a possible solution. Then, Paper E discusses this idea, and an observer-based guaranteed cost structural controller is developed.

PUBLICATIONS

The following five papers are appended and will be referred to by corresponding Latin alphabets. The papers are printed in their originally published state except for changes in format and minor errata.

[A] Y. Si, H. R. Karimi, and H. Gao, "Modelling and optimization of a passive structural control design for a spar-type floating wind turbine", *Journal of Engineering Structures*, vol. 69, pp. 168–182, 2014.

[B] Y. Si, H. R. Karimi, and H. Gao, "Modelling and parameter analysis of the OC3-Hywind floating wind turbine with a tuned mass damper in nacelle", *Journal of Applied Mathematics*, vol. 2013, Article ID 679071, 10 pages, 2013.

[C] Y. Si and H. R. Karimi, "Load reduction for floating offshore wind turbines using tuned liquid column dampers", *Proceedings of the 12th German Wind Energy Conference*, Bremen, Germany, 19–20 May, 2015.

[D] Y. Si and H. R. Karimi, "Gain scheduling H_2/H_∞ structural control of a floating wind turbine", *Proceedings of the 19th World Congress of the International Federation of Automatic Control*, pp. 6788–6793, Cape Town, South Africa, 24-29 August, 2014.

[E] Y. Si and H. R. Karimi, "Observer-based guaranteed cost structural control for an offshore floating wind turbine", *Proceedings of the 6th World*

Conference on Structural Control and Monitoring, Barcelona, Spain, 15–17 July, 2014.

CONTENTS

LIST OF FIGURES

LIST OF TABLES

CHAPTER 1

INTRODUCTION

Due to both current global environment problems and potential oil shortage, the worldwide demand for renewable energy has been increasing rapidly during the past few years. Wind power, as an alternative to fossil fuels, is plentiful, widely distributed, cost-efficient and clean, and it has been considered one of the most important and biggest sources of renewable energy. It was estimated that the total amount of economically extractable power available from the wind in the world is considerably more than present human power use from all sources. With huge amount of wind resources, many countries have been trying to promote wind energy in the past twenty years. In Denmark for example, over 20% of the electricity is generated from wind, and plans are towards reaching 50% (Breton and Moe, 2009).

Most current large wind turbines around the world are installed on land with sparse population and vast land. However, in many countries, inhabitants are concentrated in places along coastlines where land is scarce while power is in high demand. Therefore, utilizing offshore wind resources is more beneficial, which will both reduce electricity transmission loss and reserve more land space for people, animals and plants. More importantly, offshore wind quality has been evaluated to be much better than that onshore. According to (Archer and Jacobson, 2005), a wind farm located offshore could experience wind speeds that are, on average, 90% greater than that over land. Therefore, global wind

energy exploitation has been gradually moving to offshore areas (Kaldellis and Kapsali, 2013). Near offshore wind farms in shallow water have been extensively built in recent years, but they are still often blamed for visual and noise impacts, and their foundations may also leave relatively large seabed footprints (Musial et al., 2006). In contrast, with less space constraints and more consistent wind, deep sea wind energy is more promising for those coastal cities without enough ideal shallow water areas.

According to the experience borrowed from offshore oil and gas industry, floating foundations can be regarded as a possible way of wind turbine deployment. Deep offshore wind energy from floating windmills has many advantages compared to its onshore and near offshore counterparts. Firstly, the quality of wind in deep sea areas is better, since the wind tends to blow more strongly and consistently with less turbulence intensity. Secondly, the size of floating wind turbines is not limited by road or rail logistical constraints if they can be manufactured near the coastline, and seabed quality also does not restrict the turbine weight, so they can possibly grow bigger with theoretically higher efficiency. Thirdly, the visual and noise annoyances of wind turbines can be avoided if they are installed in an enough distance from shore. Fourthly, vast uninterrupted open sea areas are available, and the installations will not occupy land or interfere with other land uses. Fifthly, since floating platforms can be towed by boats, the wind turbines could be brought to shore for maintenance instead of expensive operation in feild. Last but not least, energy is mostly consumed in coastal cities with high population intensity, and the power loss can be reduced due to relatively short transmission distance.

1.1 Research Motivation

In order to access the wind resource over deep water, different floating platforms for wind turbines have being designed and studied. Figure 1.1 illustrates four popular floating wind turbine concepts, which are classified in terms of how the designs achieve static stability. The spar-buoy concept, which can be moored by catenary or taut lines, achieves stability by using ballast to lower the

center of mass below the center of buoyancy. Based on this concept, the first full-scale floating wind-turbine Hywind was launched by the company Statoil in 2009, and it has been working well so far. The tension leg platform (TLP) achieves stability through the use of mooring-line tension produced by excess buoyancy in the tank, so it will lead to a more costly mooring system despite its good stability performance. For the barge concept, it is generally moored by catenary lines and achieves stability through its water-plane area, and the shallow draft will enable easy, inexpensive onshore assembly of the system, while the modes of the platform are closer to the range of wave frequency. Another promising concept is the semi-submersible foundation with column-stabilized units, and the company Principle Power has installed a multi-megawatt full-scale floating wind turbine prototype off the coast of Portugal in 2011, called WindFloat.

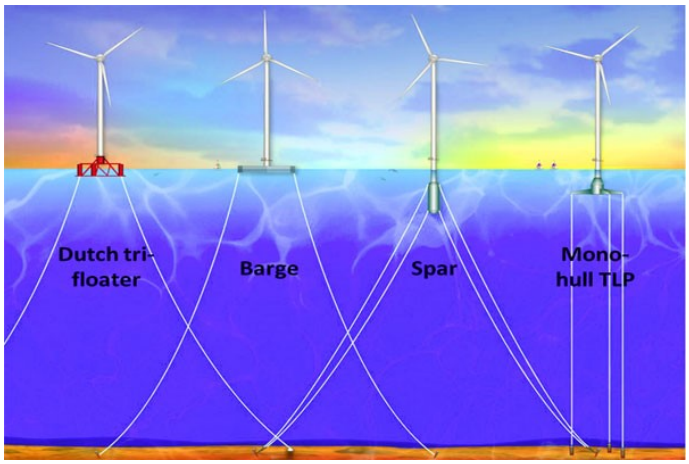

Figure 1.1: Four floating offshore wind turbine concepts. [1]

Floating platforms have been successfully used in the offshore oil or gas industry, but there remain a lot of challenges associated with the offshore floating wind turbines (Butterfield et al., 2005). One critical challenge is the increased loading on the blades and tower due to the higher inertial and gravitational forces caused by the motion of the floating platforms. The soft foundations will lead to lower natural frequency and larger scale of platform motion, which will produce more freedom of tower pitching and yawing movements. This will

[1] http://fessrg.ucsd.edu/Research/Wind/

greatly increase the fatigue loads at different parts of floating turbines, such as the tower-platform joint, connection between rotor and nacelle etc (Larsen and Hanson, 2007). The platform rotation and displacement will also lead to an unfavorable coupling between tower motion and the blade pitch control of the turbine, probably causing the failure of traditional blade pitch control design. Therefore, the ability to reduce fatigue loads is extremely important for offshore floating wind turbines, as it allows for increased reliability and possibly lighter and cheaper structures, thus they will benefit greatly from certain load reduction techniques.

One idea for wind turbine load mitigation is to improve the blade pitch control strategy. There have been many promising numerical results, see published (Larsen and Hanson, 2007; Jonkman, 2008; Lackner, 2013; Namik and Stol, 2010), while these methods will possibly increase the control complexity or decrease the power quality and control stability. At the same time, a more direct approach to reduce loading is to utilize structural control devices, which have been applied successfully in large civil structures in the past few years, such as long bridges and tall buildings. For example, as shown in Figure 1.2, Taipei World Financial Center installed a huge tuned mass damper in its 87th-92rd floors to dissipate the vibration from seismic earthquake and strong wind.

Considering the above mentioned problems and possible solutions, numerical investigation of structural control design for load reduction of offshore floating wind turbines is chosen as the subject of this doctoral research.

1.2 The State of the Art

Structural vibration control have been successfully applied in civil engineering structures, such as skyscrapers and bridges (Korkmaz, 2011), thus it is also expected to be a promising solution for extending the fatigue life of wind turbines. There have been many published results discussing this idea recent years.

In (Murtagh et al., 2008), the authors investigated the use of a tuned mass

damper (TMD) placed at the tower top of a simplified wind turbine model for vibration mitigation. Following the same installation idea, Colwell et al. explored the structural responses of a fixed-bottom offshore wind turbine with a tuned liquid column damper (TLCD) (Colwell and Basu, 2009). Later, the reliability of this idea was assessed in (Mensah and Dueñas-Osorio, 2012). Moreover, Li et al. performed an experimental study on an offshore wind turbine with a ball vibration absorber fixed on top of the nacelle (Li et al., 2012). However, these discussions are about vibration mitigation of fixed-bottom wind turbines, while their motion dynamics are quite different from that of floating wind turbines. Besides, these works are not based on the cutting edge high-fidelity codes for wind turbine models, which may not capture the comprehensive coupled nonlinear dynamics of wind turbines.

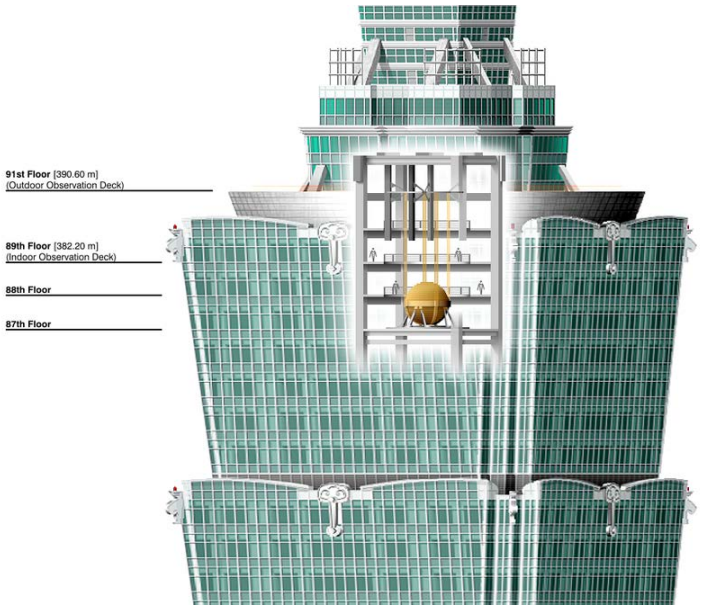

Figure 1.2: Location of Taipei 101's tuned mass damper. [2]

Based on the aero-hydro-servo-elastic wind turbine numerical simulator FAST (fatigue, aerodynamics, structures, and turbulence) (Jonkman and Buhl Jr, 2005), Lackner et al. implemented a new simulation tool, called FAST-SC, for passive, semi-active, and active structural control design of wind turbines (Lackner and Rotea, 2011a). It has incorporated TMDs into the nacelle or

[2] https://en.wikipedia.org/wiki/Tuned_mass_damper/

platform of wind turbines for load mitigation. Utilizing this code, Lackner et al. presented more realistic simulation results by installing a TMD in the nacelle of both a barge-type and a monopile supported wind turbines, and a simple parametric study was also performed to determine the TMD parameters (Lackner and Rotea, 2011a). In order to perform a more comprehensive parametric study, the authors in (Stewart, 2012; Stewart and Lackner, 2013) established a 3-DOF dynamic model for different types of floating wind turbines based on first principles, and TMD parameters are designed under different optimization methods. This limited-DOF model has greatly facilitated parametric analysis, but the coupling between platform surge and pitch motion was not captured. This effect can be ignored for the barge model, but might be a strong mode for other platforms (Namik and Stol, 2011; Jonkman, 2010). In addition, TMD was also proposed to be installed in the platform of TLP or spar-type floating wind turbines (Stewart, 2012), so that extra attention can be drawn on this idea since bigger mass becomes possible. Besides, the author in (Roderick, 2012) investigated the effectiveness of TLCD for offshore wind turbine load reduction, but the results were not based on the cutting edge simulator with fully coupled TLCD-turbine interaction. Since FAST-SC can be possibly customized for TLCD, it then becomes interesting to conduct further code development and simulation study. It was also shown more load reduction could be achieved when introducing active structural control, such as the multi-variable H_∞ control with a loop-shaping technique (Lackner and Rotea, 2011b). The actuator dynamics and control-structure interaction were also considered in (Stewart and Lackner, 2011). Alternative advanced control strategies should be also interesting to be studied.

CHAPTER 2
RESEARCH METHODOLOGY

2.1 Dynamic Modelling Techniques

In order to investigate the parameters of structural control devices, optimize system performance, or further design active controllers, establishing one dynamic mathematical model is very helpful. The following principles or techniques are used in this work to either establish dynamic models or further customize the code FAST-SC.

2.1.1 D'Alembert's Principle of Inertial Forces

D'Alembert showed that one can transform an accelerating rigid body into an equivalent static system by adding the so-called 'inertial force' and 'inertial torque'. The inertial force must act through the center of mass, but the inertial torque can act anywhere. The system can then be analyzed exactly as a static system subjected to this 'inertial force and moment' and the external forces. The advantage is that, in the equivalent static system one can take moments about any point, not just the center of mass. This often leads to simpler calculations because any force can be eliminated from the moment equations by choosing the appropriate point (Lanczos, 1986).

For a planar rigid body, moving in the plane of the body (the x–y plane),

and subjected to forces and torques causing rotation only in this plane, the inertial force is

$$\mathbf{F}_i = -m\ddot{\mathbf{r}}_c,$$

where $\mathbf{r}_c$ is the position vector of the centre of mass of the body, and m is the mass of the body. Similarly, the inertial torque is

$$T_i = -I\ddot{\theta},$$

where I is the moment of inertia of the body, and $\ddot{\theta}$ is the body rotational acceleration. In addition to the external forces and torques acting on the body, if the inertia force and the inertial torque are added. the system will be equivalent to one in static equilibrium. Thus the equations of static equilibrium

$$\sum F_x = 0,$$
$$\sum F_y = 0,$$
$$\sum T_i = 0$$

hold. The important thing is that $\sum T_i$ is the sum of torques taken about any point, while the direct application of Newton's laws requires that the angular acceleration equation be applied only about the center of mass.

Since wind turbine motion can be seen as multi-body dynamics or motion of distributed mass particles, the following equations can then be used to describe the static equilibrium for system translation and rotation about the reference point P

$$\mathbf{F} - \sum m_i\mathbf{a}_i = 0,$$
$$\boldsymbol{\tau} - \sum \mathbf{r}_i \times m_i\mathbf{a}_i = 0.$$

$\mathbf{F}$ and $\boldsymbol{\tau}$ denote vectors of external forces and moments about P, respectively, while $-\sum m_i\mathbf{a}_i$ and $-\sum \mathbf{r}_i \times m_i\mathbf{a}_i$ are vector sums of inertial forces and torques about P, respectively. m_i is the mass of particle i, and $\mathbf{r}_i$ represents the position vector from P to particle i. $\mathbf{a}_i$ is the acceleration vector for mass particle i,

It is noticed that the modelling difficulty is reduced, and the wind turbine

longitudinal motion can be seen as the sum of a translation and a rotation about the axis passing trough P and perpendicular to the surge-heave-pitch plane (Rao and Durgaiah, 2005). Also note that this will bring convenience in the parameter estimation process, since FAST code also uses the point P as the modelling reference instead of the mass center for the multi-body system.

2.1.2 Curve Fitting

Floating wind turbines are usually designed to be installed in a deep offshore environment several miles off the coast and in water depths greater than 60 m. The open sea environment will bring more loads onto the wind turbine structure than fixed bottom ones, which are usually used to govern the design of wind turbine and its floating foundation. As shown in Figure 2.1, the loads on a floating wind turbine include aerodynamic, hydrodynamic, hydrostatic, gravitational, mooring loads, etc. Detailed representations of these loads are not given here.

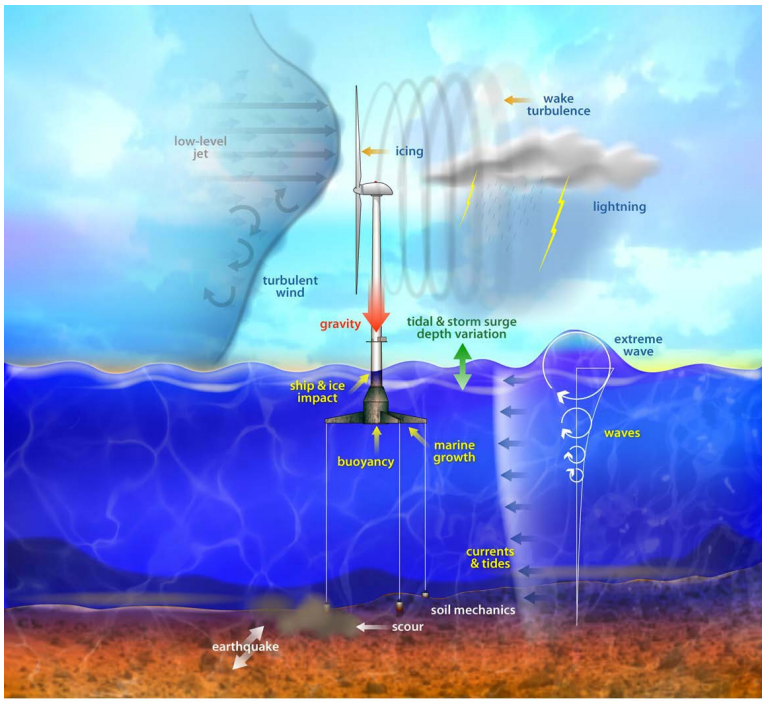

Figure 2.1: Loads on a floating wind turbine. (Jonkman, 2007)

In the beginning study of floating wind turbine modelling, most of these

external loads on the floating wind turbine, including aerodynamic, hydrodynamic and mooring loads, were approximated by linear or quadratic terms. However, it was found later that these parameters can be better represented with the curve fitting approach. For example, the mooring loads F_{sg}^{moor} and F_{hv}^{moor} of OC3-Hywind regarding the surge and heave displacement can be expressed as the following polynomials with the curve fitting results shown in Figure 2.2,

$$F_{sg}^{moor} = c_1(x_{sg}^{fair}) + c_2(x_{sg}^{fair})^2 + c_3(x_{sg}^{fair})^3,$$
$$F_{hv}^{moor} = d_1(x_{hv}^{fair})^2 + d_2(x_{sg}^{fair})^3 + d_3(x_{sg}^{fair})^4.$$

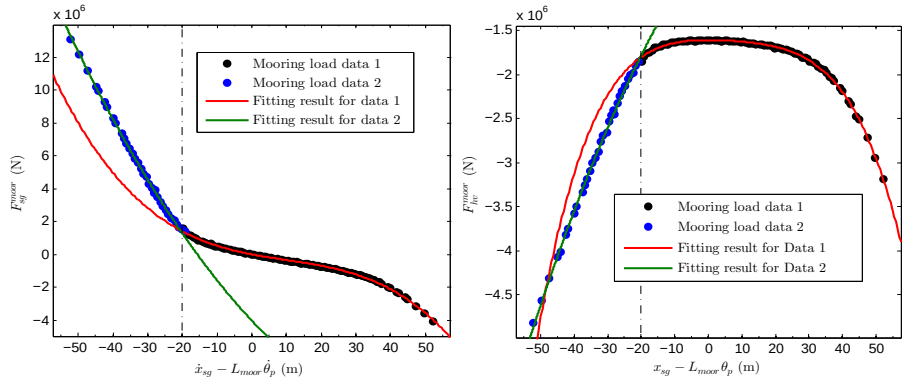

Figure 2.2: Curve fitting results for mooring loads.

The Matlab curve fitting toolbox[1] is used in the parameter estimation process of this work.

2.1.3 Kane's Dynamics

The theory of Kane's dynamics combines computational advantages of both the Newton-Euler formulas and Lagrange's equation, which will automatically eliminate the nonworking internal constraint forces without differentiating the scalar energy functions. This will lead to simpler equations of motion and less computational cost, thus it is favourable in many computational occasions (Xie, 1993).

[1] http://www.mathworks.com/products/curvefitting

The equations of motion in FAST are based on Kanes dynamics (Jonkman and Buhl Jr, 2005), which is also used in Paper C to characterize the numerical model of TLCD and its interaction with the wind turbine in FAST-SC-TLCD. It is a bit lengthy to present the details of this theory (Kane and Levinson, 1985) here, but a brief introduction is described as follows.

For a simple holonomic system with P generalized coordinates, system dynamic equation can be expressed via the following equation,

$$F_i + F_i^* = 0. \quad (i = 1, 2, ..., P)$$

For a set of W rigid bodies, and reference frame N_r, mass m_r and center of mass location X_r, the generalized active forces, F_i, and the generalized inertial forces, F_i^*, are expressed using the following equations,

$$F_i = \sum_{r=1}^{W} {}^E v_i^{X_r} \cdot F^{X_r} + {}^E \omega_i^{N_r} \cdot M^{N_r},$$
$$F_i^* = \sum_{r=1}^{W} {}^E v_i^{X_r} \cdot (-m_r {}^E a^{X_r}) + {}^E \omega_i^{N_r} \cdot (-{}^E \dot{H}^{N_r}).$$

F^{X_r} and M^{N_r} are the active force and moment vectors applied at the mass center, respectively. ${}^E a^{X_r}$ is the acceleration of point X_r in the inertial frame E, ${}^E \dot{H}^{N_r}$ is the first time derivative of the angular momentum of rigid body N_r about point X_r in the inertial frame E, ${}^E v_i^{X_r}$ is the partial linear velocity of point X_r in the inertial frame E, and ${}^E \omega_i^{N_r}$ is the partial angular velocity of rigid body N_r in the inertial frame E.

2.2 Structural Control Methods

Structural control is generally a concept in civil engineering discipline, which refers to the techniques that are used to reduce acceleration and loading in buildings and bridges due to wind, wave and earthquake. In the past decades, numerous structural control devices have been implemented for large civil structures, and there are many different types of devices or designs, ranging from massive pendulums to motor controlled mass dampers. Following

is a brief introduction of several structural control methods discussed in this dissertation.

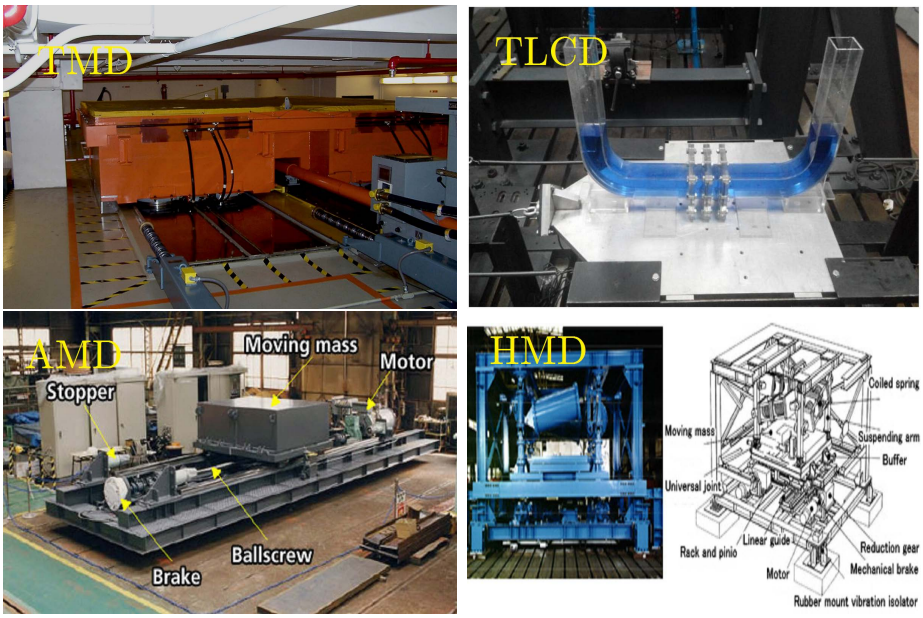

Figure 2.3: Different types of structural control devices. [2,3,4]

2.2.1 Tuned Mass Dampers

The most common structural control device is called the tuned mass damper. This device utilizes a mass on an ideally frictionless track. The TMD mass and the main structure are connected via a spring and damper, providing stiffness and damping. In an ideal TMD, both of these components are linear and have a constant spring and damping coefficient, which are also the assumptions in this work. Following is the sketch for an ideal TMD on top of the target system for horizontal acceleration mitigation, and the mathematical model can be established as

$$m_s\ddot{v}_s + D_s\dot{v}_s + K_s v_s = f_w + Kx + D\dot{x},$$
$$m\ddot{x} + Kx + D\dot{x} = 0,$$

[2]http://www.lemessurier.com/john_hancock_tower
[3]http://www.mdpi.com/1996-1073/8/1/111
[4]http://www.ihi.co.jp/iis/english/products/damper_mass.html

where m_s, D_s, K_s denote structural mass, damping coefficient and stiffness of the target system, respectively, while m, D, K represent corresponding properties of the TMD. $\ddot{v}_s$ and $\ddot{x}$ are the horizontal acceleration of the target and the TMD. f_w is the external force imposing on the target.

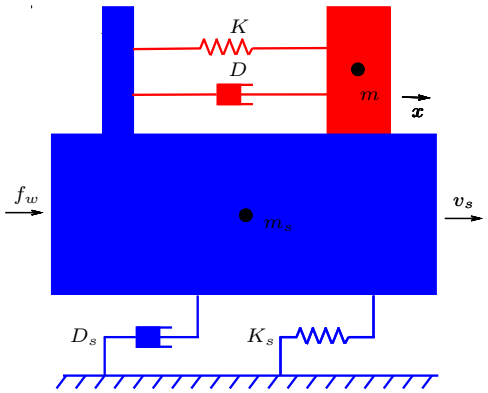

Figure 2.4: Sketch of a tuned mass damper on top of the target system.

The mass and spring are usually tuned to be consistent with the main system frequency regarding load reduction, and this will lead to the TMD mass vibrating at the same frequency. At the same time, the damper dissipates energy from the whole system in the form of heat. However, in a real TMD design, optimizing the spring and damping constants can be difficult due to space constraints and parameter nonlinearities. For structures with more degrees of freedom and nonlinearities like an offshore wind turbine, this is much more difficult.

2.2.2 Tuned Liquid Column Dampers

Tuned liquid column damper uses two attached vertical columns of liquid with an orifice between them. The difference between the heights of the two liquid columns provides an equivalent spring force, and the fluid passing through the orifice provides a damping force. Figure 2.5 gives a sketch for a TLCD on top

of the target, and the equations of motion can be described as

$$m_s\ddot{v}_s + C_s\dot{v}_s + K_s v_s = f_w - \rho AB\ddot{w} - \rho AL_{em}\ddot{v}_s,$$
$$\rho AL_{ee}\ddot{w} + 0.5\rho A\xi|\dot{w}|\dot{w} + 2\rho Agw = -\rho AB\ddot{v}_s m,$$
$$|w| < \frac{L-B}{2},$$

where w represents the liquid relative displacement. A and A_1 denote cross-sectional area of liquid column vertical and horizontal sections, respectively. B is the horizontal length, and L is the total length of the liquid. $\alpha = A/A_1$ is the area ratio, and $L_{ee} = L - B + \alpha B$. ρ is the liquid density, and ξ is coefficient of head loss. $L_{em} = B/\alpha + (L - B)$ is the length of an equivalent uniform crosssectional area liquid column with area A which has the same mass as the TLCD.

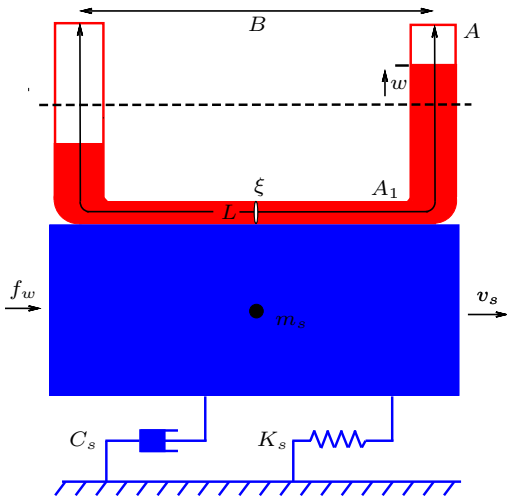

Figure 2.5: Sketch of a tuned liquid column damper on top of the target system.

Compared with TMD, TLCD will significantly reduce the cost as it only uses liquid instead of huge concrete or steel. This can be seen as an advantage over other structural control methods, since cost of energy is a main topic in wind industry. Similar with TMD, how to define the dimension and position of TLCD needs to be investigated. Also, TLCD provides a semi-active

control channel because of the tunable orifice, which is promising for further performance improvement.

2.2.3 Hybrid Mass Dampers

An active mass damper (AMD) consists of a mass and an actuator, which can be actively controlled to apply a force to the mass and an equal and opposite force on the structure. Since there is no physical spring and damper in this system, the actuator must provide all of the forces to the mass. There is also the potential to destabilize the system if the control scheme is not well designed.

Based on this, the hybrid mass damper combines the TMD and AMD. It usually consists of a tuned mass, spring, and damper system as well as an actuator, such as servomotor or hydraulic actuator. Figure 2.6 sketches an HMD on top of the target, and its dynamics are similar to that of TMD, except a force F from the actuator is added.

$$m_s\ddot{v}_s + D_s\dot{v}_s + K_s v_s = f_w + Kx + D\dot{x},$$
$$m\ddot{x} + Kx + D\dot{x} = F.$$

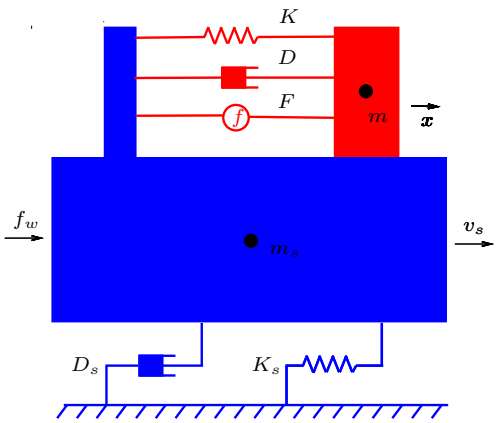

Figure 2.6: Sketch of a hybrid mass damper on top of the target system.

With the added actuator, the HMD gains the potential for improved per-

formance over a passive system. However, HMD can add energy to the system, thus instability will be possibly introduced, and how to design a proper controller for the actuator is one of the topics in this research. Besides, the HMD includes a passive system, so it can still provide load reduction with no actuation power.

2.3 Design Optimization

Optimal parameter tuning of the vibration absorber is an important design consideration in structural control problems. One task in this work is to find the optimal coefficients of structural control devices for wind turbine load reduction. These include TMD spring and damping coefficients, TLCD dimensions, as well as their locations. The following techniques are used in the design optimization.

2.3.1 Frequency Analysis

In engineering applications, the natural frequency of TMD is usually tuned to be near to that of the target system, so that it will effectively dissipate the undesirable system vibration energy. In order to systematically describe this phenomenon, Den Hartog analyzed the response of undamped main system with TMD subjected to harmonic external forces (Den Hartog, 1985). Then, he derived an explicit expression to determine the optimal TMD natural frequency and damping ratio for vibration inhibition, which has been widely adopted in practical applications. The optimal solution is given by

$$f_{tmd} = \frac{f}{1+\mu}, \quad \xi_{tmd} = \sqrt{\frac{3\mu}{8(1+\mu)}},$$

where μ denotes the mass ratio $\frac{m_{tmd}}{m}$. f and ξ are the natural frequency and damping ratio of target system, respectively. f_{tmd} and ξ_{tmd} represent, respectively, the optimal natural frequency and damping ratio of TMD. However, all systems contain damping, which should not be neglected in the parameter tuning process. It is also found that the optimum tuning frequency is strongly

influenced by the system damping level. In face of this, Tsai et al. presented a numerical searching procedure to determine the optimum parameters with target system damping considered, and a curve fitting scheme was then used to produce the equations for the optimal tuning parameters (Tsai and Lin, 1993), given as

$$f_{tmd} = ((\frac{\sqrt{1+0.5\mu}}{1+\mu} + \frac{1}{\sqrt{1-2\xi^2}} - 1) - (0.288 - 0.661\sqrt{\mu} + 1.12\mu)\sqrt{\mu}\xi$$
$$- (2.298 - 6.739\sqrt{\mu} + 8.316\mu)\sqrt{\mu}\xi^2)f,$$
$$\xi_{tmd} = \sqrt{\frac{3\mu}{8(1+\mu)}} + 0.151\xi - 0.187\xi^2 + 0.238\xi\mu.$$

Their results also showed that the higher the system's damping is, the more the optimum parameters deviate from those in undamped systems.

2.3.2 Intelligent Algorithms

Since a mathematical model describing floating wind turbine surge-heave-pitch motion can be derived and solving these equations is much more efficient than running the FAST code, then it becomes a possible solution to determine the optimal TMD parameters by using exhaustive search or intelligent algorithms.

Before optimization, the performance indices have to be introduced. In fact, the fore-aft tower top deflection is the best indicator of tower bottom bending moments, and the author in (Stewart and Lackner, 2013) used standard deviation of the tower top displacement as the performance index, which is also adopted in this work as the first index J_1. Similarly, the standard deviation of platform pitch angle is another criterion J_2, since platform pitch motion is the source of extra tower fatigue load, and it will also introduce extra loading on the important devices in nacelle such as drivetrain and generator. Ultimate loading should also be checked in the design process, since we need to make sure the turbine will survive in the extreme events. Therefore, the range of tower top displacement and platform pitch angle in the free decay test are treated as another two evaluation indices J_3 and J_4.

In the past few years, genetic algorithm has been widely applied in a broad

Table 2.1: Performance indices

Index	Description
$J_1 = \sqrt{\frac{1}{T}\int_0^T (x_{tt} - \tilde{x}_{tt})^2 \mathrm{d}t}$	Standard deviation of tower top displacement
$J_2 = \sqrt{\frac{1}{T}\int_0^T (\theta_p - \tilde{\theta}_p)^2 \mathrm{d}t}$	Standard deviation of platform pitch angle
$J_3 = \max(x_{ttd}) - \min(x_{ttd})$	Maximum range of tower top displacement
$J_4 = \max(\theta_p) - \min(\theta_p)$	Maximum range of platform pitch angle

spectrum of real-world systems (Wang and Ohmori, 2013). This approach starts with randomly generated population, and individuals with better fitness will be selected as the basis of next generation. The improved population will keep evolving after inheritance, mutation, selection, and crossover procedures until it meets the final requirement. As a global optimization method, genetic algorithm is based on stochastic variables and does not require the derivatives of object function, which brings the advantages of global evaluation and objective tolerance when compared with other gradient based local optimization methods. It usually helps to obtain a better result in optimization problems with non-smooth objective functions, thus is suitable for the optimization problem in this work.

However, the genetic algorithm may still suffer from the slow convergence that brings about high computational cost. Considering this problem, several researchers tried to furnish genetic algorithm with the ability to simulate the fast convergence of local search methods. The simplex coding genetic algorithm (SCGA) proposed by Hedar et al. is adopted in this work for efficient parameter optimization (Hedar and Fukushima, 2003). SCGA combines the genetic algorithm and simplex-based local optimization algorithm called Nelder-Mead method (Kelley, 1999), which is one of the most efficient derivative-free nonlinear optimization approaches. In SCGA, each chromosome in the population is a simplex and the gene is a vertex of this simplex. Nelder-Mead method is applied to improve the population in the initial stage and every intermediate step when new children are generated. Matlab source code of SCGA can be

found here[5].

2.4 Control Synthesis

If incorporating a hybrid mass damper into the wind turbine, the active structural control strategy becomes possible and offers the potential for further load mitigation. Note that this work only considers the model based control design. Based on small deviation approximation, the system dynamic model around each equilibrium point can be linearized into the following state-space representation,

$$\begin{aligned} \dot{x}(t) &= Ax(t) + Bu(t), \\ z(t) &= C_1 x(t), \\ y(t) &= C_2 x(t), \end{aligned} \tag{2.1}$$

where $x = \left[\dot{x}_{sg}, \dot{x}_{hv}, \dot{\theta}_p, \dot{x}_{hmd}, \dot{\theta}_t, x_{sg}, x_{hv}, \theta_p, x_{hmd}, \theta_t \right]^T$ is the state vector. It includes the velocity and displacement of platform surge, heave, pitch, HMD mass translation, as well as tower pitch motion. $u = F$ is the control input, $z = \theta_p - \theta_t$ is the controlled output, and $y = [x_{sg} + (\theta_p - \theta_t) l_{twr}, \theta_p, x_{hmd}]^T$ is the measured output. The matrices A, B, C_1 and C_2 are of appropriate dimensions.

2.4.1 H_2/H_∞ Control Design

Consider the linear system around a certain setpoint

$$\begin{cases} \dot{x}(t) = Ax(t) + Bu(t) + B_w w(t) \\ z(t) = Cx(t) \end{cases}$$

where $w(t)$ is the aerodynamic disturbance acting on the rotor. We would like to design a state feedback controller $u(t) = Kx(t)$ that keeps the closed-loop system

[5] http://www-optima.amp.i.kyoto-u.ac.jp/member/student/hedar/Hedar_files/go_files/Page341.htm

$$\begin{cases} \dot{x}(t) = (A + BK)x(t) + B_w w(t) \\ z(t) = Cx(t) \end{cases} \tag{2.2}$$

asymptotically stable and improves the dynamic performance of the closed-loop system simultaneously. More specifically, regarding performance improvement, the controller should keep the closed-loop system robust to disturbance $w(t)$, i.e. the H_∞ norm of the transfer function T_{wz} in the closed-loop system does not exceed a given upper bound γ_1. More importantly, the H_2 norm of T_{wz} should be as small as possible (e.g. less than γ_2) so that the vibration energy of tower top deflection will be reduced.

Therefore, this problem is equivalent to a mixed H_2/H_∞ control design, see (Scherer, 1995; Doyle et al., 1994), and the design objective is to determine a desired state feedback gain K such that the closed-loop system is asymptotically stable and γ_2 is minimal for the controllers such that

$$\|T_{wz}\|_\infty < \gamma_1, \|T_{wz}\|_2 < \gamma_2.$$

The following theorem helps to convert the H_2/H_∞ control design problem into an optimization process for several linear matrix inequalities (LMIs). It is then more convenient to solve by using well developed LMI toolbox in Matlab.

Theorem 2.1 For the closed-loop system (2.2), if there exists a given $\gamma_1 > 0$ and the following LMIs have an optimal solution,

$$\begin{aligned} &\min \gamma_2 \\ s.t. &\begin{bmatrix} AX + BW + (AX + BW)^T & B_w & (CX)^T \\ B_w^T & -\gamma_1 I & 0 \\ CX & 0 & -\gamma_1 I \end{bmatrix} < 0 \\ &AX + BW + (AX + BW)^T + B_w B_w^T < 0 \\ &\begin{bmatrix} -Z & CX \\ (CX)^T & -X \end{bmatrix} < 0 \\ &Trace(Z) < \gamma_2 \end{aligned}$$

where $X = X^T > 0$, $Z = Z^T > 0$ and W are matrices of appropriate dimensions, then the state feedback H_2/H_∞ control design is feasible, and the control law is

$$u = WX^{-1}x.$$

2.4.2 Observer Design

Implementing a full state-feedback controller is usually not practical due to the lack of sensors or low measurement accuracy, so designing an observer based controller becomes a possible solution. Consider the observer for (2.1)

$$\begin{aligned}\dot{\hat{x}}(t) &= A\hat{x}(t) + Bu(t) - L(y(t) - \hat{y}(t)),\\ \hat{y}(t) &= C_2\hat{x}(t),\end{aligned}$$

where L is the observer gain. If the state estimation error is defined as $e(t) = x(t) - \hat{x}(t)$, then

$$\begin{aligned}\dot{\hat{e}}(t) &= \dot{x}(t) - \dot{\hat{x}}(t),\\ &= Ax(t) + Bu(t) - A\hat{x}(t) - Bu(t) + L(y(t) - \hat{y}(t)),\\ &= (A + LC_2)e(t).\end{aligned}$$

In order to keep the the estimation error asymptotically stable, we need to design L such that all the eigenvalues of $A + LC$ have negative real parts. Here we use the pole placement technique for the observer design, and the following theorem is introduced (Chilali and Gahinet, 1996).

Theorem 2.2 Let $\mho(\eta, r)$ denote any disk region centered in η with radius r in the complex plane (η, $r \in \mathbb{R}$ and $r > 0$). Then, all the eigenvalues of $A + LC$ in (E.4) lie in the region $\mho(\eta, r)$ if and only if there exists a symmetric matrix $P_1 > 0$ satisfying

$$\begin{bmatrix} -P_1 & P_1(A + LC_2 - \eta I) \\ * & -r^2 P_1 \end{bmatrix} < 0.$$

Then, the desired observer gain can be obtained by simply solving this linear

matrix inequality (LMI).

2.4.3 Guaranteed Cost Control Design

Regarding load reduction, the guaranteed cost control design could offer a solution to keep the closed-loop system stable and improve the system performance simultaneously. The design objective can be converted to find a desired control law $u(t) = K\hat{x}(t)$ such that the closed-loop system

$$\begin{aligned} \dot{x}(t) &= Ax(t) + BK\hat{x}(t) \\ &= (A + BK)x(t) - BKe(t) \\ &\approx (A + BK)x(t), \\ z(t) &= C_1 x(t), \end{aligned} \tag{2.3}$$

is asymptotically stable and the cost function

$$\begin{aligned} J &= \int_0^\infty \left[u^T(\tau)Ru(\tau) + x^T(\tau)Qx(\tau)\right] \mathrm{d}\tau \\ &= \int_0^\infty x^T(\tau)\left[K^T RK + Q\right] x(\tau)\mathrm{d}\tau, \end{aligned}$$

satisfies $J \leq \bar{J}$. Here R and Q are given positive-definite symmetric matrices, and note that the term $BKe(t)$ could be ignored in (2.3) since the designed observer has governed the convergence rate of $e(t)$. Next, the guaranteed control design approach is presented.

Theorem 2.3 For a given K, the closed-loop system in (2.3) is asymptotically stable and the performance index has an upper bound $\bar{J} = x^T(0)P_2x(0)$, if there exists a matrix $P_2 > 0$ satisfying

$$\left[P_2(A + BK)\right]_s + Q + K^T RK < 0. \tag{2.4}$$

Notice that (2.4) can be transformed into an LMI for easier numerical solution. Consider the closed-loop system in (2.3), if there exist matrices

$X > 0$ and Y with appropriate dimensions such that the LMI

$$\begin{bmatrix} [AX + BY]_s & X & Y^T \\ * & -Q^{-1} & 0 \\ * & * & -R^{-1} \end{bmatrix} < 0,$$

holds, then there will exist a proper controller such that the closed-loop system is asymptotically stable and the performance index J has an upper bound as follows

$$J \leq \bar{J} = \mathit{Trace}(X^{-1}).$$

The desired state-feedback control gain will be given by

$$K = YX^{-1}.$$

2.5 Load Analysis Techniques

This work focuses on the evaluation of load reduction effectiveness for different structural control methods, so proper load analysis techniques are needed. Note that the loads mentioned here mainly refer to mechanical loads. Both ultimate and fatigue loads are studied in different design load case simulations. Loads on each primary component of the turbine including the blades, tower, nacelle, drivetrain, and mooring system need to be examined.

2.5.1 Design Load Cases

The IEC 61400-3 standard (DNV, 2011) requires to run a number of design load case (DLC) simulations to verify the structural integrity of an offshore wind turbine design. The results from each DLC are analyzed to determine the ultimate and fatigue loads expected over the lifetime of the turbine.

Although limited, the design load cases in Table 2.2 are selected in the simulation process of this work. Here, NTM, EWM, NSS, and ESS denote normal turbulence model, turbulent extreme wind model, normal sea state, and extreme sea state, respectively. In total, we consider three different DLCs.

The wind and wave conditions in (Lackner and Rotea, 2011b) are adopted as two cases. For wind condition, the mean value of the turbulent wind at hub height is defined as 10 m/s and 18 m/s, respectively. Kaimal spectra and the power law exponent of 0.14 are used for the wind field. The normal turbulence intensity is set as level B, i.e. 18% (10 m/s case) and 15%(18 m/s case). For wave condition, JONSWAP spectrum is utilized to generate the stochastic wave inputs. The significant wave height is set as 2.3 m (10 m/s case) and 3.7 m (18 m/s case), and the peak spectral period is both defined as 14s. Besides, the parked case with 50-year extreme wind and wave is also considered. Mean value of the extreme turbulent wind is defined as 37 m/s with 11% intensity and 0.11 power law exponent, and the significant wave height and wave period are defined as 13.8 m and 19 s. In this case, the generator torque and blade pitch controller is turned off, and all the blades are feathered to 90 degree to minimize the aerodynamic loading. For each case, at least two sets of random seeds are used to generate wind and wave data.

Table 2.2: Selected design load cases

DLC	Wind conditions		Wave Conditions		Events
	Model	Wind Speed	Model	Wave Height	
1.1a	NTM	V_{hub}^{mean}=10m/s	NSS	H_s=2.3m	Normal operation
1.1b	NTM	V_{hub}^{mean}=18m/s	NSS	H_s=3.7m	Normal operation
6.1a	EWM	V_{hub}^{mean}=34m/s	ESS	H_s=13.8 m	Parked

2.5.2 Ultimate Loads

As described above, this work examines the ultimate loads with normal wind conditions in combination with normal machine states, and extreme wind and wave conditions in combination with normal machine states. The occurrence of fault should also be examined in the ultimate loads evaluation process, which will be considered in future study.

In this work, 95th percentile of the loads, including fore-aft and side-side tower base bending moments, flapwise bending moment at the first blade root

and tension of the first anchor are calculated and compared with the baseline results. Besides, the 95th percentile of platform pitch and roll rotation angle are also checked. These values will indicate the load reduction effectiveness and whether the structural control devices will excite any mode of the wind turbine.

2.5.3 Fatigue Loads

In fact, the design of most wind turbine components is not governed by ultimate loads but by fatigue loads (Matha, 2010). According to (Burton et al., 2011), the rotor of a 2 MW onshore wind turbine will rotate some 10^8 times during a 20-year life, with each revolution causing a complete gravity stress reversal in the low speed shaft and in each blade, together with a cycle of blade out-of-plane loading due to the combined effects of wind shear, yaw error, shaft tilt, tower shadow and turbulence. This number will probably be higher with extra hydrodynamic and mooring loads for a floating wind turbine. Therefore, special attention should be drawn on the fatigue load evaluation of floating wind turbine structures.

Since only a limited number of wind speeds are used in the simulations, the short-term damage-equivalent load (DEL), instead of lifetime DEL, for each time-series is seen as the indicator of fatigue load. The post-processing Matlab scripts Mlife [6] is used in this work to calculate the DELs and other statistics for one or more time series.

For the calculation of DEL, rainflow counting (Downing and Socie, 1982) should be firstly performed, where the fluctuating loads are broken down into individual hysteresis cycles by matching local peaks with local valleys. Normal rainflow counting procedure is listed below.

(1) Reduce the time-series to a sequence of peaks and valleys.

(2) Imagine that the time-series is a template for a rigid sheet, and rotate it clockwise 90°.

(3) Each peak is imagined as a source of water that drips down.

[6] https://nwtc.nrel.gov/MLife

(4) Count the number of half-cycles by looking for terminations in the flow occurring when either:

- It reaches the end of the time history;
- It merges with a flow that started at an earlier peak; or
- It flows when an opposite peak has greater magnitude.

(5) Repeat step (4) for valleys.

(6) Assign a load range to each half-cycle equal to the magnitude difference between its start and termination.

(7) Pair up half-cycles of identical magnitude (but opposite sense) to count the number of complete cycles.

Figure 2.7 illustrates an example of how to perform the rainflow counting for a time-series, and the results are shown in Table 2.3.

Table 2.3: Rainflow counting results.

Load range (kN·m)	Whole cycles	Half cycles
10	2	0
13	0	1
16	0	2
17	0	2
19	1	0
20	0	1
22	0	1
24	0	1
27	0	1

Based on the rainflow counting numbers, a DEL can be calculated, representing a constant-amplitude fatigue load that occurs at a fixed load-mean and frequency and produces the equivalent damage as the variable spectrum

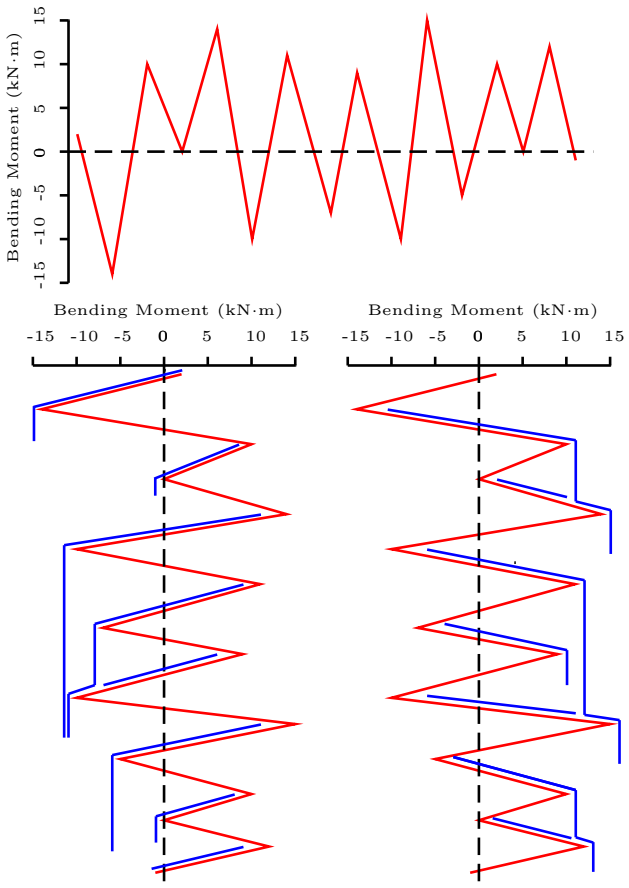

Figure 2.7: Example for rainflow counting.

loads such that,

$$
\begin{aligned}
D_j^{ST} &= \sum_i \frac{n_{ji}}{N_{ji}} = \frac{n_j^{STeq}}{N_j^{eq}}, \\
n_j^{STeq} &= f^{eq} T_j, \\
N_j^{eq} &= \left(\frac{L^{ult} - |L^{MF}|}{0.5 D E L_f^{STF}}\right)^m, \\
N_{ji} &= \left(\frac{L^{ult} - |L^{MF}|}{0.5 L_{ji}^{RF}}\right)^m,
\end{aligned}
$$

where D_j^{ST} is short-term damage rate for time-series j. N_{ji} and n_{ji} denote the cycle number to failure for load range L_{ji}^{RF} and its rainflow counting number,

respectively. f^{eq} is the DEL frequency, T_j is the elapsed time of time-series j. L^{ult} is the ultimate design load of the component, L^{MF} is the fixed load-mean. n_j^{STeq} is the total equivalent fatigue counts for time-series j, DEL_f^{STF} is the short term DEL for time-series j about a fixed mean, and N_j^{eq} is the equivalent number of cycles until failure for time-series j. m denotes the Whöler exponent, which is specific to the component. In this work, m is set as 3 for steel structures, such as tower, and 10 for fiberglass components, like blades. Solving these equations will yield

$$DEL_f^{STF} = \left(\frac{\sum_i \left(n_{ji}(L_{ji}^{RF})^m\right)}{n_j^{STeq}}\right)^{\frac{1}{m}}.$$

2.6 Numerical Simulation Tools

The simulation and data analysis tools used in this work include TurbSim[7], FAST, FAST-SC [8], and Matlab/Simulink.

TurbSim is developed by National Wind Technology Center to simulate inflow turbulence environments that incorporate many of the important fluid dynamic features known to adversely affect turbine aeroelastic response and loading. It has the ability to drive the state-of-the-art wind turbine design code (e.g., FAST or MSC.Adams) for simulations of advanced turbine designs. Therefore, it is used in this work to generate the wind data for various scenarios, including below-rated, rated, and parked occasions.

FAST (Fatigue, Aerodynamics, Structures, and Turbulence) is a fully coupled aero-hydro-servo-elastic open source code that simulates the performance of wind turbines (Jonkman and Buhl Jr, 2005). It is being developed through a subcontract between National Renewable Energy Laboratory (NREL) and Oregon State University. The FAST code models the wind turbine as a combination of rigid and flexible bodies. It uses Blade Element-Momentum (BEM) theory or generalized dynamic wake theory to calculate aerodynamic loads, a linear modal representation for structural components, and a non-linear hydro-

[7]https://nwtc.nrel.gov/TurbSim

[8]http://www.umass.edu/windenergy/research/software/fastsc

dynamic subroutine that calculates wave loading on the platform for offshore applications. This code is interfaced through Matlab/Simulink, and a controller can be implemented graphically with Simulink. FAST is widely used in current research areas on dynamics modelling and load analysis of wind turbines, and the version of FASTv7 [9] is used in this work.

FAST-SC is a modified version of FAST, and was developed by Dr. Matthew Lackner at the University of Massachusetts Amherst in 2009 and modified through 2013. FAST-SC was created in order to model additional degrees-of-freedom (DOFs) in wind turbines, specifically structural control devices (the SC stands for 'structural control'). It has incorporated structural control devices into the nacelle or platform of wind turbines for load mitigation, and passive, semi-active, as well as active structural control designs can be numerically investigated (Lackner and Rotea, 2011a). Simulations for passive structural control methods in this work are mainly based on this code. Besides, the S-function featuring the wind turbine dynamics can also be built from FAST-SC, so that active structural control simulations are run in the Matlab/Simulink environment, which has greatly facilitated model based control designs.

[9] https://nwtc.nrel.gov/FAST7

CHAPTER 3

CONCLUDING REMARKS

3.1 Conclusions

This thesis proposed different structural control strategies for floating wind turbine load reduction, and numerical simulation results showed both the promises and limits for different designs.

In paper A and B, parameter optimization of passive structural control devices, i.e. tuned mass dampers, was performed for a spar-type floating wind turbine. A mathematical model for wind turbine surge-heave-pitch motion was established based on the D'Alembert's principle of inertial forces, and different performance indices and parameter optimization methods were adopted for TMD parameter determination, including frequency analysis, exhaustive search, and intelligent algorithms. For platform installation, the simulation results illustrated that TMD was more effective when placed in the upper side of the spar platform. It was also found that the design of TMD with small spring coefficients would achieve more load reduction and power quality improvement when the turbine was working above rated in resonant motion. However, it did not take much effect for the below rated condition. It would even deteriorate the system performance when the turbine was parked in extreme wind and wave condition, since external load mainly comes from wave in the parked condition, and the platform pitch frequency is dominated by wave,

so that the proposed TMD design loses effect. In contrast, the design with large spring and damping constants would produce moderate load reduction in both resonant and non-resonant motions. One problem for this idea is the stroke restriction due to the lack of horizontal space in the spar platform, and a huge mass in the platform also means an additional cost in manufacture and installation. Similar results were also obtained for the nacelle installation case. It was again shown that inappropriate TMD design would not contribute to wind turbine load reduction, especially in below-rated stage. This is mainly because that the TMD might lean on one side of the nacelle or platform if the turbine fore-aft pitch angle does not cross 0 degree.

Paper C dealt with the idea of installing tuned liquid column dampers in a spar-type floating wind turbine. The code FAST-SC-TLCD is further customized based on FAST-SC, making it possible for fully coupled wind turbine numerical simulation with TLCD incorporated. Only nacelle installation was considered in this work, and a mathematical model for the wind turbine longitudinal motion was again established with TLCD dynamics included. It is usually believed that a larger ratio of the TLCD horizontal length to its total length will be more effective for load reduction, but technically the length of a TLCD is restricted by the dimension of the nacelle if installed on top of the tower. Therefore, both total length and horizontal length of the TLCD were predetermined according to the wind turbine nacelle dimension, leaving the horizontal area, vertical area, and the head loss to be optimized. Because of the intrinsic nonlinearity, it is difficult to obtain an analytical solution for these parameters, and they were determined in this work by using genetic searching algorithm with considering different performance indices. Although limited, the results from a small number of simulations showed its decent performance in load reduction. Also, the low cost of TLCD makes it more promising compared with installing a huge steel or contrate mass damper into the wind turbine. On the other hand, it needs to be noted that more numerical investigations, including evaluating the length of TLCD in the optimization process, should have been performed to demonstrate its effectiveness.

Paper D proposed a gain scheduling H_2/H_∞ active structural control deign

for a hybrid mass damper installed at the tower top of the OC3-Hywind floating wind turbine. External loads imposing on the wind turbine, including aerodynamic, hydrodynamic, and mooring loads, were better approximated based on the polynomial curve fitting approach. Different steady-state points were also derived, which had facilitated the model based control design. Here, H_2 design aimed at reducing the tower top vibration, and H_∞ design was used for mitigate the aerodynamic disturbance. A gain scheduling technique was also used to switch the controller according to the rotor speed and blade pitch angle. Results demonstrated that more load reduction could be achieved at the expense of more energy consumption. However, this will at the same time bring the risk of instability. Moreover, the full-state feedback controller is not very practical from a technical point of view due to the lack of sensors and measurement inaccuracy. Considering this problem, an observer was designed in Paper E with the same installation idea, and guaranteed cost structural control design was be performed to improve the concerned system performance, i.e. the loads and power consumption. Simulation results showed that the designed observer managed to estimate the system states and the designed guaranteed cost controller would help to achieve more load reduction than the passive case. However, these model based controllers, especially the observer based design, highly reply on the model fidelity, while it is almost impossible to describe in practical applications, so that data based control design will be more interesting to be evaluated.

3.2 Contribution to Knowledge

This work aims at conducting a numerical study on the floating wind turbine load reduction effectiveness with different structural control methods and providing useful reference for possible future applications. Also, the efforts on dynamic modelling, design optimization, code development, and structural control design, will lay a solid foundation on the research in this line. Underneath follows a brief statement about what the contributions are in this work.

- A mathematical model for floating wind turbine surge-heave-pitch motion, including the modes of platform surge, heave, pitch, as well as tower tilt motion, is established based on the D'Alembert's principle of inertial forces. The dynamics of structural control devices and their interaction with the wind turbine are also featured in the model.

- External loads imposing on the wind turbine, including aerodynamic, hydrodynamic, and mooring loads, are approximated based on the polynomial curve fitting approach.

- Design optimization process is performed on TMD and TLCD for floating wind turbine load mitigation, and the obtained numerical simulation results have indicated the their effectiveness and limits regarding different properties and installations.

- The code FAST-SC-TLCD is developed based on FAST-SC, making it possible for fully coupled numerical wind turbine simulation with TLCD incorporated.

- A gain scheduling H_2/H_∞ active structural full-state feedback controller is deigned for a HMD installed at the tower top of a spar-type floating wind turbine, aiming at both reducing tower bottom load and mitigating the aerodynamic disturbance.

- Moreover, an observer based guaranteed cost structural controller is designed to work with fewer sensors and improve the concerned system performance regarding load reduction and less power consumption.

3.3 Future Work

A number of research directions can be proposed to further investigate different structural control designs for load reduction of offshore wind turbines.

- It will be interesting to see the effectiveness of structural control ideas on other types of offshore wind turbine models, such as monopile, barge,

TLP and semi-submersible. In this work, the supporting spar produces a constant platform pitch angle due to the wind turbine mass distribution, and it will be harmful for the proposed structural control design, as it is difficult for the mass damper to come across the neutral point. Therefore, the structural control strategy might be more useful for other supporting foundations.

- This work lacks of a comprehensive simulation analysis, especially regarding other design load cases defined in the offshore wind turbine design standard. Therefore, it is necessary to perform more numerical simulations to evaluate the performance of any structural control method. Besides, it will be interesting to look at more performance evaluation methods, such as parameter sensitivity analysis, power spectrum density analysis, etc.

- A TLCD also offers the possibility of the semi-active control design by using the tunable orifice, which leaves the space for further load reduction without too much energy consumption.

- Due to lack of measured data, state-feedback is almost impossible for control design in practice. Alternatively, output feedback theory provides a possible method to deal with this problem, which only require a few types of measurable data, such as the acceleration on tower top and platform tilt angle.

- Despite extensive numerical simulations, the more convincing measure is to perform the field test to demonstrate the effectiveness of structural control. The test can be firstly performed on a scaled wind turbine model with structural vibration control devices mounted.

REFERENCES

Archer, C. and Jacobson, M. (2005). Evaluation of global wind power. *Journal of Geophysical Research*, 110:D12110.

Breton, S. P. and Moe, G. (2009). Status, plans and technologies for offshore wind turbines in europe and north america. *Renewable Energy*, 34(3):646–654.

Burton, T., Jenkins, N., Sharpe, D., and Bossanyi, E. (2011). *Wind energy handbook*. John Wiley & Sons.

Butterfield, S., Musial, W., Jonkman, J., Sclavounos, P., and Wayman, L. (2005). Engineering challenges for floating offshore wind turbines. In *Copenhagen Offshore Wind 2005 Conference and Expedition Proceedings, 26–28 October 2005, Copenhagen, Denmark*.

Chilali, M. and Gahinet, P. (1996). H_∞ design with pole placement constraints: an LMI approach. *IEEE Transactions on Automatic Control*, 41(3):358–367.

Colwell, S. and Basu, B. (2009). Tuned liquid column dampers in offshore wind turbines for structural control. *Engineering Structures*, 31(2):358–368.

Den Hartog, J. P. (1985). *Mechanical vibrations*. Dover publications.

DNV (2011). Offshore standard: design of offshore wind turbine structures. Technical report, DET NORSKE VERITAS.

Downing, S. D. and Socie, D. (1982). Simple rainflow counting algorithms. *International Journal of Fatigue*, 4(1):31–40.

Doyle, J., Zhou, K., Glover, K., and Bodenheimer, B. (1994). Multiobjective H_2/H_∞ control. *IEEE Transactions on Automatic Control*, 39(8):1575–1587.

Hedar, A. R. and Fukushima, M. (2003). Minimizing multimodal functions by simplex coding genetic algorithm. *Optimization Methods and Software*, 18(3):265–282.

Jonkman, J. (2007). *Dynamics modeling and loads analysis of an offshore floating wind turbine*. PhD thesis, Department of Aerospace Engineering Sciences, University of Colorado.

Jonkman, J. (2008). Influence of control on the pitch damping of a floating wind turbine. In *2008 ASME Wind Energy Symposium. Reno, Nevada. January 7-10*. National Renewable Energy Laboratory.

Jonkman, J. (2010). Definition of the floating system for phase IV of OC3. *NREL/TP-500-38060. Golden, Colorado: National Renewable Energy Laboratory*.

Jonkman, J. and Buhl Jr, M. (2005). FAST users guide. Technical report, NREL/EL-500-29798. Golden, Colorado: National Renewable Energy Laboratory.

Jonkman, J., Butterfield, S., Musial, W., and Scott, G. (2009). Definition of a 5-MW reference wind turbine for offshore system development. Technical report, NREL/TP-500-47535. Golden, Colorado: National Renewable Energy Laboratory.

Kaldellis, J. K. and Kapsali, M. (2013). Shifting towards offshore wind energy - recent activity and future development. *Energy Policy*, 53:136–148.

Kane, T. R. and Levinson, D. A. (1985). *Dynamics, theory and applications*. McGraw Hill.

Kelley, C. (1999). *Iterative Methods for Optimization*. Frontiers in Applied Mathematics, Society for Industrial and Applied Mathematics.

Korkmaz, S. (2011). A review of active structural control: challenges for engineering informatics. *Computers & Structures*, 89:2113–2132.

Lackner, M. A. (2013). An investigation of variable power collective pitch control for load mitigation of floating offshore wind turbines. *Wind Energy*, 16(3):435–444.

Lackner, M. A. and Rotea, M. A. (2011a). Passive structural control of offshore wind turbines. *Wind Energy*, 14(3):373–388.

Lackner, M. A. and Rotea, M. A. (2011b). Structural control of floating wind turbines. *Mechatronics*, 21(4):704–719.

Lanczos, C. (1986). *The variational principles of mechanics*. Dover Publications.

Larsen, T. J. and Hanson, T. D. (2007). A method to avoid negative damped low frequent tower vibrations for a floating, pitch controlled wind turbine. *Journal of Physics: Conference Series*, 75(1).

Li, J., Zhang, Z., and Chen, J. (2012). Experimental study on vibration control of offshore wind turbines using a ball vibration absorber. *Energy and Power Engineering*, 4(3):153–157.

Matha, D. (2010). Model development and loads analysis of an offshore wind turbine on a tension leg platform with a comparison to other floating turbine concepts. Technical report, NREL/SR-500-45891. National Renewable Energy Laboratory (NREL), Golden, CO.

Mensah, A. and Dueñas-Osorio, L. (2012). Reliability analysis of wind turbines equipped with tuned liquid column dampers (TLCD). In *Structures Congress*, pages 1190–1200.

Murtagh, P. J., Ghosh, A., Basu, B., and Broderick, B. M. (2008). Passive control of wind turbine vibrations including blade/tower interaction and rotationally sampled turbulence. *Wind Energy*, 11(4):305–317.

Musial, W., Butterfield, S., and Ram, B. (2006). Energy from offshore wind. In *Offshore Technology Conference*, pages 1888–1898.

Namik, H. and Stol, K. (2010). Individual blade pitch control of floating offshore wind turbines. *Wind Energy*, 13(1):74–85.

Namik, H. and Stol, K. (2011). Performance analysis of individual blade pitch control of offshore wind turbines on two floating platforms. *Mechatronics*, 21(4):691–703.

Rao, S. and Durgaiah, R. (2005). *Engineering Mechanics*. Universities Press, India.

Roderick, C. (2012). Vibration reduction of offshore wind turbines using tuned liquid column dampers. Master's thesis, University of Massachusetts Amherst.

Scherer, C. W. (1995). Multiobjective H_2/H_∞ control. *IEEE Transactions on Automatic Control*, 40(6):1054–1062.

Stewart, G. (2012). Load reduction of floating wind turbines using tuned mass dampers.

Stewart, G. and Lackner, M. (2013). Offshore wind turbine load reduction employing optimal passive tuned mass damping systems. *IEEE Transactions on Control Systems Technology*, 21(4):1090–1104.

Stewart, G. M. and Lackner, M. A. (2011). The effect of actuator dynamics on active structural control of offshore wind turbines. *Engineering Structures*, 33(5):1807–1816.

Tsai, H.-C. and Lin, G.-C. (1993). Optimum tuned-mass dampers for minimizing steady-state response of support-excited and damped systems. *Earthquake Engineering & Structural Dynamics*, 22(11):957–973.

Wang, H. and Ohmori, H. (2013). Elasto-plastic analysis based truss optimization using genetic algorithm. *Engineering Structures*, 50:1–12.

Xie, M. (1993). *Flexible Multibody System Dynamics: Theory and Applications*. CRC Press.

PAPER A

MODELLING AND OPTIMIZATION OF A PASSIVE STRUCTURAL CONTROL DESIGN FOR A SPAR TYPE FLOATING WIND TURBINE

Yulin Si, Hamid Reza Karimi and Huijun Gao

This paper has been published as:

Y. Si, H. R. Karimi, and H. Gao, "Modelling and optimization of a passive structural control design for a spar-type floating wind turbine", *Journal of Engineering Structures*, vol. 69, pp. 168–182, 2014.

Modelling and Optimization of a Passive Structural Control Design for a Spar Type Floating Wind Turbine

Yulin Si, Hamid Reza Karimi and Huijun Gao
*Department of Engineering
Faculty of Engineering and Science, University of Agder
Jon Lilletunsvei 9, 4879 Grimstad, Norway.
**Research Institute of Intelligent Control and Systems,
Harbin Institute of Technology, Harbin, 150001, China

Abstract **— Compared with fixed-bottom installation, deep water floating wind turbine has to undergo more severe structural loads due to extra degrees of freedom. Aiming for effective load reduction, this paper deals with the evaluation of a passive structural control design for a spar-type floating wind turbine, and the proposed strategy is to install a tuned mass damper (TMD) into the spar platform. Firstly, a mathematical model for wind turbine surge-heave-pitch motion is established based on the D'Alembert's principle of inertial forces. Then, parameter estimation is performed by comparing the outputs from the proposed model and the state-of-the-art simulator. Further, different optimization methods are adopted to optimize TMD parameters when considering different performance indices. Finally, high fidelity nonlinear simulations with previous optimized TMD designs are conducted under different wind and wave conditions. Simulation results demonstrate both the effectiveness and limitation of different TMD parameter choices, providing parametric analysis and design basis for future improvement on floating wind turbine load reduction with structural control methods.**

Keywords — Floating wind turbine; Spar; Passive Structural Control; Modelling; Identification; Optimization; FAST-SC

Nomenclature

$\mathbf{a_i^k}$	Component k of acceleration vector for mass particle i
A_i^j	Generalized added mass for DOF i with regard to DOF j
D_i^j	Equivalent damping coefficient for DOF i with regard to DOF j
F_i^j	Generalized force for DOF i due to effect or DOF j
g	Gravitational acceleration
I_i^j	Generalized inertia tensor for DOF i with regard to DOF j
J_u^X	Inertia tensor for u with regard to point X
K_i^j	Equivalent spring coefficient for DOF i with regard to DOF j
L_u	Length of part u
m_u	Mass of part u
M_i^j	Generalized mass for DOF i with regard to DOF j
x_i	Displacement of DOF i
$\boldsymbol{\alpha_i}$	Angular acceleration vector for mass particle i
θ_i	Rotation angle of DOF i
τ_i^j	Generalized torque for DOF i due to effect or DOF j

Acronyms and Abbreviations

am	Added mass effect
Anch1Ten	Tension of the first anchor
CB	Center of buoyancy
CG_u	Gravity center of part u
ctr	Centripetal effect
d	Misalignment between RNA mass center and tower centerline
DEL	Damage equivalent load
gr	Gravitational effect
hdr	Hydro effect
hv	DOF of platform have motion
LM	Levenberg-Marquardt
jot	Joint between platform and tower
moor	Mooring lines effect
NREL	National Renewable Energy Laboratory
p	DOF of platform pitch motion
ptfm	Platform
PtfmHeave	Platform heave displacement
PtfmPitch	Platform pitch angle
PtfmSurge	Platform surge displacement
RootMyc1	flapwise bending moment at the first blade root
RMS	root mean square
RNA	Rotor nacelle assembly
sg	DOF of platform surge motion
spr.damp	Spring and damping effect of TMD
SA	Platform symmetric axis
SCGA	simplex coding genetic algorithm
STD	Standard deviation
SSE	Sum of squared errors
SWL	Sea water level
t	DOF of tower fore-aft bending
tmd	DOF of TMD motion
twr	Tower
TmdXDxt	TMD displacement in platform frame
TwrBsMxt	side-side tower base bending moment
TwrBsMyt	fore-aft tower base bending moment
TLP	Tension-leg platform
TTD	Tower top displacement
TTDspFA	Fore-aft tower top displacement
VA	Vertical axis

1 Introduction

Most current large wind turbines around the world are installed on land with sparse population and vast land. However, in many countries, inhabitants are concentrated in places along coastlines where land is scarce while power is in high demand. Therefore, utilizing offshore wind resources is more beneficial, which will both reduce electricity transmission loss and reserve more land space for people, animals and plants. More importantly, offshore wind quality has been evaluated to be much better than that onshore. According to (Archer and Jacobson, 2005), a wind farm located offshore could experience wind speeds that are, on average, 90% greater than that over land. Therefore, global wind energy exploitation has been gradually moving to offshore areas (Kaldellis and Kapsali, 2013). Near offshore wind farms in shallow water have been extensively built in recent years, but they are still often blamed for visual and noise impacts, and their foundations may also leave relatively large seabed footprints (Musial et al., 2006). In contrast, with less space constraints and more consistent wind, deep sea wind energy is more promising for those coastal cities without enough ideal shallow water areas.

Instead of fixed bottom installations, floating foundations are generally considered to be an economical and feasible way of deployment if the water depth is between 60m and 900m (Jonkman, 2007). Based on decades of experience from offshore oil and gas industry, several different traditional floating platforms have been proposed to support large wind turbines in deep sea regions, including spar-buoy, tension-leg, barge, and semi-submersible (Jonkman, 2009). In detailed design, they each correspond to the models of OC3-Hywind, MIT/NREL TLP, ITI Barge, and Principle Power WindFloat (Roddier et al., 2010).

One of the challenges for floating wind turbines is the wave and wind induced platform tilt motion, which will heavily increase the loads on turbine structure due to high inertial and gravitational forces (Butterfield et al., 2005). Large tower and platform healing angle will cause great tower top displacement, which will bring severe fatigue and ultimate loading on tower and blades, disturb the lubrication distribution of gearbox, alter yaw bearing loading etc. Ac-

cording to (Jonkman and Matha, 2009), when comparing a spar-type floating wind turbine with an onshore design, the sea-to-land ratio of fatigue damage equivalent loads (DEL) with respect to fore-aft tower base bending moments is 2.5, and the number has reached 7 for the barge-type, thus special mechanical design or advanced control technique is required to improve wind turbine reliability. Besides, soft foundation properties of floating wind turbines will lead to low natural frequency platform motion, so that commonly used blade pitch control strategy for fixed bottom wind turbines may cause negative damping or even large resonant motion (Larsen and Hanson, 2007). These problems have drawn a lot of attention from both academia and industry on improving the load reduction mechanisms of floating wind turbines. In literature, different methods have been proposed to effectively reduce extra loads brought by platform tilt motion, which can be classified into two different categories.

One idea is to improve the blade pitch control strategy for load mitigation. In order to avoid negative damping, Larsen et al. developed a collective pitch control system for a spar-type floating wind turbine, ensuring the desired natural frequency of control structure is lower than the lowest critical tower frequency (platform fore-aft pitch mode) (Larsen and Hanson, 2007). At the same time, Skaare et al. proposed an estimator based control strategy in order to avoid large resonant platform pitch motion and increase tower fatigue life (Skaare et al., 2007). Jonkman also proposed several modified collective blade pitch control strategies for a barge-type floating wind turbine, including tower top feedback and controller gain detuning (Jonkman, 2008). Besides, in (Namik and Stol, 2010, 2011), Namik et al. proposed an advanced individual blade pitch control for floating wind turbines, which would achieve remarkable platform motion inhibition and tower load reduction, but requiring more blade pitch usage and more complex control strategy.

A more direct approach is to utilize structural vibration control devices, which have been successfully applied in civil engineering structures, such as skyscrapers and bridges (Korkmaz, 2011). It is also expected to be a promising solution for extending the fatigue life of floating wind turbines. In (Murtagh et al., 2008), Murtagh et al. investigated the use of a tuned mass damper

(TMD) placed at the tower top of a simplified wind turbine model for vibration mitigation. Following the same installation idea, Colwell et al. explored the structural responses of a fixed-bottom offshore wind turbine with a tuned liquid column damper (TLCD) (Colwell and Basu, 2009). Later, Mensah et al. assessed the reliability of this idea (Mensah and Dueñas-Osorio, 2012). Moreover, Li et al. performed an experimental study on an offshore wind turbine with a ball vibration absorber fixed on top of the nacelle (Li et al., 2012). However, these discussions are about vibration mitigation of fixed-bottom wind turbines, while their motion dynamics are quite different from that of floating wind turbines. Besides, these works are not based on the cutting edge high-fidelity codes for wind turbine models, which may not capture the comprehensive coupled nonlinear dynamics of wind turbines. Based on the aero-hydro-servo-elastic wind turbine numerical simulator FAST (fatigue, aerodynamics, structures, and turbulence) (Jonkman and Buhl Jr, 2005), Lackner et al. implemented a new simulation tool, called FAST-SC, for passive, semi-active, and active structural control design of wind turbines (Lackner and Rotea, 2011a), which has incorporated TMDs into the nacelle or platform of wind turbines for load mitigation. Utilizing this code, Lackner et al. presented more realistic simulation results by installing a TMD in the nacelle of both a barge-type and a monopile supported wind turbines, and a simple parametric study was also performed to determine the TMD parameters (Lackner and Rotea, 2011a). It was shown more load reduction could be achieved when introducing active structural control, such as the multi-variable H_∞ control with a loop-shaping technique (Lackner and Rotea, 2011b). The actuator dynamics and control-structure interaction were also considered in (Stewart and Lackner, 2011). Furthermore, in order to perform a more comprehensive parametric study, the authors in (Stewart, 2012; Stewart and Lackner, 2013) established a 3-DOF dynamic model for different types of floating wind turbines based on first principles, and TMD parameters are designed under different optimization methods. This limited-DOF model has greatly facilitated parametric analysis and active control design, but the coupling between platform surge and pitch motion was not captured. This effect can be ignored for the barge

model, but might be a strong mode for other platforms (Namik and Stol, 2011; Jonkman, 2010). In addition, TMD was also proposed to be installed in the platform of TLP or spar-type floating wind turbines (Stewart, 2012), so that extra attention can be drawn on this idea since bigger mass becomes possible. Motivated by the above mentioned problems and research potentials, this work will investigate the feasibility of a TMD installed in the floating wind turbine spar platform for load reduction. Modelling, identification, optimization and simualtion will be performed to evaluate the effectiveness of this passive structural control design.

The remainder of this paper will be organized as follows. Section 2 introduces the OC3-Hywind spar-type floating wind turbine, and a 5-DOF model is established based on the D'Alembert's principle of inertial forces. In Section 3, parameter estimation and validation are performed by using the Levenberg-Marquardt algorithm. In Section 4, different optimization methods and performance indices are used for TMD parameter determination. Section 5 presents the nonlinear simulation results from FAST-SC under different wind and wave conditions, and both advantages and limitations of different designs are analyzed. At last, we draw conclusions and point out some interesting directions for future work in Section 6.

2 Dynamic Modelling

In 2009, one Norwegian company Statoil developed the world first full-scale experimental floating wind turbine Hywind, where a Seimens 2.3MW wind turbine was mounted on a spar floater. In cooperation with Statoil, Jonkman from National Renewable Energy Laboratory (NREL) specified a detailed OC3-Hywind wind turbine model, which combined the data of the NREL 5MW baseline turbine and the Statoil Hywind spar (Jonkman, 2010; Jonkman et al., 2009). Properties and illustrations of OC3-Hywind are shown in Table A.1 and Figure A.1 respectively. It needs noting that its control strategy when operating at rated power, i.e. Region 3, was modified by Jonkman to avoid negative damping. In detail, the gains of blade pitch-to-feather controller were

reduced, and the generator torque was kept constant (Jonkman, 2010).

Table A.1: Properties of the OC3-Hywind (Jonkman, 2010; Jonkman et al., 2009).

Item	Value
Rating	5 MW
Rotor configuration	Upwind, 3 blades
Cut-in, rated, cut-out wind speed	3 m/s, 11.4 m/s, 25 m/s
Total draft below sea water level (SWL)	120 m
Tower base above SWL	10m
Hub height above SWL	90m
Nacelle dimension (length, width, height)	14.2m, 2.3m, 3.5m
Platform diameter above taper	6.5m
Platform diameter below taper	9.4m
RNA mass	350,000kg
Tower mass	249,718 kg
Platform mass	7,466,000 kg
Number of mooring lines	3
Depth to fairleads below SWL	70m
Control modifications in Region 3	Gains reduction, constant torque

Aiming for load reduction, this work proposes to install one TMD into the OC3-Hywind spar. Instead of a specific device, an ideal TMD is used in this preliminary study, which is assumed to move on a linear non-friction track, and its stiffness and damping coefficients are kept constant during operation. Besides, the TMD in the platform may be placed at different height in the spar, so that its location is also regarded as a pending parameter.

In order to investigate these parameters, optimize system performance, or further design an active controller, establishing one dynamic mathematical model is very helpful. In (Lackner and Rotea, 2011b), a 3-DOF (platform pitch, tower tilt, TMD motion) dynamic model for a barge-type floating wind turbine is obtained from numerical linearization, but it is an approximation around the set point and will become less accurate when getting away from it. Besides, it might ignore system nonlinearities which could be important intrinsic dynamics. Therefore, establishing a model from first principles is a better choice. In (Stewart, 2012), based on Newton's Second Law, the author

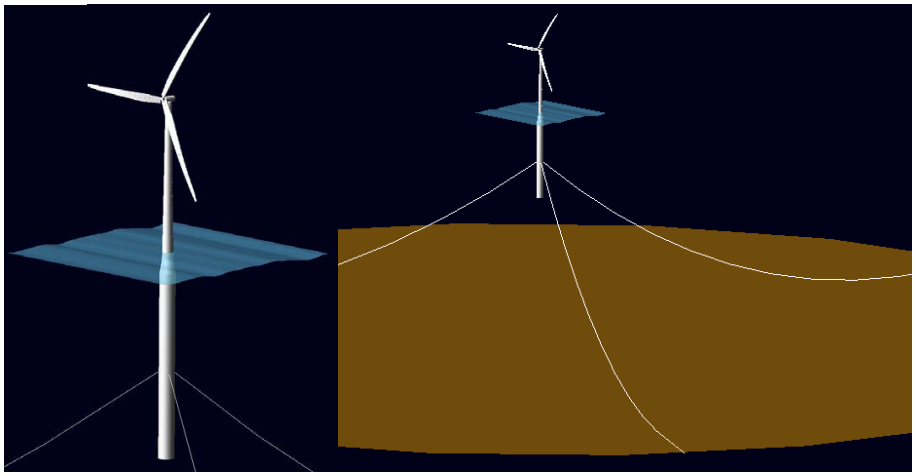

Figure A.1: Illustrations of the NREL 5-MW wind turbine on the OC3-Hywind spar (Jonkman, 2010).

built another 3-DOF dynamic model for floating wind turbines, while their surge and heave DOFs are disabled. In fact, it was pointed out in (Namik and Stol, 2011) from frequency analysis that surge DOF almost does not have impact on system dynamic response for the barge-type turbine, but it is of great importance to the spar buoy, which cannot be simply omitted. Besides, to certain extent, heave motion is also affected by surge and pitch. Therefore, in order to better describe the OC3-Hywind coupled dynamics and the additional TMD motion, in this part, we will establish a model from first principles to represent the system surge-heave-pitch motion and their coupling with tower flexibility and TMD. Figure A.2 is the diagram.
Before presenting the dynamic model, the following premises and assumptions need to be made.

- OC3-Hywind is treated as a multi-body dynamic system, and the motion of reference point P is chosen for output analysis, which is in accordance with the definition in (Jonkman, 2010). Rigid bodies in the model include the spar platform, tower, rotor nacelle assembly (RNA) and the TMD, while the tower flexibility, similar to (Stewart and Lackner, 2011), is captured by introducing the hinge at tower bottom. This equivalent hinge includes a linear spring and damper, representing the structural stiffness and damping of tower bending. The correctness is guaranteed by

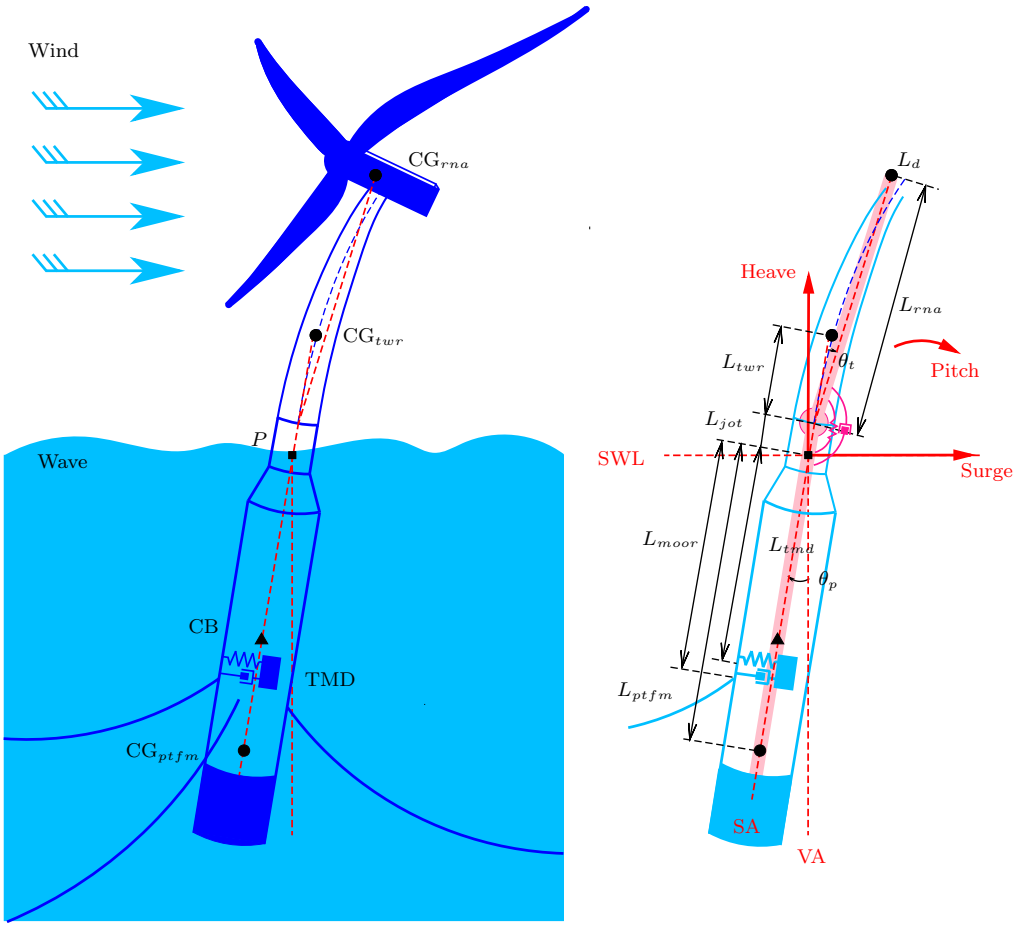

Figure A.2: Diagram of the OC3-Hywind surge-pitch-heave motion with tower fore-aft flexibility and passive structural control.

minimizing the difference of tower top displacement (TTD) between the established model and FAST-SC under the same simulation condition.

- TMD with linear spring and damper is installed in the platform, which could move on a non-friction linear track along the fore-aft direction in the platform frame. The location of the TMD in platform L_{tmd} is defined as the distance from the reference point P to the neutral TMD position along the spar platform center line.

- This model focuses on system intrinsic coupled dynamics with hydro and mooring loads, and turbulent wind and incident wave loads have not yet been considered in the modelling process. That is to say, the wind turbine is placed in still water without wind effect.

- In this work, we do not consider the dynamics in rotor, generator and gearbox in the design process, and the whole RNA structure is treated as a lumped mass. In total, the model has five DOFs, i.e. platform surge, heave, pitch, tower fore-aft bending, and TMD motion. The other DOFs, such as rotor yaw motion, are not included.

Based on the above descriptions, the overall system dynamics can be regarded as the motion of a rigid body with distributed mass particles in the surge-heave-pitch plane. In other words, the system motion is seen as the sum of a translation and a rotation about the axis passing trough P and perpendicular to the surge-heave-pitch plane (Rao and Durgaiah, 2005). However, P is not the overall mass center, so that it is not easy to directly derive the dynamic model from the Newton's law. In this case, it is more convenient to apply the D'Alembert's principle of inertial forces (Lanczos, 1986), which can transform an accelerating rigid body into an equivalent static system by adding inertial forces or moments. The advantage is that, in the equivalent static system, it becomes possible to consider forces and moments about any point, not just the center of mass, which is more appropriate to this problem. Based on the D'Alembert's principle of inertial forces, the following equations manage to

describe the static equilibrium for system translation and rotation about P

$$\begin{aligned} \mathbf{F} - \sum m_i \mathbf{a}_i = 0, \\ \boldsymbol{\tau} - \sum \mathbf{r}_i \times m_i \mathbf{a}_i = 0. \end{aligned} \tag{A.1}$$

$\mathbf{F}$ and $\boldsymbol{\tau}$ denote vectors of external forces and moments about P, respectively, while $-\sum m_i \mathbf{a}_i$ and $-\sum \mathbf{r}_i \times m_i \mathbf{a}_i$ are vector sums of inertial forces and torques about P, respectively. m_i is the mass of particle i, i.e. platform, tower, RNA and TMD, and $\mathbf{r}_i$ represents the position vector from P to particle i. $\mathbf{a}_i$ is the acceleration vector for mass particle i, and it consists of the translational, normal and tangential components of acceleration as illustrated in Figure A.3. Besides, platform and tower have huge inertia tensor around their mass center,

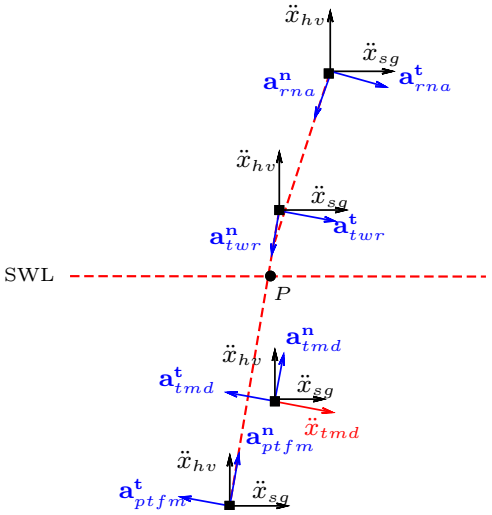

Figure A.3: Acceleration components of each particle for the OC3-Hywind surge-pitch-heave motion with tower fore-aft flexibility and passive structural control.

which should also be included. Therefore, the equations of surge-heave-pitch motion for OC3-Hywind about P can be established as

$$\begin{aligned} \sum m_i({}^{sg}\mathbf{a}^{\mathbf{l}}_i + {}^{sg}\mathbf{a}^{\mathbf{n}}_i + {}^{sg}\mathbf{a}^{\mathbf{t}}_i) = \mathbf{F}^{gr}_{sg} + \mathbf{F}^{hdr.moor}_{sg}, \\ \sum m_i({}^{hv}\mathbf{a}^{\mathbf{l}}_i + {}^{hv}\mathbf{a}^{\mathbf{n}}_i + {}^{hv}\mathbf{a}^{\mathbf{t}}_i) = \mathbf{F}^{gr}_{hv} + \mathbf{F}^{hdr.moor}_{hv}, \\ \sum (\mathbf{r}_i \times m_i(\mathbf{a}^{\mathbf{l}}_i + \mathbf{a}^{\mathbf{n}}_i + \mathbf{a}^{\mathbf{t}}_i) + J_i \boldsymbol{\alpha}_i) = \boldsymbol{\tau}^{gr}_p + \boldsymbol{\tau}^{hdr.moor}_p, \end{aligned} \tag{A.2}$$

where $\mathbf{a}_i^{\mathbf{l}}$ is the linear acceleration vector for mass particle i, consisting of translational accelerations for surge, heave and TMD motion, while $\mathbf{a}_i^{\mathbf{n}}$ and $\mathbf{a}_i^{\mathbf{t}}$ denote normal and tangential acceleration vectors for particle i. ${}^{sg}\mathbf{a}$ and ${}^{hv}\mathbf{a}$ are surge and heave components of acceleration $\mathbf{a}$. J_i is the moment of inertia for particle i about its mass center, and $\boldsymbol{\alpha}_i$ is its angular acceleration vector. $\mathbf{F}_{sg}^{gr}$, $\mathbf{F}_{hv}^{gr}$ and $\boldsymbol{\tau}_p^{gr}$ are, respectively, gravitational force and moment vectors about P for system surge, heave and pitch motion, while $\mathbf{F}_{sg}^{hdr.moor}$, $\mathbf{F}_{hv}^{hdr.moor}$ and $\boldsymbol{\tau}_p^{hdr.moor}$ are the force and moment vectors due to hydro and mooring effects, respectively. Similarly, the dynamics of TMD is represented by

$$m_{tmd}({}^{tmd}\mathbf{a}_{tmd}^{\mathbf{l}} + \mathbf{a}_{tmd}^{\mathbf{t}}) = \mathbf{F}_{tmd}^{gr} + \mathbf{F}_{tmd}^{spr.damp}, \tag{A.3}$$

where ${}^{tmd}\mathbf{a}$ denotes the TMD linear acceleration component along its moving direction, and $\mathbf{F}_{tmd}^{spr.damp}$ is the force vector from the TMD spring and damper. Then, the tower flexibility is considered, where the tower-platform interaction is represented by a linear spring damper as mentioned above. The motion equation of tower fore-aft bending can be described as

$$\sum (\mathbf{r}_i \times m_i(\mathbf{a}_i^{\mathbf{l}} + \mathbf{a}_i^{\mathbf{n}} + \mathbf{a}_i^{\mathbf{t}})) + I_t^t \boldsymbol{\alpha}_t = \boldsymbol{\tau}_t^{gr} + \boldsymbol{\tau}_t^p, \tag{A.4}$$

which is also based on the D'Alembert's principle of inertial forces. m_i denotes the mass of tower and RNA. I_t^t is the equivalent moment of inertia for tower and RNA about tower bottom, and $\boldsymbol{\alpha}_t$ denotes the angular acceleration vector of tower pitch motion. $\boldsymbol{\tau}_t^p$ is the torque vector due to the spring-damping effect between tower and platform. To be consistent with the output of FAST simulator, the tower top displacement (TTD) is also calculated, which is given by

$$x_{ttd} = \sin(\theta_t - \theta_p) L_{ttd}, \tag{A.5}$$

where L_{ttd} is the length of flexible tower.

Next, hydrodynamic loads are characterized. It is stated in (Jonkman, 2007) that the hydrodynamic loads mainly include contributions from hydrostatics (from water-plane area and buoyancy), diffraction (from incident waves), and radiation (from outgoing waves generated by platform motion). In accordance

with this analysis, the hydrodynamic load calculation in this work follows a similar path. Firstly, hydrostatic load mainly comes from the buoyancy effect, which is almost constantly proportional to platform displacement and tilt angle as specified in (Jonkman, 2010). Secondly, the platform is assumed to be located in still water in this model, so that the diffraction effect resulting from incident waves is not included. Thirdly, the radiation load consists of nonlinear viscous drag, hydrodynamic radiation damping and the added-mass effect.

- In FAST, the viscous drag load on OC3-Hywind is mainly from the surge motion of the slender platform, and it is described by the viscous drag term in Morison's equation (Sarpkaya, 1986), i.e.

$$F^{viscous} = \frac{1}{2}\rho C_d A(v_{sg}^{wave} - \dot{x}_{sg})|v_{sg}^{wave} - \dot{x}_{sg}|. \tag{A.6}$$

  C_d denotes the effective platform normalized hydrodynamic viscous drag coefficient. A is the effective platform diameter, and ρ is water density. v_{sg}^{wave} is wave flow velocity along surge direction. Following previous premise, incident waves are not considered in this model, thus the value of viscous drag force is proportional to the directional quadratic power of platform surge velocity. Considering platform pitch motion, the viscous drag load should be in the following integration form,

$$\begin{aligned} F_{sg}^{damp} &= \alpha \int_0^{L_{spar}} (\dot{x}_{sg} - L\dot{\theta}_p)|\dot{x}_{sg} - L\dot{\theta}_p|dL, \\ \tau_p^{damp} &= \beta \int_0^{L_{spar}} (\dot{x}_{sg} - L\dot{\theta}_p)|\dot{x}_{sg} - L\dot{\theta}_p|LdL. \end{aligned} \tag{A.7}$$

  Here α and β are proper coefficients. However, the integration form is too complicated and not computationally efficient for design optimization. Therefore, the quadratic terms $\dot{x}_{sg}^2$ and $\dot{\theta}_p^2$, together with linear ones $\dot{x}_{sg}$ and $\dot{\theta}_p$, are simply treated as polynomial approximation of the viscous load in the model.

- The radiation damping in FAST is captured through the time-convolution of wave-radiation-retardation kernel with platform velocities, but it is

quite computationally expensive, and the values of this load for most of modes are considerably smaller than those of added mass and viscous drag (Jonkman, 2010), thus this effect is omitted here.

- In this work, for the surge-heave-pitch motion of OC3-Hywind, the added mass effect is represented as

$$\begin{aligned} A_{sg}^{sg}\ddot{x}_{sg} + A_{sg}^{hv}\ddot{x}_{hv} + A_{sg}^{p}\ddot{\theta}_p &= F_{sg}^{am}, \\ A_{hv}^{sg}\ddot{x}_{sg} + A_{hv}^{hv}\ddot{x}_{hv} + A_{hv}^{p}\ddot{\theta}_p &= F_{hv}^{am}, \\ A_{p}^{sg}\ddot{x}_{sg} + A_{p}^{hv}\ddot{x}_{hv} + A_{p}^{p}\ddot{\theta}_p &= \tau_{p}^{am}, \end{aligned} \tag{A.8}$$

  where $\ddot{x}_{sg}$, $\ddot{x}_{hv}$, $\ddot{\theta}_p$ represent, respectively, accelerations for system surge, heave and pitch motion about P. A_i^j is the added mass for DOF i with regard to motion j. F_{sg}^{am}, F_{hv}^{am} and τ_p^{am}, respectively, are the force and torque components due to added mass effect. For OC3-Hywind, the added mass matrix has already been specified in (Jonkman, 2010), and it varies little across oscillation frequency, thus is regarded as constant here.

- Besides, additional linear damping should be added onto the overall hydrodynamic loads in order to be consistent with the data provided by Statoil (Jonkman, 2010).

Regarding the mooring system, FAST simulator uses a quasi-static model to calculate the load of each individual mooring line, which exhibits nonlinear behaviors due to both mooring dynamics and the asymmetry of the three-point mooring system. However, considering the small displacement range in the model and its computational simplicity, the constant mooring stiffness approximation is used here.

In sum, except for added mass, the hydrodynamic loads and mooring effect are modelled as

$$\begin{aligned} F_{sg}^{hdr.moor} &= -D_{sg}^{sg}\dot{x}_{sg} - \hat{D}_{sg}^{sg}\dot{x}_{sg}^2 - K_{sg}^{sg}x_{sg} - D_{sg}^{p}\dot{\theta}_p - K_{sg}^{p}\theta_p, \\ F_{hv}^{hdr.moor} &= -D_{hv}^{hv}\dot{x}_{hv} - K_{hv}^{hv}x_{hv} - F_{moor}^{0} + F_{buoy}^{0} - K_{hv}^{p.sg}(x_{sg} - L_{moor}\sin\theta_p)^2, \\ \tau_{p}^{hdr.moor} &= -D_{p}^{p}\dot{\theta}_p - K_{p}^{p}\theta_p - D_{p}^{sg}\dot{x}_{sg} - \hat{D}_{p}^{sg}\dot{x}_{sg}^2 - K_{p}^{sg}x_{sg}. \end{aligned} \tag{A.9}$$

D_i^j, $\hat{D}_i^j$ and K_i^j, respectively, denote equivalent damping and spring coefficients for DOF i with regard to DOF j. F_{moor}^0 and F_{buoy}^0 represent initial mooring line and buoyancy forces when there is no platform displacement or rotation. It is later found that the mooring load for platform heave motion shows strong nonlinear relationship with the surge and pitch modes, thus it is not simplified.

Based on the above analysis and equations (A.2)-(A.9), the nonlinear dynamic model of OC3-Hywind surge-heave-pitch motion can be established in the following implicit form

$$\begin{bmatrix} M_{sg}^{sg} & 0 & I_{sg}^{p} & M_{sg}^{tmd} & I_{sg}^{t} \\ 0 & M_{hv}^{hv} & I_{hv}^{p} & M_{hv}^{tmd} & I_{hv}^{t} \\ M_{p}^{sg} & M_{p}^{hv} & I_{p}^{p} & M_{p}^{tmd} & 0 \\ M_{tmd}^{sg} & M_{tmd}^{hv} & I_{tmd}^{p} & M_{tmd}^{tmd} & I_{tmd}^{t} \\ M_{t}^{sg} & M_{t}^{hv} & 0 & M_{t}^{tmd} & I_{t}^{t} \end{bmatrix} \begin{bmatrix} \ddot{x}_{sg} \\ \ddot{x}_{hv} \\ \ddot{\theta}_{p} \\ \ddot{x}_{tmd} \\ \ddot{\theta}_{t} \end{bmatrix} = \begin{bmatrix} F_{sg}^{hdr.moor} + F_{sg}^{ctr} \\ F_{hv}^{gr} + F_{hv}^{hdr.moor} + F_{hv}^{ctr} \\ \tau_{p}^{gr} + \tau_{p}^{hdr.moor} + \tau_{p}^{ctr} \\ F_{tmd}^{gr} + F_{tmd}^{spr.damp} \\ \tau_{t}^{gr} + \tau_{t}^{p} + \tau_{t}^{ctr} \end{bmatrix}. \tag{A.10}$$

In this model, sg, hv, p, tmd, t represent, respectively, the enabled 5 DOFs, i.e. platform surge, heave, pitch motion about P, TMD translation, and tower rotation about tower bottom. On the left side, M_i^j and I_i^j denote, respectively, generalized mass and generalized inertial tensor for DOF i with regard to DOF j. On the right side, gr, hdr, moor, ctr, spr and damp describe gravitational, hydro, centripetal, spring and damping effects in forces and moments, respectively. Expanded expressions of this model are presented in Appendix.

The mass matrix on the left side of (A.10) exhibits the system inertial property, i.e. mass and inertia tensor, and it also includes hydro added mass and acceleration coupling terms. The coupling terms are induced forces or moments due to acceleration of other DOFs, which will lead the model into an implicit expression, so that it needs an additional matrix inversion operation when solving this differential equation. The terms on the right side of (A.10) can be classified into several different effects. Gravitational forces and moments are the first type, labeled as gr. It is worth noting that there exists misalignment between the tower centerline and RNA mass center, so the equilibrium of pitch mode does not equal to zero due to this constant gravitational pitch moment. The second effect, labeled as hdr.moor, is the hydrodynamic and mooring loading, which consists of hydrostatics, viscous drag, additional linear damp-

ing, and mooring effects. The third type, which is obtained from D'Alembert's principle, is the centripetal forces and moments originated from the rotation of platform, tower and TMD about the reference point P, and they are labeled as ctr. Tower and platform interaction is the fourth effect captured in this model, and the bending moment is described by a linear spring-damper between them. The final consideration is the spring and damping effect in TMD, so it is labeled as spr.damp.

After obtaining the OC3-Hywind dynamic model for its surge-heave-pitch motion in still water, parameter estimation should be performed to quantize the unknown parameters and verify the correctness of the proposed model.

3 Parameter Estimation

The FAST simulator (Jonkman and Buhl Jr, 2005) has been extensively used in scientific research and engineering on load analysis and control design of wind turbines. Based on the Kane's method (Kane and Levinson, 1985), this code captures the fully coupled aero-hydro-servo-elastic dynamics of both onshore and offshore wind turbines, and system dynamic responses can be obtained by activating different DOFs under various wind and wave conditions. It is also discovered that our proposed model essentially leads to the same form as that from Kane's dynamics, but in this case, the D'Alembert's principle of inertial forces and certain approximations provide a more simple and direct modelling process.

In order to adopt additional structural control features, Lackner et al. implemented the FAST-SC module (Lackner and Rotea, 2011a) based on the FAST code. Two TMDs in nacelle and two in platform were added into the system, which could move independently in the fore-aft or side-side direction in local frame. Their equations of motion were also based on the Kane's method, and each TMD can be controlled in a passive, semi-active or active manner. For the passive case, the TMD spring and damping coefficients are configured as constants in the input file before running the simulation.

Here FAST-SC is used to estimate the unknown parameters in the proposed

model. In total, there are 17 parameters to be identified, and they are classified into two categories, i.e. $\mathbf{U} = [\mathbf{U}_1{}^T, \mathbf{U}_2{}^T]^T$, where

$$\mathbf{U}_1 = [D_{sg}^{sg}, \hat{D}_{sg}^{sg}, K_{sg}^{sg}, D_{sg}^{p}, K_{sg}^{p}, D_{hv}^{hv}, K_{hv}^{hv}, K_{hv}^{sg.p}, D_{p}^{p}, K_{p}^{p}, D_{p}^{sg}, \hat{D}_{p}^{sg}, K_{p}^{sg}]^T,$$
$$\mathbf{U}_2 = [D_t, K_t, I_t]^T.$$

In $\mathbf{U}_1$, most of the parameters belong to spring and damping coefficients related with hydrodynamic and mooring effects. $\mathbf{U}_2$ is the parameter vector for tower rotation. I_t also needs to be estimated since the tower flexibility in this model is an approximation, which does not exhibit exactly the same inertial property as that of OC3-Hywind wind turbine tower bending.

In this section, specifically, the Levenberg-Marquardt (LM) algorithm (More, 1978) is used to estimate the unknown parameters by minimizing the sum of squared errors (SSE) between the model response and FAST-SC simulation result. This technique helps to locate the minimum of a function that is expressed as the sum of squares of nonlinear functions, and it has been widely adopted in parameter estimation, system identification and curve fitting problems (Shawash and Selviah, 2013). In detail, the LM approach combines the advantages of two minimization methods, the gradient descent algorithm and the Gauss-Newton approach (Gavin, 2011). It acts more like the gradient descent method when the parameters are far from their optimal value, providing a steady and convergent process for multi-variable identification problem, and acts more like the Gauss-Newton method when the parameters are close to their optimal value, so it will converge rapidly and accurately to the local minimum. Therefore, the LM method is chosen in this work since it will both guarantee the convergence of this multi-variable identification problem and improve estimation efficiency and accuracy.

The SSE between outputs from FAST-SC and the proposed model is defined as

$$S(\mathbf{U}) = \frac{1}{2}\sum_{j=1}^{m}\sum_{i=1}^{n} w_j(y_j(t_i) - f_j(t_i, \mathbf{U}))^2,$$

$$= \frac{1}{2}\sum_{i=1}^{n}(\mathbf{y}(t_i) - \mathbf{f}(t_i, \mathbf{U}))^T \mathbf{W}(\mathbf{y}(t_i) - \mathbf{f}(t_i, \mathbf{U})),$$

where m denotes the number of outputs, and n is the data length for one output. $y_j(t_i)$ is the jth FAST-SC output at time t_i, while $y_j(t_i, \mathbf{U})$ is the jth output of the established model with parameter vector $\mathbf{U}$ at time t_i. $\mathbf{y}(t_i)$ and $\mathbf{y}(t_i, \mathbf{U})$ are their vector notations. $\mathbf{W}$ represents the diagonal weight matrix for normalization.

Since the effects of turbulent wind and incident waves are not characterized in this model, simple free decay test is chosen here for system parameter estimation, where a small platform pitch angle is set as the initial disturbance. The parameter estimation procedure has three steps. Firstly, in the FAST-SC input file, activate the platform surge, heave, pitch DOFs, deactivate all the others, disable wind and incident wave effects, and set the initial platform pitch angle as 5°. Then, run FAST-SC and obtain the fully coupled nonlinear free decay simulation result. Next, quantify the difference of platform surge, heave, pitch responses between the established model and FAST-SC, and estimate all the unknown parameters in $\mathbf{U}_1$. Secondly, in addition to the previous setup, enable tower 1st fore-aft bending mode and obtain the FAST-SC free decay test result. Then, calculate the SSE of platform surge, heave, pitch outputs and the fore-aft tower top displacement, and continue to estimate the rest unknown parameters in $\mathbf{U}_2$. Thirdly, activate the TMD DOF both in FAST-SC and the identified model, run the free decay simulation and compare the results in order to verify the proposed model.

The LM algorithm used in this work adopts the embedded `lsqnonlin` solver in MATLAB. Before estimation, the initial algorithm damping parameter λ is set as 0.01, which is adaptive during the iteration process. Parameter and cost tolerance is set as 0.001 when estimation accuracy and efficiency are both considered. For brevity, detailed steps of LM algorithm (More, 1978) in the solver are not described in this paper. It should be noted that the initial guess of unknown parameters are important in this nonlinear iterative estimation problem, since there are a big amount of parameters to be estimated compared with the number of outputs, and it will usually lead to a slow convergence process

and unsatisfied result if the initial values are placed too far away from the best estimation. Luckily, some parameters, such as hydrostatic, mooring and linear damping coefficients, have been presented in (Jonkman, 2010), which could be treated as the initial guess before estimation. However, D_t and K_t do not have reference values, so that it takes some trial and error to produce a rough initial guess for these parameters. To illustrate the parameter estimation process, the initial guess and the estimation result are given in Table A.2, and the estimation iteration process is shown in Figure A.4. The parameters have metric units, which are not presented in this table and figure for conciseness.

Table A.2: Initial guess and the parameter estimation result

Term	Guess	Estimation	Term	Guess	Estimation
D_{sg}^{sg}	5.0000 $\times 10^5$	1.2474 $\times 10^5$	K_{sg}^{sg}	4.1180 $\times 10^4$	4.0328 $\times 10^4$
D_{sg}^{p}	-3.0000 $\times 10^6$	-6.2164 $\times 10^6$	K_{sg}^{p}	-2.8210 $\times 10^6$	-2.6383 $\times 10^6$
D_{p}^{p}	7.0000 $\times 10^7$	5.2121 $\times 10^8$	K_{p}^{p}	-4.6881 $\times 10^9$	-4.7330 $\times 10^9$
D_{p}^{sg}	-3.0000 $\times 10^6$	-2.9784 $\times 10^6$	K_{p}^{sg}	-2.8160 $\times 10^6$	-2.7198 $\times 10^6$
D_{hv}^{hv}	1.3000 $\times 10^5$	1.3001 $\times 10^5$	K_{hv}^{hv}	3.4488 $\times 10^5$	3.4361 $\times 10^5$
$\hat{D}_{sg}^{sg}$	0	1.3156 $\times 10^5$	$K_{hv}^{sg.p}$	0	2.4806 $\times 10^2$
$\hat{D}_{p}^{sg}$	0	-4.8626 $\times 10^6$	K_t	2.0000 $\times 10^{10}$	1.4019 $\times 10^{10}$
D_t	1.3817 $\times 10^8$	7.4400 $\times 10^7$	I_t	2.3862 $\times 10^9$	1.8945 $\times 10^9$
I_t^{nac}	1.8945 $\times 10^9$	1.9978 $\times 10^9$			

Based on the estimation result, free decay response comparison between the identified model and FAST-SC numerical simulation for the OC3-Hywind surge-pitch-heave motion without TMD is illustrated in Figure A.5, where two results coincide well with each other. In this figure, PtfmSurge, PtfmHeave and PtfmPitch denote the displacement of platform surge, heave and pitch motion, and TTDspFA represents the fore-aft tower top displacement. Besides, as shown in Figure A.6, if the initial platform pitch angle is changed into a bigger value, 10° for instance, the two responses are still in high overlap ratio. Then, in order to further verify the established model, free decay response comparisons are performed again with TMD installed. The TMD parameters in Table A.3 are chosen for verification, and the comparison results are shown in Figure A.7. In this figure, TmdXDxt means TMD displacement in platform

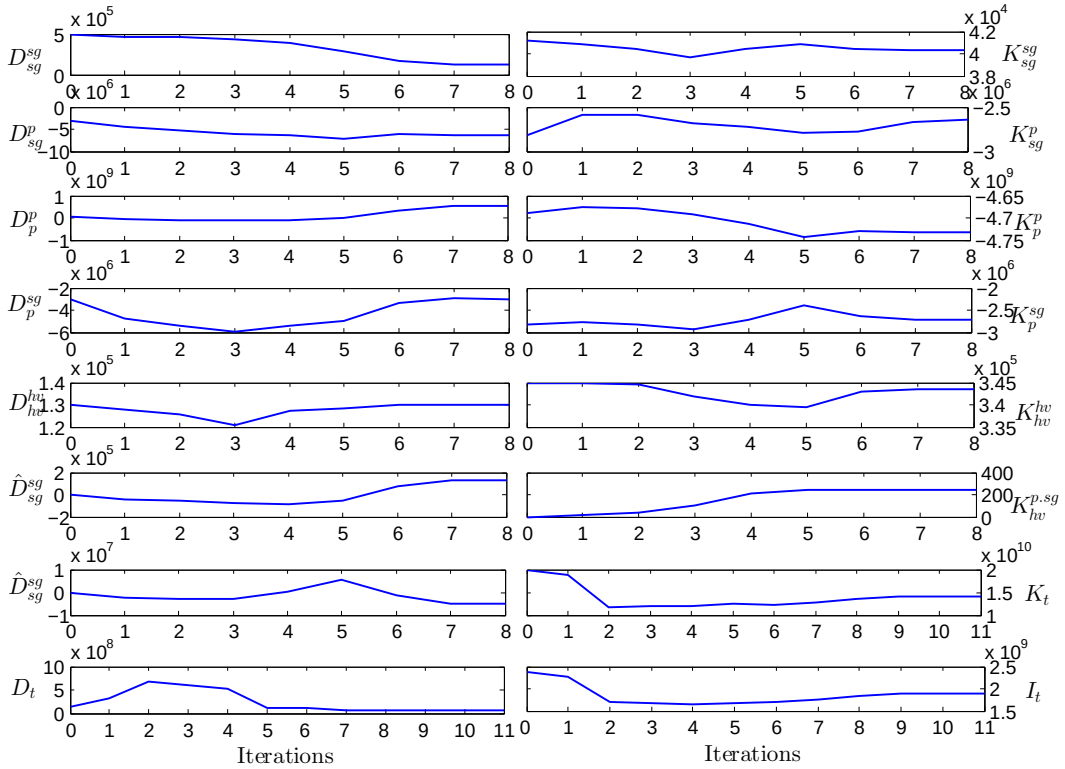

Figure A.4: Iteration process for parameter estimation under LM algorithm.

frame. Still, the outputs of the established model are almost the same as the responses from FAST-SC. It should be noted that the minor misalignment, as pointed out in Figure A.7, is mainly due to the nonlinearity of mooring loads. Besides, huge additional mass of TMD will cause fierce platform heave motion and also bring the coefficient alternation in mooring and viscous drag loads.

Table A.3: TMD parameters for system validation

Mass	1×10^5 kg
Spring coefficient	5×10^3 N/m
Damping coefficient	1×10^4 N·s/m
TMD location	-100 m
Stop positions	$\pm$ 4 m
Stop spring coefficient	1×10^6 N/m
Stop damping coefficient	5×10^6 N·s/m

In fact, one of the most important restrictions for TMD spar installation is the

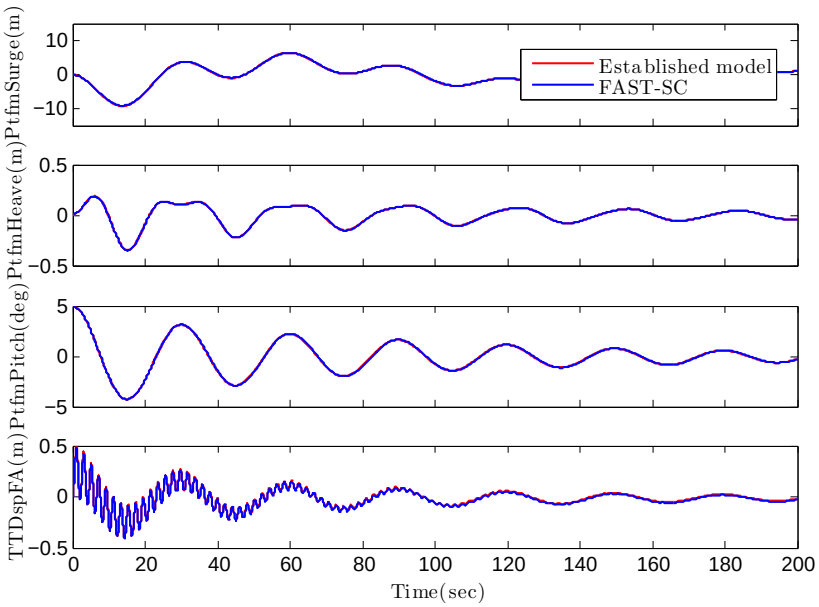

Figure A.5: Free decay response comparison for the OC3-Hywind surge-pitch-heave motion without TMD (5° initial platform pitch).

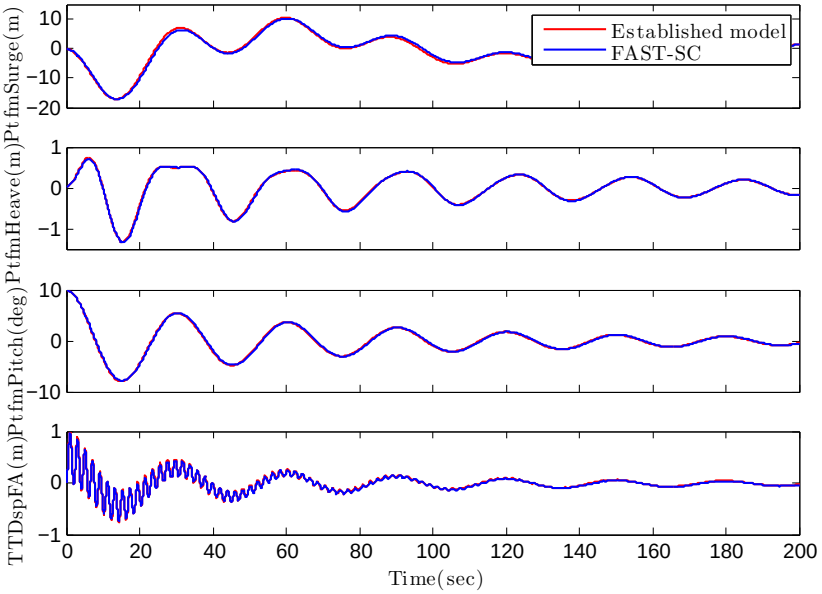

Figure A.6: Free decay response comparison for the OC3-Hywind surge-pitch-heave motion without TMD (10° initial platform pitch).

space limitation, so the TMD displacement should be restricted into a certain range in the model. According the platform dimension (9.4m in diameter)

described in (Jonkman, 2010), the TMD displacement range in platform is defined as ± 4m in this work. In FAST-SC, the TMD motion constraints were modelled as stops, where there would be spring stiffness and damping interaction between TMD and platform when its displacement exceeds the predefined constraints. For example, if TMD in platform moves beyond the predefined platform limits, the stop spring damper will take effect to prevent TMD from exceeding the bounds until it is back in platform. The stops effect in this work is characterized in the same way, and the stop spring and damping coefficients in Table A.3 are used in simulation. Figure A.8 illustrates the free decay response comparison result when TMD stops in platform are considered. As expected, the established model still manages to capture the system dynamics including TMD stop interaction. It is worth mentioning that the stops with various spring and damping coefficients could have very different impacts on system dynamics, but further analysis of stop parameters is not within the scope of this paper. The TMD stop parameters in Table A.3 are chosen because they usually lead to relatively smooth TMD motion when the interaction happens.

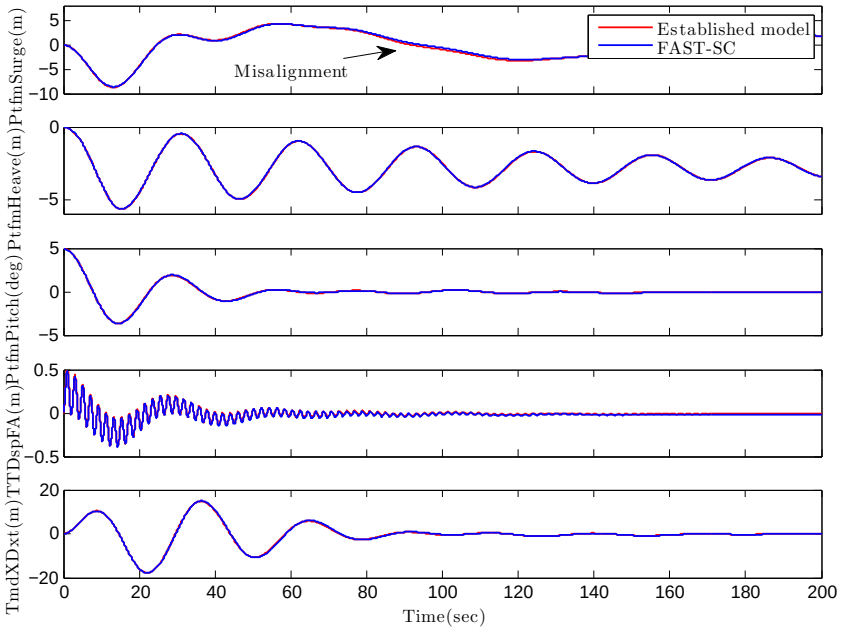

Figure A.7: Free decay response comparison with TMD in platform.

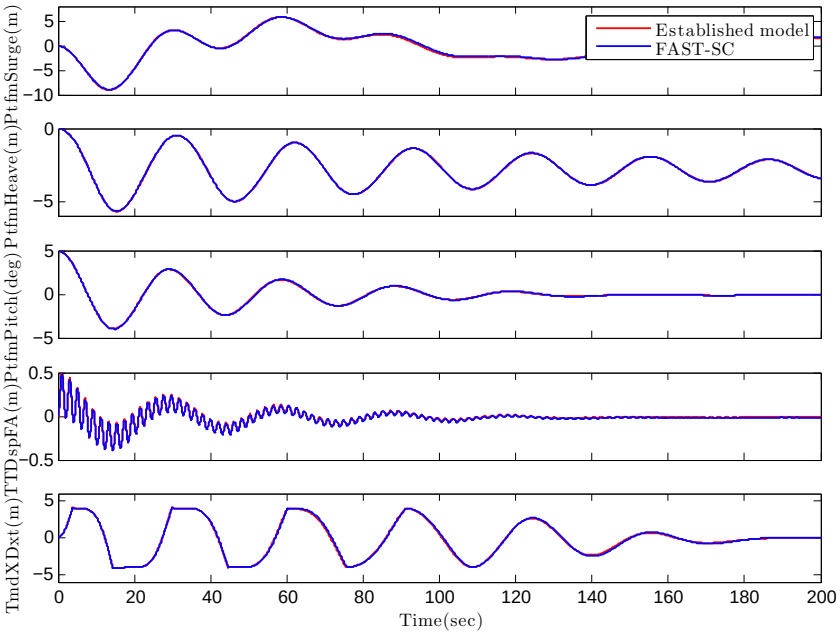

Figure A.8: Free decay response comparison with TMD and stops in platform.

Based on the above analysis, it can be concluded that the proposed model has captured most of the intrinsic dynamics for OC3-Hywind surge-heave-pitch motion, including hydrodynamic and mooring loads, tower flexibility and TMD-platform interactions. Next step is to analyze and optimize TMD parameters for system load reduction.

4 Parameter Optimization

Optimal parameter tuning of the vibration absorber is an important design consideration in passive structural control problems. The design aim in this work is to find the optimal TMD coefficients for wind turbine load reduction. The parameters to be determined include TMD spring and damping coefficients and its location in platform. Mass of TMD is usually determined by cost and installation space, and the mass ratio is below 5% for most vibration control applications (Connor and Connor, 2003). Since the TMD moving space is limited and large mass is difficult for marine operation, a small mass ratio is chosen, i.e. 100,000kg, about 1.25% of the whole platform-tower-RNA weight.

In fact, the most convincing optimization solution here is to try all possible values of these parameters in FAST-SC. However, this global searching process will take tens of thousands of calls from FAST-SC, and it even takes minutes to run it for only one time. Therefore, exhaustive search based on FAST-SC is almost impossible with ordinary computers, and appropriate optimization methods are needed.

4.1 Frequency and Damping Analysis

In engineering applications, the natural frequency of TMD is usually tuned to be near to that of the target system, so that it will effectively dissipate the undesirable system vibration energy. In order to systematically describe this phenomenon, Den Hartog (Den Hartog, 1985) analyzed the response of undamped main system with TMD subjected to harmonic external forces, and derived an explicit expression to determine the optimal TMD natural frequency and damping ratio for vibration inhibition, which has been widely adopted in many practical applications. The optimal solution is given by

$$f_{tmd} = \frac{f}{1+\mu}, \quad \xi_{tmd} = \sqrt{\frac{3\mu}{8(1+\mu)}}, \tag{A.11}$$

where μ denotes the mass ratio $\frac{m_{tmd}}{m}$. f and ξ are the natural frequency and damping ratio of target system. f_{tmd} and ξ_{tmd} represent, respectively, the optimal natural frequency and damping ratio of TMD. However, all systems contain damping, which should not be neglected in the parameter tuning process. It is also found that the optimum tuning frequency is strongly influenced by the system damping level (Tsai and Lin, 1993). In face of this, Tsai et al. presented a numerical searching procedure to determine the optimum parameters with target system damping considered, and a curve fitting scheme was then used to produce the equations for the optimal tuning parameters (Tsai and Lin, 1993), given as

$$\begin{aligned} f_{tmd} = ((&\frac{\sqrt{1+0.5\mu}}{1+\mu} + \frac{1}{\sqrt{1-2\xi^2}} - 1) - (0.288 - 0.661\sqrt{\mu} + 1.12\mu)\sqrt{\mu}\xi \\ &- (2.298 - 6.739\sqrt{\mu} + 8.316\mu)\sqrt{\mu}\xi^2)f, \end{aligned} \tag{A.12}$$

$$\xi_{tmd} = \sqrt{\frac{3\mu}{8(1+\mu)}} + 0.151\xi - 0.187\xi^2 + 0.238\xi\mu.$$

Their results also showed that the higher the system's damping is, the more the optimum parameters deviate from those in undamped systems. In the OC3-Hywind dynamics, there exist high structural damping (above 0.1) for the main translational and rotational modes, thus the solution (A.12) is more appropriate than (A.11) for this optimization problem.

In order to adopt Tsai's method, eigenanalysis based on model linearization result should be performed first to obtain system natural frequencies and damping ratios for the modes of interest. In the FAST linearization process, all the platform translation and rotation DOFs, all tower bending DOFs, drivetrain DOF, and blade flexibility DOFs are enabled. Rotor speed and wind speed are both set as 0. Incident wave and hydro radiation damping effects are disabled. Part of the eigenanalysis result is presented in the following table, which agrees with the data in (Matha, 2010).

Table A.4: Natural frequencies and damping ratios of modes for OC3-Hywind surge-heave-pitch motion

DOF	f (Hz)	ξ
Platform surge	0.0080	0.1364
Platform heave	0.0324	0.0384
Platform pitch	0.0342	0.1418
1st tower fore-aft bending	0.4732	0.0087
2nd tower fore-aft bending	3.7505	0.0102

Among these DOFs for OC3-Hywind surge-heave-pitch motion, the most critical modes that affect system performance are the 1st tower fore-aft bending mode and the low frequency platform pitch mode, which is also the dominant cause of tower bending. Therefore, the natural frequency and damping ratio of these two modes are used here for TMD parameter optimization. Based on formula (A.12), the TMD spring and damping coefficients are determined and listed in Table A.6. It should be noted that the TMD location in platform is not analyzed, and it is intuitively specified as -100m.

However, the nonlinearity of TMD stops due to space constraints is not considered in this design process, which has been shown to have strong influence on TMD load reduction effectiveness according to the nonlinear FAST-SC simulation results. Besides, parametric study of TMD location in platform cannot be performed based on this method. Therefore, a more thorough method should be proposed to find the best combination of TMD parameters.

4.2 Exhaustive Search (ES)

In last section, we have obtained a mathematical model describing OC3-Hywind surge-heave-pitch motion, which manages to capture most of system structural dynamics, hydro and mooring effects. More importantly, the time for solving this dynamic equation is less than 1s, thus exhaustive search, a global parameter tuning method, becomes a possible solution to determine the optimal TMD parameters.

Before presenting the result, the performance indices are introduced which are used in the performance evaluation process. In fact, the fore-aft tower top deflection is the best indicator of tower bottom bending moments, and the author in (Stewart, 2012) used standard deviation of the tower top displacement as the performance index, which is also adopted in this work as the first index J_1. Similarly, the standard deviation of platform pitch angle is another criterion J_2, since platform pitch motion is the source of extra tower fatigue load, and it will also introduce extra loading on the important devices in nacelle such as drivetrain and generator. Secondly, we also care about load reduction effectiveness of the proposed method in extreme events, thus the range of tower top displacement and platform pitch angle in the free decay test are treated as another two evaluation indices J_3 and J_4.

Exhaustive search is performed based on these indices. The parameter searching range and interval are chosen when both time consumption and accuracy are considered. The slice plot for J_1 illustrated in Figure A.9, and the optimization results are listed in Table A.6.

Although exhaustive search could be regarded as a global optimization method, it is still limited by pre-defined parameter searching range and interval. Be-

Table A.5: Performance indices

Index	Description
$J_1 = \sqrt{\frac{1}{T}\int_0^T (x_{tt} - \tilde{x}_{tt})^2 \mathrm{d}t}$	Standard deviation of tower top displacement under its equilibrium point
$J_2 = \sqrt{\frac{1}{T}\int_0^T (\theta_p - \tilde{\theta}_p)^2 \mathrm{d}t}$	Standard deviation of platform pitch angle under its equilibrium point
$J_3 = \max(x_{ttd}) - \min(x_{ttd})$	Maximum range of tower top displacement
$J_4 = \max(\theta_p) - \min(\theta_p)$	Maximum range of platform pitch angle

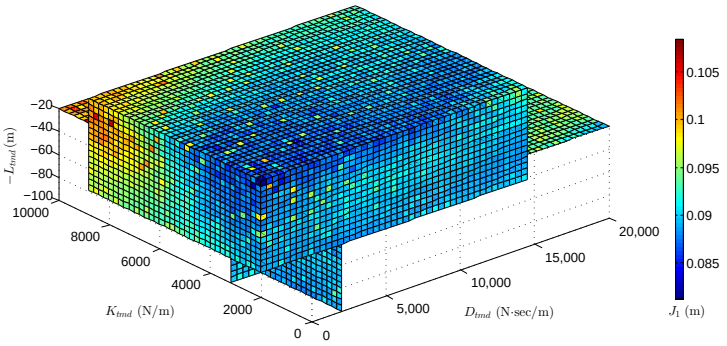

Figure A.9: Slice plot subjected to performance index J_1 with TMD installed in platform.

sides, it is very computationally expensive, which will take hours or days long to finish one optimization process. Moreover, there might exist better solution if the parameter interval is not small enough. Therefore, more intelligent and efficient optimization algorithms are demanded.

4.3 Simplex Coding Genetic Algorithm (SCGA)

In the past few years, genetic algorithm has been widely applied in a broad spectrum of real-world systems (Wang and Ohmori, 2013; Martínez et al., 2014). This approach starts with randomly generated population, and individuals with better fitness will be selected as the basis of next generation. The improved population will keep evolving after inheritance, mutation, selection, and crossover procedures until it meets the final requirement. As a global optimization method, genetic algorithm is based on stochastic variables and does

not require the derivatives of object function, which brings the advantages of global evaluation and objective tolerance when compared with other gradient based local optimization methods. It usually helps to obtain a better result in optimization problems with non-smooth objective functions, thus is suitable for the optimization problem in this paper.

However, the genetic algorithm may still suffer from the slow convergence that brings about high computational cost. Considering this problem, several researchers tried to furnish genetic algorithm with the ability to simulate the fast convergence of local search methods. The simplex coding genetic algorithm (SCGA) proposed by Hedar et al. is adopted in this work for efficient parameter optimization (Hedar and Fukushima, 2003). SCGA combines the genetic algorithm and simplex-based local optimization algorithm called Nelder-Mead method (Kelley, 1999), which is one of the most efficient derivative-free nonlinear optimization approaches. In SCGA, each chromosome in the population is a simplex and the gene is a vertex of this simplex. Nelder-Mead method is applied to improve the population in the initial stage and every intermediate step when new children are generated. Detailed steps of SCGA are not presented here for brevity, while only the values of important parameters are given in the following. In the simplex searching parameters, number of simplices per coordinate direction is set as 5, and maximum number of local iterations is 2. For the GA initialization, probability of the roulette wheel uniform crossover is chosen as 0.6, and the mutation probability 0.01 is used.

Based on the same evaluation indices in Table A.5, the optimization results are shown in Table A.6. Firstly, it can be easily noticed that SCGA gives a better result with respect to J_3, but the exhausted searching range is limited by its searching scope. Secondly, compared with GA, the SCGA searching range is not strictly restricted by the initial lower and upper limits, since the reflection and expansion steps in the simplex searching process will possibly cross the pre-defined bounds. This feature also brings the advantage of wider searching range, where the optimal values may exceed the pre-determined limits in the J_3 case. Thirdly, SCGA is more efficient than GA, which only takes 10 minutes to finish one optimization process.

Table A.6: Parameter optimization result (m_{tmd}=100,000kg)

Method	Performance index	K_{tmd} (N/m)	D_{tmd} (N·s/m)	L_{tmd} (m)
Tsai	Tower bending (Tsai1)	868010	40134	N/A
Tsai	Platform pitch (Tsai2)	4660	3663	N/A
ES	$J_1 = 0.0812$ m	2000	3200	20
ES	$J_2 = 1.2327$ deg	0	6400	20
ES	$J_3 = 0.8880$ m	3000	0	20
ES	$J_4 = 8.8926$ deg	0	14800	20
SCGA	$J_1 = 0.0826$ m	719	3389	20
SCGA	$J_2 = 1.2312$ deg	0	11733	20
SCGA	$J_3 = 0.7600$ m	959526	5733	20
SCGA	$J_4 = 8.8924$ deg	0	14595	20

5 Simulation and Analysis

In this section, based on the optimization result, fully nonlinear simulations are performed in FAST-SC with all wind turbine DOFs enabled. Each test runs 630 seconds, and the output data in first 30s are not recorded, waiting for generator torque and blade pitch motion arriving normal operation state. The modified generator torque and blade pitch controller from NREL is used in the form of a dynamic link library for all tests (Jonkman, 2010).

In total, we consider three different simulation scenarios. The wind and wave conditions in (Lackner and Rotea, 2011b) are adopted as two cases in this experiment. For wind condition, the mean value of the turbulent wind is defined as 10 m/s and 18 m/s, respectively. The wind field is generated by TurbSim (B. and M.L., 2005), where Kaimal spectra and the power law exponent of 0.14 are used according to the IEC61400-3 offshore wind turbine design standard. The normal turbulence intensity is set as level B, i.e. 18% (10 m/s case) and 15%(18 m/s case). For wave condition, JONSWAP spectrum is utilized to generate the stochastic wave inputs. The significant wave height is set as 2.3 m (10 m/s case) and 3.7 m (18 m/s case), and the peak spectral period is both defined as 14s. Besides, the parked case with 50-year extreme wind and wave is also considered. Mean value of the extreme turbulent wind is defined as 37 m/s with 11% intensity and 0.11 power law exponent, and the significant

wave height and wave period are defined as 13.8 m and 19 s. In this case, the generator torque and blade pitch controller is turned off, and all the blades are feathered to 90 degree to minimize the aerodynamic loading. For each case, at least two sets of random variables are used to generate wind and wave data. Percentage of load reduction with different TMD parameter choice is shown in Table A.7. In the cases Tsai1 and Tsai2, TMD is placed near to the top of the spar, i.e. 20m from P, while L_{tmd} is 100m for Tsai1' and Tsai2'. Regarding J_1 to J_4, the better design parameters are chosen when comparing the index values between ES and SCGA in the optimization results. In order to measure the fatigue and extreme loading, damage equivalent load (DEL) and the 95th percentile of fore-aft and side-side tower base bending moments (TwrBsMyt abd TwrBsMxt), flapwise bending moment at the first blade root (RootMyc1) and tension of the first anchor (Anch1Ten) are calculated. Standard deviation (STD) and the 95th percentile of platform pitch and roll rotation angle are also calculated. In above rated situation, the root mean square (RMS) of generated power is considered as another index. Three time series simulation results based on the $J1$ design are shown in Figure A.10-A.12, and our remarks on these data are presented below.

- Firstly, when comparing the results of Tsai1-Tsai2 and Tsai1'-Tsai2', it is interesting to find out that this TMD is more effective when placed at the upper side of the spar instead of the bottom. This agrees with the other optimization results, and it could also be indicated from the fact that most tall buildings have TMDs installed on top floors.

- Secondly, it can be seen that the design of TMD with small spring coefficient ($J1$, $J2$ and $J4$ cases) achieves much load reduction in above rated condition, and the RMS of generated power is even improved by over 40%. Also, the load reduction effectiveness can be clearly noticed from Figure A.11, where the TMD is taking effect when the platform is in resonant motion. Besides, from the other point of view, only a damper is needed for the above rated case to achieve such performance based on the value of optimized parameters.

- Thirdly, with these designs, however, it does not bring much load reduction when the turbine is working below rated in non-resonant motion. This ineffectiveness is due to the constant wind force component acting on the turbine rotor, so that the TMD is leaning on one side most of time (Stewart, 2012), which can be seen from Figure A.10. Besides, in parked condition, the system performance is also worse since external load mainly comes from wave, and the platform pitch frequency is dominated by wave, so that the proposed TMD design loses effect.

- Fourthly, the design with large spring and damping constants ($J3$ case), in contrast, will produce moderate load reduction in all three working conditions, no matter the platform is in resonant motion or not. At this time, the TMD behaves like a high frequency load absorber, working around its original position and never exceeding its motion constraints. Therefore, it will not contribute too much when the wind turbine platform is working above rated or in low frequency resonant motion.

6 Conclusion

This work dealt with the modelling and parameter optimization of a passive structural control design for a spar-type floating wind turbine. Firstly, the coupled surge-heave-pitch dynamic model with a TMD installed in platform was established based on the D'Alembert's principle of inertial forces. Secondly, parameter estimation was performed based on LM algorithm, and the proposed model was verified when comparing its simulation results with the outputs from FAST-SC. Thirdly, different performance indices and parameter optimization methods were adopted for TMD parameter determination. Especially, SCGA provides a more efficient and accurate optimization method compared with the other methods. At last, FAST-SC was used for fully coupled nonlinear simulation with various wind and wave conditions.
The results illustrated that TMD is more effective when placed in the upper side of the spar platform. It was also found that the design of TMD with

Table A.7: Percentage of load reduction with different TMD parameters

Case	Evaluation index	Tsai1	Tsai1'	Tsai2	Tsai2'	J_1	J_2	J_3	J_4
	DEL TwrBsMyt	5.40	-0.28	2.21	-0.35	1.71	1.32	3.30	1.33
	DEL TwrBsMxt	17.59	-0.90	-1.36	-2.16	-2.05	-2.64	18.73	-2.54
	DEL RootMyc1	0.31	-1.32	0.77	-0.01	0.51	0.36	0.56	0.32
	DEL Anch1Ten	5.25	2.75	5.25	2.75	0.51	0.36	0.56	0.32
10m/s	95th TwrBsMyt	1.12	2.57	0.40	1.58	0.27	0.05	0.68	0.05
	95th TwrBsMxt	4.44	1.60	1.33	1.70	0.81	0.33	3.11	0.34
	95th RootMyc1	0.42	0.37	0.47	0.42	0.47	0.51	0.42	0.47
	95th Anch1Ten	4.09	4.07	4.06	4.05	4.06	4.07	4.09	4.07
	95th PtfmPitch	1.92	7.91	0.49	5.46	0.25	0.02	1.96	0.04
	95th PtfmRoll	0.90	2.11	2.74	3.53	2.49	2.11	0.81	2.11
	DEL TwrBsMyt	0.80	0.06	14.26	6.77	13.89	13.24	- 0.38	13.1
	DEL TwrBsMxt	18.70	5.46	-4.76	4.52	-6.88	1.25	9.17	2.93
	DEL RootMyc1	-0.89	4.47	8.05	7.14	7.80	7.28	-0.98	7.29
	DEL Anch1Ten	4.81	1.41	-3.52	2.40	-2.01	-0.97	4.82	-0.97
18m/s	95th TwrBsMyt	-0.78	2.00	12.84	6.54	13.17	12.16	-1.03	11.95
	95th TwrBsMxt	3.82	2.40	1.90	3.61	0.64	3.03	1.54	3.65
	95th RootMyc1	-0.90	-0.61	7.11	2.41	7.56	7.07	-0.75	6.97
	95th Anch1Ten	4.55	4.60	2.96	4.38	3.15	3.39	4.55	3.41
	95th PtfmPitch	-0.38	7.12	18.80	13.78	18.53	17.50	-0.40	17.27
	95th PtfmRoll	-3.64	8.42	13.92	12.60	12.97	12.10	-3.66	12.07
	RMS GenPwr	-8.32	12.63	46.90	37.29	46.47	42.45	-8.29	41.86
	DEL TwrBsMyt	3.73	-2.50	-7.14	-1.98	-7.75	-7.39	2.69	-6.12
	DEL TwrBsMxt	-0.56	0.53	-0.61	0.73	-0.42	-0.49	-0.67	-0.27
	DEL RootMyc1	0.93	-2.51	-8.66	-3.28	-8.41	-5.70	0.45	-4.40
	DEL Anch1Ten	3.29	3.87	3.13	3.38	3.25	3.66	3.14	3.25
37m/s	95th TwrBsMyt	2.27	-3.70	2.42	-2.76	1.21	0.39	3.09	1.26
	95th TwrBsMxt	0.36	1.33	-0.02	1.44	0.15	0.17	0.34	0.47
	95th RootMyc1	1.01	-1.12	-4.73	-1.00	-4.40	-0.62	1.14	-1.57
	95th Anch1Ten	3.67	3.82	3.52	3.67	3.54	3.53	3.66	3.55
	95th PtfmPitch	2.15	-8.16	4.30	-5.23	4.00	2.87	2.17	2.98
	95th PtfmRoll	1.32	6.22	1.22	6.37	1.06	0.59	1.32	0.37

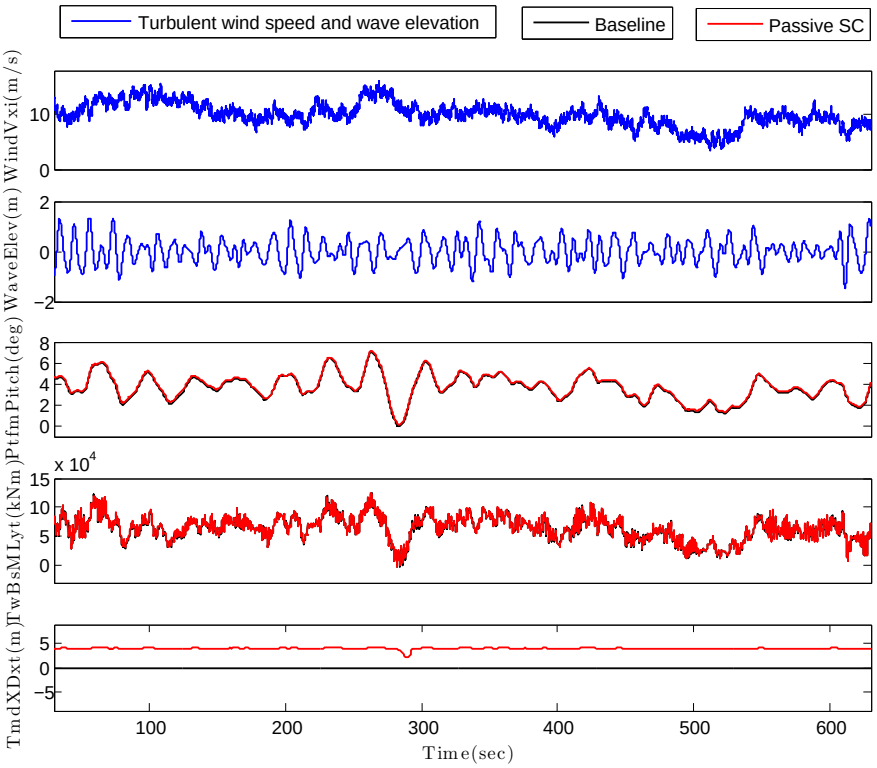

Figure A.10: FAST-SC simulation results with 10m/s turbulent wind and 2.3m wave height.

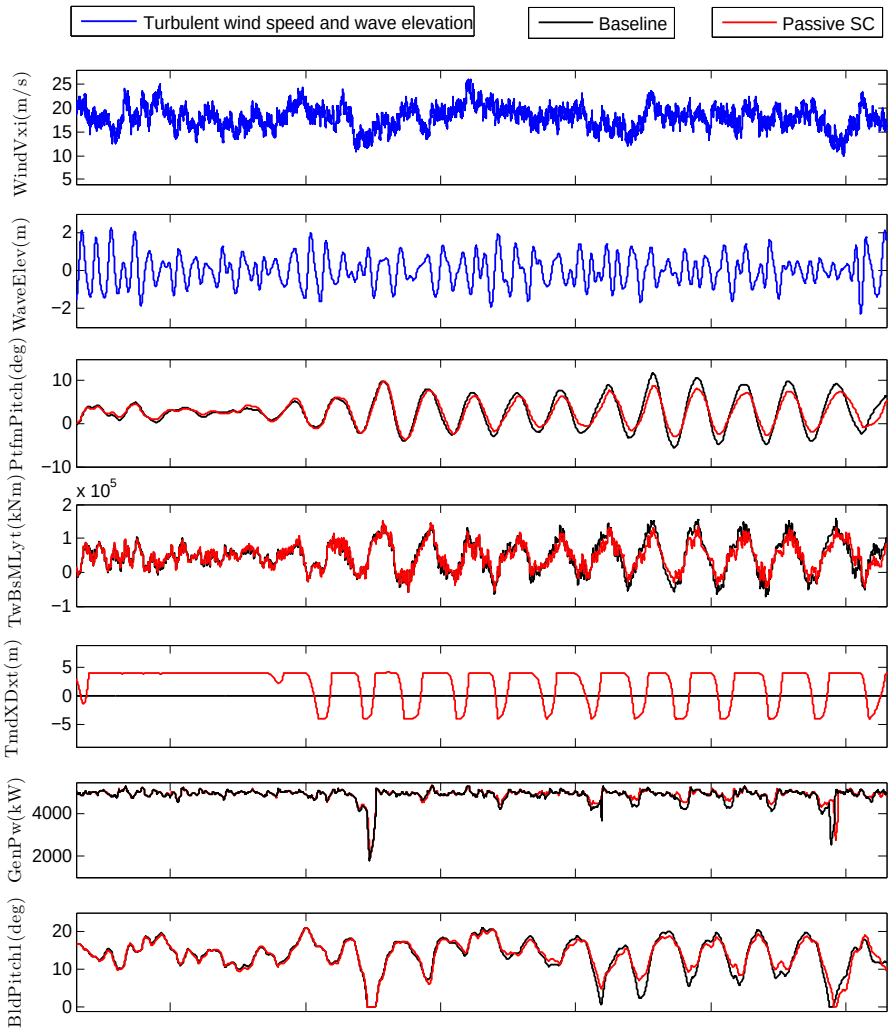

Figure A.11: FAST-SC simulation results with 18m/s turbulent wind and 3.7m wave height.

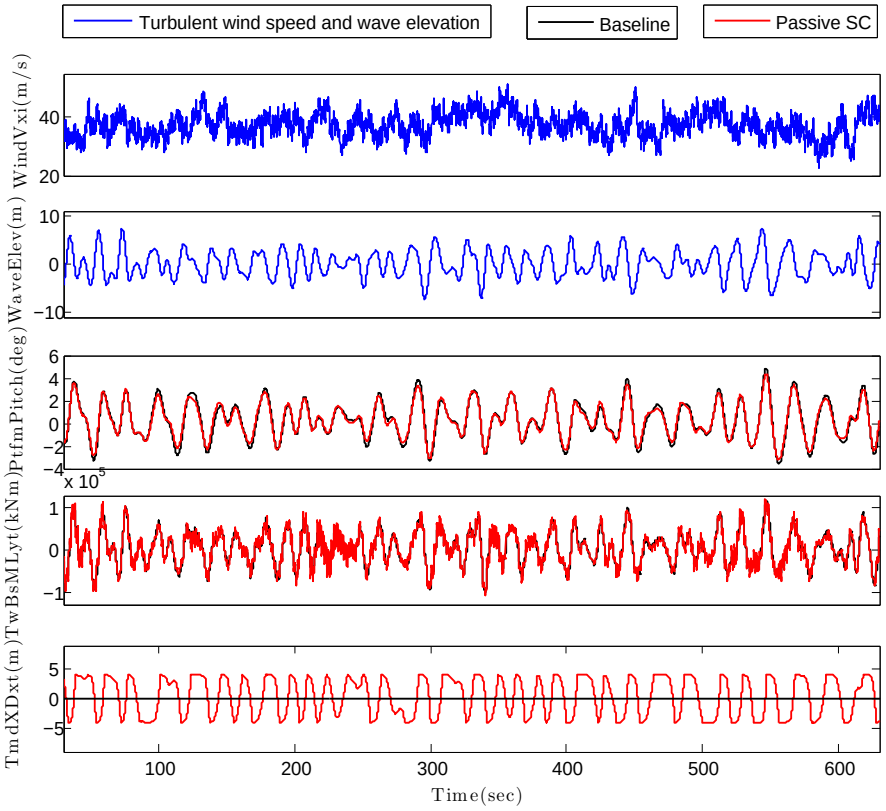

Figure A.12: FAST-SC simulation results with 37m/s 50-year extreme turbulent wind and 13.8m wave height.

small spring coefficients would achieve much load reduction and power quality improvement when the platform is working above rated in resonant motion, but it did not take much effect for the below rated condition, and would even deteriorate the system performance when the turbine was parked in extreme wind and wave condition. In contrast, the design with large spring and damping constants would produce moderate load reduction in both resonant and non-resonant motions.

On direction for future work is to consider the wind loads on the rotor, which might affect the optimization result. Also, semi-active and active structural control design are also worth investigating for this problem.

Appendix

$$
\begin{aligned}
M_{sg}^{sg} &= A_{sg}^{sg} + m_{ptfm} + m_{twr} + m_{rna} + m_{tmd} \\
I_{sg}^{p} &= A_{sg}^{p} + m_{twr}(L_{twr} + L_{jot})\cos\theta_p - m_{ptfm}L_{ptfm}\cos\theta_p - m_{tmd}L_{tmd}\cos\theta_p \\
M_{sg}^{tmd} = M_{tmd}^{sg} &= m_{tmd}\cos\theta_p \\
I_{sg}^{t} &= m_{rna}(L_{rna} + L_{jot})\cos\theta_t \\
M_{hv}^{hv} &= A_{hv}^{hv} + m_{ptfm} + m_{twr} + m_{rna} + m_{tmd} \\
I_{hv}^{p} &= -m_{twr}(L_{twr} + L_{jot})\sin\theta_p + m_{ptfm}L_{ptfm}\sin\theta_p + m_{tmd}L_{tmd}\sin\theta_p \\
M_{hv}^{tmd} = M_{tmd}^{hv} &= -m_{tmd}\sin\theta_p \\
I_{hv}^{t} &= -m_{rna}(L_{rna} + L_{jot})\sin\theta_t \\
M_{p}^{sg} &= A_{p}^{sg} + m_{rna}(L_{rna} + L_{jot})\cos\theta_t + m_{twr}(L_{twr} + L_{jot})\cos\theta_p \\
&\quad - m_{ptfm}L_{ptfm}\cos\theta_p - m_{tmd}L_{tmd}\cos\theta_p \\
M_{p}^{hv} &= -m_{rna}(L_{rna} + L_{jot})\sin\theta_t - m_{twr}(L_{twr} + L_{jot})\sin\theta_p \\
&\quad + m_{ptfm}L_{ptfm}\sin\theta_p + m_{tmd}L_{tmd}\sin\theta_p \\
I_{p}^{p} &= A_{p}^{p} + J_{ptfm}^{CG_{ptfm}} + m_{ptfm}{L_{ptfm}}^2 + J_{twr}^{CG_{twr}} \\
&\quad + m_{twr}(L_{twr} + L_{jot})^2 + m_{rna}(L_{rna} + L_{jot})^2 + m_{tmd}L_{tmd}^2 \\
M_{tmd}^{p} = I_{p}^{tmd} &= -m_{tmd}L_{tmd} \\
M_{tmd}^{tmd} &= m_{tmd} \\
M_{t}^{tmd} = I_{tmd}^{t} &= 0 \\
M_{t}^{sg} &= m_{rna}L_{rna}\cos\theta_t + m_{twr}L_{twr}\cos\theta_p \\
M_{t}^{hv} &= -m_{rna}L_{rna}\sin\theta_t - m_{twr}L_{twr}\sin\theta_p \\
F_{hv}^{gr} &= -(m_{ptfm} + m_{twr} + m_{rna} + m_{tmd})g \\
\tau_{p}^{gr} &= m_{rna}g(L_{rna} + L_{jot})\sin\theta_t + m_{twr}g(L_{twr} + L_{jot})\sin\theta_p \\
&\quad - m_{ptfm}gL_{ptfm}\sin\theta_p - m_{rna}gL_{d}\cos\theta_t \\
&\quad + m_{tmd}gx_{tmd}\cos\theta_p - m_{tmd}gL_{tmd}\sin\theta_p \\
F_{tmd}^{gr} &= m_{tmd}g\sin\theta_p \\
\tau_{t}^{gr} &= m_{twr}gL_{twr}\sin\theta_p + m_{rna}gL_{rna}\sin\theta_t - m_{rna}gL_{d}\cos\theta_t \\
F_{sg}^{hdr.moor} &= -D_{sg}^{sg}\dot{x}_{sg} - \hat{D}_{sg}^{sg}\dot{x}_{sg}^2 - K_{sg}^{sg}x_{sg} - D_{sg}^{p}\dot{\theta}_p - K_{sg}^{p}\theta_p \\
F_{hv}^{hdr.moor} &= -D_{hv}^{hv}\dot{x}_{hv} - K_{hv}^{hv}x_{hv} - F_{moor} + F_{buoy} - K_{hv}^{p.sg}(x_{sg} - L_{moor}\sin\theta_p)^2 \\
\tau_{p}^{hdr.moor} &= -D_{p}^{p}\dot{\theta}_p - K_{p}^{p}\theta_p - D_{p}^{sg}\dot{x}_{sg} - \hat{D}_{p}^{sg}\dot{x}_{sg}^2 - K_{p}^{sg}x_{sg}
\end{aligned}
$$

$$
\begin{aligned}
F_{sg}^{ctr} &= m_{twr}\dot{\theta}_p^2(L_{twr}+L_{jot})\sin\theta_p + m_{rna}\dot{\theta}_t^2(L_{rna}+L_{jot})\sin\theta_t \\
&\quad - m_{ptfm}\dot{\theta}_p^2 L_{ptfm}\sin\theta_p - m_{tmd}\dot{\theta}_p(\dot{\theta}_p L_{tmd} - \dot{x}_{tmd})\sin\theta_p \\
F_{hv}^{ctr} &= m_{twr}\dot{\theta}_p^2(L_{twr}+L_{jot})\cos\theta_p + m_{rna}\dot{\theta}_t^2(L_{rna}+L_{jot})\cos\theta_t \\
&\quad - m_{ptfm}\dot{\theta}_p^2 L_{ptfm}\cos\theta_p - m_{tmd}\dot{\theta}_p(\dot{\theta}_p L_{tmd} - \dot{x}_{tmd})\cos\theta_p \\
\tau_p^{ctr} &= m_{tmd}\dot{\theta}_p(\dot{\theta}_p L_{tmd} - \dot{x}_{tmd})x_{tmd} \\
\tau_t^{ctr} &= 0 \\
F_{tmd}^{spr.damp} &= -D_{tmd}\dot{x}_{tmd} - K_{tmd}x_{tmd} \\
\tau_t^{p} &= D_t(\dot{\theta}_t - \dot{\theta}_p) + K_t(\theta_t - \theta_p)
\end{aligned}
$$

Acknowledgment

This work has been (partially) funded by Norwegian Centre for Offshore Wind Energy (NORCOWE) under grant 193821/S60 from Research Council of Norway (RCN). NORCOWE is a consortium with partners from industry and science, hosted by Christian Michelsen Research.
The authors would like to give sincere thanks to Dr. Lackner in University of Massachusetts Amherst for his generosity on the FAST-SC code sharing and Dr. Jonkman from National Renewable Energy Laboratory for his enthusiastic help and support with the specifications of OC3-Hywind model.

REFERENCES

Archer, C. and Jacobson, M. (2005). Evaluation of global wind power. *Journal of Geophysical Research*, 110:D12110.

B., J. and M.L., B. (2005). Turbsim users guide. Technical report, NREL/EL-500-36970. Golden, Colorado: National Renewable Energy Laboratory.

Butterfield, S., Musial, W., Jonkman, J., Sclavounos, P., and Wayman, L. (2005). Engineering challenges for floating offshore wind turbines. In *Copenhagen Offshore Wind 2005 Conference and Expedition Proceedings, 26–28 October 2005, Copenhagen, Denmark*.

Colwell, S. and Basu, B. (2009). Tuned liquid column dampers in offshore wind turbines for structural control. *Engineering Structures*, 31(2):358–368.

Connor, J. J. and Connor, J. (2003). *Introduction to structural motion control*. Prentice Hall Pearson Education.

Den Hartog, J. P. (1985). *Mechanical vibrations*. Dover publications.

Gavin, H. (2011). The levenberg-marquardt method for nonlinear least squares curve-fitting problems. Technical report, Duke University.

Hedar, A. R. and Fukushima, M. (2003). Minimizing multimodal functions by simplex coding genetic algorithm. *Optimization Methods and Software*, 18(3):265–282.

Jonkman, J. (2007). *Dynamics modeling and loads analysis of an offshore floating wind turbine*. PhD thesis, Department of Aerospace Engineering Sciences, University of Colorado.

Jonkman, J. (2008). Influence of control on the pitch damping of a floating wind turbine. In *2008 ASME Wind Energy Symposium. Reno, Nevada. January 7-10*. National Renewable Energy Laboratory.

Jonkman, J. (2009). Dynamics of offshore floating wind turbines - model development and verification. *Wind Energy*, 12(5):459–492.

Jonkman, J. (2010). Definition of the floating system for phase IV of OC3. *NREL/TP-500-38060. Golden, Colorado: National Renewable Energy Laboratory.*

Jonkman, J. and Buhl Jr, M. (2005). FAST users guide. Technical report, NREL/EL-500-29798. Golden, Colorado: National Renewable Energy Laboratory.

Jonkman, J., Butterfield, S., Musial, W., and Scott, G. (2009). Definition of a 5-MW reference wind turbine for offshore system development. Technical report, NREL/TP-500-47535. Golden, Colorado: National Renewable Energy Laboratory.

Jonkman, J. and Matha, D. (2009). A quantitative comparison of the responses of three floating platform concepts. In *European Offshore Wind 2009 Conference & Exhibition*, pages 14–16.

Kaldellis, J. K. and Kapsali, M. (2013). Shifting towards offshore wind energy - recent activity and future development. *Energy Policy*, 53:136–148.

Kane, T. R. and Levinson, D. A. (1985). *Dynamics, theory and applications.* McGraw Hill.

Kelley, C. (1999). *Iterative Methods for Optimization.* Frontiers in Applied Mathematics, Society for Industrial and Applied Mathematics.

Korkmaz, S. (2011). A review of active structural control: challenges for engineering informatics. *Computers & Structures*, 89:2113–2132.

Lackner, M. A. and Rotea, M. A. (2011a). Passive structural control of offshore wind turbines. *Wind Energy*, 14(3):373–388.

Lackner, M. A. and Rotea, M. A. (2011b). Structural control of floating wind turbines. *Mechatronics*, 21(4):704–719.

Lanczos, C. (1986). *The variational principles of mechanics.* Dover Publications.

Larsen, T. J. and Hanson, T. D. (2007). A method to avoid negative damped low frequent tower vibrations for a floating, pitch controlled wind turbine. *Journal of Physics: Conference Series*, 75(1):012073.

Li, J., Zhang, Z., and Chen, J. (2012). Experimental study on vibration control of offshore wind turbines using a ball vibration absorber. *Energy and Power Engineering*, 4(3):153–157.

Martínez, C. A., Curadelli, O., and Compagnoni, M. E. (2014). Optimal placement of nonlinear hysteretic dampers on planar structures under seismic excitation. *Engineering Structures*, 65:89 – 98.

Matha, D. (2010). Model development and loads analysis of an offshore wind turbine on a tension leg platform with a comparison to other floating turbine concepts. Technical report, NREL/SR-500-45891. National Renewable Energy Laboratory (NREL), Golden, CO.

Mensah, A. and Dueñas-Osorio, L. (2012). Reliability analysis of wind turbines equipped with tuned liquid column dampers (TLCD). In *Structures Congress*, pages 1190–1200.

More, J. (1978). The levenberg-marquardt algorithm: implementation and theory. *Numerical Analysis*, pages 105–116.

Murtagh, P. J., Ghosh, A., Basu, B., and Broderick, B. M. (2008). Passive control of wind turbine vibrations including blade/tower interaction and rotationally sampled turbulence. *Wind Energy*, 11(4):305–317.

Musial, W., Butterfield, S., and Ram, B. (2006). Energy from offshore wind. In *Offshore Technology Conference*, pages 1888–1898.

Namik, H. and Stol, K. (2010). Individual blade pitch control of floating offshore wind turbines. *Wind Energy*, 13(1):74–85.

Namik, H. and Stol, K. (2011). Performance analysis of individual blade pitch control of offshore wind turbines on two floating platforms. *Mechatronics*, 21(4):691–703.

Rao, S. and Durgaiah, R. (2005). *Engineering Mechanics*. Universities Press, India.

Roddier, D., Cermelli, C., Aubault, A., and Weinstein, A. (2010). Windfloat: A floating foundation for offshore wind turbines. *Journal of Renewable and Sustainable Energy*, 2(3):033104.

Sarpkaya, T. (1986). Forces on a circular cylinder in viscous oscillatory flow at low keulegan-carpenter numbers. *Journal of Fluid Mechanics*, 165(61-71):11–15.

Shawash, J. and Selviah, D. (2013). Real-time nonlinear parameter estimation using the levenberg-marquardt algorithm on field programmable gate arrays. *IEEE Transactions on Industrial Electronics*, 60(1):170–176.

Skaare, B., Hanson, T., and Nielsen, F. (2007). Importance of control strategies on fatigue life of floating wind turbines. In *Proceedings of the 26th International Conference on Offshore Mechanics and Arctic Engineering*. ASME.

Stewart, G. (2012). Load reduction of floating wind turbines using tuned mass dampers.

Stewart, G. and Lackner, M. (2013). Offshore wind turbine load reduction employing optimal passive tuned mass damping systems. *IEEE Transactions on Control Systems Technology*, 21(4):1090–1104.

Stewart, G. M. and Lackner, M. A. (2011). The effect of actuator dynamics on active structural control of offshore wind turbines. *Engineering Structures*, 33(5):1807–1816.

Tsai, H.-C. and Lin, G.-C. (1993). Optimum tuned-mass dampers for minimizing steady-state response of support-excited and damped systems. *Earthquake Engineering & Structural Dynamics*, 22(11):957–973.

Wang, H. and Ohmori, H. (2013). Elasto-plastic analysis based truss optimization using genetic algorithm. *Engineering Structures*, 50:1–12.

PAPER B

MODELLING AND PARAMETER ANALYSIS OF THE OC3-HYWIND FLOATING WIND TURBINE WITH A TUNED MASS DAMPER IN NACELLE

Yulin Si, Hamid Reza Karimi and Huijun Gao

This paper has been published as:

Y. Si, H. R. Karimi, and H. Gao, "Modelling and parameter analysis of the OC3-Hywind floating wind turbine with a tuned mass damper in nacelle", *Journal of Applied Mathematics*, vol. 2013, Article ID 679071, 10 pages, 2013.

Modelling and Parameter Analysis of the OC3-Hywind Floating Wind Turbine with a Tuned Mass Damper in Nacelle

Yulin Si, Hamid Reza Karimi and Huijun Gao
*Department of Engineering
Faculty of Engineering and Science, University of Agder
Jon Lilletunsvei 9, 4879 Grimstad, Norway.
**Research Institute of Intelligent Control and Systems,
Harbin Institute of Technology, Harbin, 150001, China

Abstract **— Floating wind turbine will suffer from more fatigue and ultimate loads compared with fixed bottom installation due to its floating foundation, while structural control offers a possible solution for direct load reduction. This paper deals with the modelling and parameter tuning of a spar type floating wind turbine with a tuned mass damper (TMD) installed in nacelle. First of all, a mathematical model for the platform surge-heave-pitch motion and TMD-nacelle interaction is established based on the D'Alembert's principle. Both intrinsic dynamics and external hydro and mooring effects are captured in the model, while tower flexibility is also featured. Then, different parameter tuning methods are adopted to determine the TMD parameters for effective load reduction. Finally, fully coupled nonlinear wind turbine simulations with different designs are conducted in different wind and wave conditions. The results demonstrate that the design of TMD with small spring and damping coefficients will achieve much load reduction in above rated condition. However, it will deteriorate system performance when the turbine is working below rated or parked. In contrast, the design with large spring and damping constants will produce moderate load reduction in all working conditions.**

Keywords — OC3-Hywind; Floating wind turbine; TMD; Modelling; Parameter analysis; FAST-SC

1 Introduction

With less space constraints and more consistent wind, offshore deep sea wind energy has attracted great worldwide attention in recent years. Wind turbines in deep water are usually installed at places where sea depth is between 60m and 900m, thus floating foundations are generally considered to be an economical and feasible way of deployment (Jonkman, 2007). Based on decades of experience from offshore oil and gas industry, several different traditional floating platforms have been proposed to support large wind turbines in deep sea regions, including spar-buoy, tension leg, barge, and semi-submersible (Jonkman, 2009). One of the most promising concepts is the spar-type supporting structure, based on which one Norwegian company Statoil has developed the world first experimental large floating offshore wind turbine in 2009.

Different from fixed-bottom wind turbines, the very first challenge for floating windmills is the wave and wind induced platform tilt motion, which will heavily increase the loads on turbine structure due to high inertial and gravitational forces (Butterfield et al., 2005). According to (Jonkman and Matha, 2009), when comparing a barge type floating wind turbine with an onshore design, the sea-to-land ratio of fatigue loads with respect to tower base bending moments has reached 7. The ratio is still over 1.5 for the OC3-Hywind spar, which may require extra reinforcement or advanced control technique to improve wind turbine reliability. Besides, soft foundation properties of floating wind turbines will lead to low natural frequency platform motion, so that commonly used blade pitch control strategy for fixed-bottom wind turbines may cause negative damping of tower bending and even large platform resonant motion (Larsen and Hanson, 2007). These problems have drawn a lot of attention from researchers on improving the system design and control strategy of floating wind turbines for load reduction.

One approach for vibration inhibition is to utilize structural vibration control

devices. This method has been successfully applied in civil engineering structures (Korkmaz, 2011), such as buildings and bridges, thus is also expected to be a promising solution for extending the fatigue life of floating wind turbines. In (Murtagh et al., 2008), Murtagh et al. investigated the use of a tuned mass damper (TMD) placed at the tower top for the vibration mitigation due to the along-wind forced vibration response of a simplified wind turbine. Following the same installation idea, Colwell et al. explored the structural responses of fixed-bottom offshore wind turbines with tuned liquid column dampers (TLCD) to control the vibrations (Colwell and Basu, 2009). Moreover, Li et al. performed an experimental study on an offshore wind turbines with a ball vibration absorber fixed on top of the nacelle (Li et al., 2012). However, these discussions are about vibration mitigation of fixed-bottom wind turbines, while their dynamics are quite different from that of floating ones. Besides, these works are not based on the cutting edge high-fidelity codes for wind turbine simulations, which can not capture the comprehensive coupled nonlinear dynamics of wind turbines.

FAST (fatigue, aerodynamics, structures, and turbulence) is one of the state-of-the-art aero-hydro-servo-elastic wind turbine numerical simulators (Jonkman and Buhl Jr, 2005). Based on FAST, Lackner et al. implemented a new simulation tool, called FAST-SC, for passive, semi-active, and active structural control design of wind turbines (Lackner and Rotea, 2011a). Utilizing this code, Lackner et al. presented more realistic simulation results with a TMD installed in the nacelle of either a barge-type or a monopile supported wind turbine, and a simple parametric study was also performed to determine the optimal TMD parameters (Lackner and Rotea, 2011a). Further, it was shown that more load reduction could be achieved when introducing active structural control in their following works (Lackner and Rotea, 2011b; Stewart and Lackner, 2011). In order to perform a more comprehensive parametric study of passive structural control design, the authors in (Stewart, 2012; Stewart and Lackner, 2012) established a 3-DOF dynamic model for different types of floating wind turbines based on first principles. This limited DOF model has greatly facilitated the parameter analysis and active control design, while the

coupling between surge and pitch motion, however, was not captured, which can be ignored for the barge design but might be an important mode for other platforms, such as spar (Jonkman, 2010; Namik and Stol, 2011).

Motivated by the above mentioned problems and research potentials, this work focuses on modelling and parameter analysis of a passive structural control design for a spar-type floating wind turbine. The remainder of this paper is organized as follows. Section 2 introduces the OC3-Hywind floating wind turbine, and the coupled surge-heave-pitch dynamic model with a TMD installed in nacelle is established. Parameter estimation is also performed for model validation. In Section 3, different parameter tuning methods and performance indices are used for TMD parameter determination. Section 4 presents the nonlinear simulation results under different wind and wave conditions. Advantages and limitations of this design with different TMD parameters are also analyzed. At last, we draw conclusions in Section 5.

2 Dynamic Modelling

In cooperation with Statoil, Jonkman from NREL has specified a detailed OC3-Hywind spar-type floating wind turbine model, which is a combination of the data for the 5MW baseline wind turbine from NREL and the Hywind floating platform from Statoil (Jonkman, 2010; Jonkman et al., 2009). Properties of the OC3-Hywind model are shown in Table B.1. According to (Jonkman, 2010), in order to avoid resonant platform pitch motion, the conventional controller in Region 3 is modified into a combination of gain reduced gain-scheduled proportional-integral (GSPI) collective blade pitch control and constant torque control, which is used all through this work as the baseline.

The passive structural control strategy in this work is to install one TMD in the nacelle, which is assumed to move on an ideal non-friction linear track along the fore-aft direction. The stiffness and damping parameters of TMD can be tuned, and they are regarded as constant in all simulations. In order to investigate these parameters, optimize system performance, or design an active controller, establishing one dynamic mathematical model is usually helpful. Figure B.1

Table B.1: Properties of the OC3-Hywind model. (Jonkman, 2010; Jonkman et al., 2009)

Item	Value
Rating	5 MW
Rotor configuration	Upwind, 3 blades
Cut-in, rated, cut-out wind speed	3 m/s, 11.4 m/s, 25 m/s
Total draft below sea water level (SWL)	120 m
Tower base above SWL	10m
Hub height above SWL	90m
Nacelle dimension (length, width, height)	14.2m, 2.3m, 3.5m
Platform diameter above taper	6.5m
Platform diameter below taper	9.4m
Rotor nacelle assembly (RNA) mass	350,000kg
Tower mass	249,718 kg
Platform mass	7,466,000 kg
Number of mooring lines	3
Depth to fairleads below SWL	70m
Baseline control in Region 3	GSPI and constant torque

shows a diagram of the OC3-Hywind surge-heave-pitch motion with tower fore-aft bending and the TMD-nacelle interaction. Definition of each term in this figure can be found in Table B.2. Before presenting the dynamic model, the following premises and assumptions need to be listed.

1. OC3-Hywind is treated as a multi-body dynamic system, and the motion of reference point P is chosen for output analysis, which is in accordance with the definition in (Jonkman, 2010). Rigid bodies in the model include the spar platform, tower and rotor nacelle assembly (RNA). Dynamics in rotor, generator, and gearbox are not considered in this work.

2. Based on the same assumption, the tower fore-aft flexibility is represented as that in (Stewart and Lackner, 2011), where the tower, for simplicity, is treated as a linear rigid rotating beam hinged at tower bottom. It is also assumed that the spring and damping coefficients of this hinge are constant.

3. In total, the model has five DOFs, i.e. platform surge, heave, pitch, tower

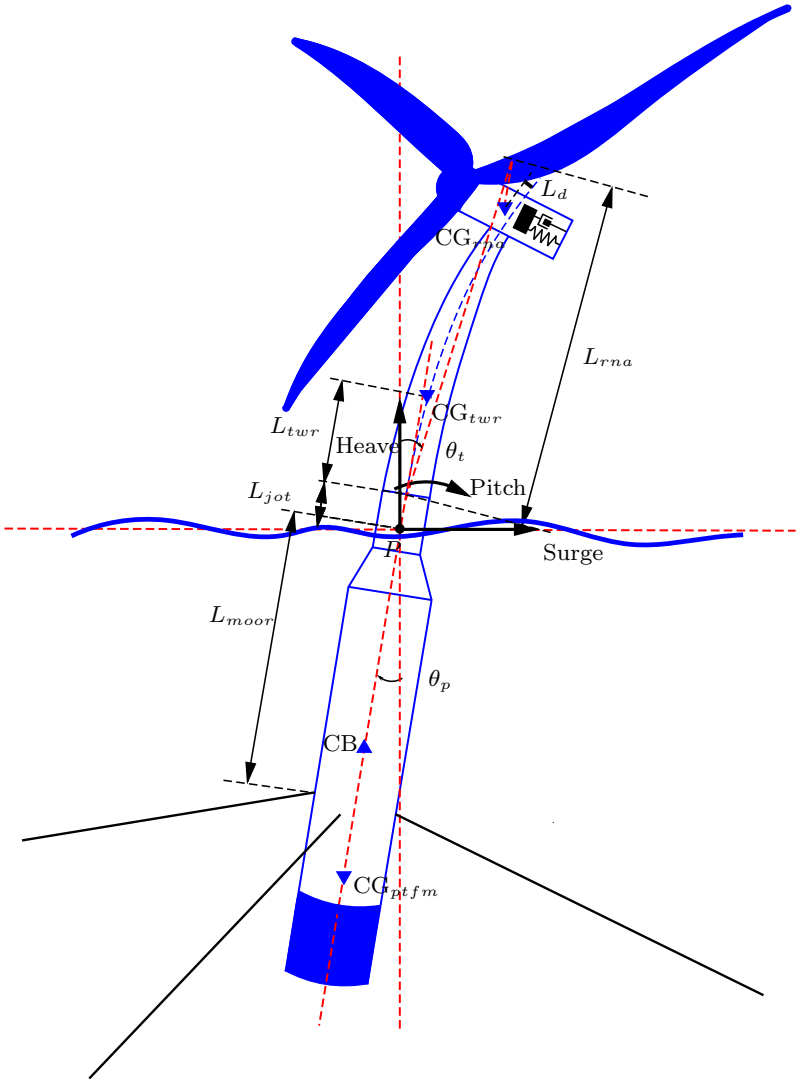

Figure B.1: Diagram of the OC3-Hywind surge-pitch-heave motion with tower fore-aft flexibility and passive structural control

fore-aft bending, and TMD motion. The other DOFs, such as rotor yaw motion and generator rotation, are not included.

4. This model focuses on the system intrinsic coupled dynamics with hydro and mooring loads, while the loads from winds and incident waves have not yet been considered in the modelling process.

Based on the above descriptions, we treat the overall system dynamics as the

motion of a rigid body with distributed mass particles in the surge-heave-pitch plane, which can be seen as the sum of a translation and a rotation about the axis passing trough P and perpendicular to this plane (Rao and Durgaiah, 2005). According to D'Alembert's principle of inertial forces, the following static equilibrium equations for system translation and rotation about the reference point P

$$\begin{aligned} \mathbf{F} - \sum m_i \mathbf{a}_i = 0, \\ \boldsymbol{\tau} - \sum \mathbf{r}_i \times m_i \mathbf{a}_i = 0, \end{aligned} \tag{B.1}$$

hold. $\mathbf{F}$ and $\boldsymbol{\tau}$ denote vectors of external forces and moments about P, while $-\sum m_i \mathbf{a}_i$ and $-\sum \mathbf{r}_i \times m_i \mathbf{a}_i$ are vector sums of inertial forces and torques about P. m_i is the mass of particle i, i.e. platform, tower, RNA and TMD, and $\mathbf{r}_i$ represents the position vector from P to particle i. $\mathbf{a}_i$ is the acceleration vector for mass particle i, and it consists of the translational acceleration, normal and tangential rotational acceleration components.

When considering the tower translation and rotation about tower bottom, the motion of tower fore-aft bending can be described as

$$\sum (\mathbf{r}_i \times m_i \mathbf{a}_i) + I_t^t \boldsymbol{\alpha}_t = \boldsymbol{\tau}_t^{gr} + \boldsymbol{\tau}_t^p, \tag{B.2}$$

which is also based on D'Alembert's principle. m_i denotes the mass of tower, RNA, and TMD. I_t^t is the equivalent moment of inertia for tower and RNA about tower bottom, and $\boldsymbol{\alpha}_t$ denotes the angular acceleration vector of tower pitch motion. $\boldsymbol{\tau}_t^p$ is the torque vector due to the spring-damping effect between tower and platform. To be consistent with the output of FAST simulator, the tower top displacement is also calculated, which is given by

$$x_t = \sin(\theta_t - \theta_p) l_{twr}, \tag{B.3}$$

where l_{twr} is the length of flexible tower. However, in the system validation process, one problem is found that there will exist huge misalignment between the responses of FAST-SC and established model when the spring and damping coefficients of TMD are in small scale. This is mainly due to the inaccuracy of nacelle rotation angle when flexible tower is modeled as a rigid rotating beam.

When TMD has tiny spring and damping constants, its acceleration will be mainly contributed by gravity, so that inaccuracy of θ_t will lead to tremendous difference of TMD dynamics. Therefore, the nacelle rotation angle should be calibrated in order to produce more convincing dynamic responses. In FAST, the tower flexibility is depicted by the pre-defined mode shapes Φ, where tower top rotation angle is determined by the product of tower top mode shape slope $\frac{\partial \Phi(h)_{rna}}{\partial h}$ and tower top displacement x_t. Following similar calculation procedure, the diagram for tower top rotation calibration is illustrated in Figure B.2, and the calibrated nacelle rotation angle $\tilde{\theta}_t$ satisfies

$$\tilde{\theta}_t = \left.\frac{\partial \Phi(h)}{\partial h}\right|_{h=L_{rna}} x_{tmd} + \theta_p. \tag{B.4}$$

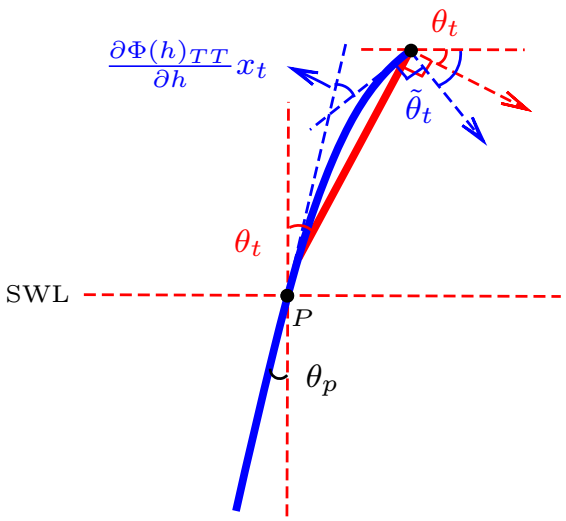

Figure B.2: Diagram for calibration of nacelle rotation angle.

Next, the hydrodynamic loads are characterized. When formulating the motion of object submerged in water, we must also consider the added mass effect, resulting from its surrounding fluid (Newman, 1977). It is summarized in (Jonkman, 2007) that the hydrodynamic loads mainly include contributions from hydrostatics (from water-plane area and buoyancy), radiation (from outgoing waves generated by platform motion), and diffraction (from incident waves). In accordance with this analysis, the hydrodynamic load calculation

in this work follows a similar path. Firstly, hydrostatic load in this model consists of buoyancy force and restoring load resulting from the effects of water-plane area and buoyancy, and the restoring force and moment are set to be constantly proportional to platform displacement and tilt angle which have been specified in (Jonkman, 2010). Secondly, the radiation loads can be represented by nonlinear vicious drag, hydrodynamic radiation damping and the above mentioned added-mass effects. Thirdly, incident wave loads are not considered here since wind turbine is supposed to be located in still water in design process.

Regarding the mooring system, FAST simulator uses a quasi-static model to calculate the load of an individual mooring line, which exhibits nonlinear behaviors due to both mooring dynamics and the asymmetry of the three-point mooring system. In the simulations of this work, the platform displacement and tilt angle are usually not in big scale where the mooring system load-displacement relationship does not show strong nonlinearities in surge and pitch modes, so that we still choose the simple linear model to represent this effect.

In sum, except for added mass, the hydrodynamic loads and mooring effect are modeled as

$$\begin{aligned} F_{sg}^{hdr.moor} &= -D_{sg}^{sg}\dot{x}_{sg} - \hat{D}_{sg}^{sg}\dot{x}_{sg}^2 - K_{sg}^{sg}x_{sg} - D_{sg}^{p}\dot{\theta}_p - K_{sg}^{p}\theta_p, \\ F_{hv}^{hdr.moor} &= -D_{hv}^{hv}\dot{x}_{hv} - K_{hv}^{hv}x_{hv} - F_{moor}^{0} + F_{buoy}^{0} - K_{hv}^{p.sg}(x_{sg} - L_{moor}\sin\theta_p)^2, \\ \tau_{p}^{hdr.moor} &= -D_{p}^{p}\dot{\theta}_p - K_{p}^{p}\theta_p - D_{p}^{sg}\dot{x}_{sg} - \hat{D}_{p}^{sg}\dot{x}_{sg}^2 - K_{p}^{sg}x_{sg}. \end{aligned} \tag{B.5}$$

D_i^j, $\hat{D}_i^j$ and K_i^j denote equivalent damping and spring coefficients for DOF i with regard to DOF j for the calculation of hydro and mooring effects. F_{moor}^0 and F_{buoy}^0 represent initial mooring line and buoyancy forces when there are no platform displacement or rotation. It should be noted that the mooring load for platform heave motion shows strong nonlinear relationship with the surge and pitch modes, thus it is not simplified.

Based on the above analysis and equations, the nonlinear dynamic model of OC3-Hywind surge-heave-pitch motion can be established in the following im-

plicit form

$$\begin{bmatrix} M_{sg}^{sg} & 0 & I_{sg}^{p} & M_{sg}^{tmd} & I_{sg}^{t} \\ 0 & M_{hv}^{hv} & I_{hv}^{p} & M_{hv}^{tmd} & I_{hv}^{t} \\ M_{p}^{sg} & M_{p}^{hv} & I_{p}^{p} & M_{p}^{tmd} & 0 \\ M_{tmd}^{sg} & M_{tmd}^{hv} & I_{tmd}^{p} & M_{tmd}^{tmd} & I_{tmd}^{t} \\ M_{t}^{sg} & M_{t}^{hv} & 0 & M_{t}^{tmd} & I_{t}^{t} \end{bmatrix} \begin{bmatrix} \ddot{x}_{sg} \\ \ddot{x}_{hv} \\ \ddot{\theta}_{p} \\ \ddot{x}_{tmd} \\ \ddot{\theta}_{t} \end{bmatrix} = \begin{bmatrix} F_{sg}^{hdr.moor} + F_{sg}^{ctr} \\ F_{hv}^{gr} + F_{hv}^{hdr.moor} + F_{hv}^{ctr} \\ \tau_{p}^{gr} + \tau_{p}^{hdr.moor} + \tau_{p}^{ctr} \\ F_{tmd}^{gr} + F_{tmd}^{spr.damp} \\ \tau_{t}^{gr} + \tau_{t}^{p} + \tau_{t}^{ctr} \end{bmatrix}. \tag{B.6}$$

In this model, *sg*, *hv*, *p*, *tmd*, *t* represent, respectively, the enabled 5 DOFs, i.e. platform surge, heave, pitch motion about P, TMD translation, and tower rotation. On the left side, M_i^j and I_i^j denote generalized mass and generalized inertial tensor for DOF i with regard to DOF j. On the right side, *gr*, *hdr*, *moor*, *ctr*, *spr* and *damp* describe gravitational, hydro, centripetal, spring and damping effects in forces and moments. Expanded expressions of this model for TMD platform installation is presented in Appendix, and the detailed term descriptions are listed in Table B.2.

The mass matrix on the left side of (B.6) exhibits the system inertial property, i.e mass and inertia tensor, and it also includes hydro added mass and acceleration coupling terms. The terms on the right side of (B.6) are external loads, which can be classified into several different effects. Gravitational forces and moments are the first type of loads, labeled as *gr*. The second effect, labeled as *hdr.moor*, is the hydrodynamic and mooring loading, which consists of hydrostatics, vicious drag, radiation damping, additional linear damping, and mooring effects. The third type, which is produced by D'Alembert's principle, is the centripetal forces and moments originated from the rotation of platform, tower and TMD about the reference point P, and they are labeled as *ctr*. Tower and platform interaction is the fourth effect captured in this equation, and the bending moment is described by a linear spring-damper between them. The final consideration is the spring and damping effect in TMD, so it is labeled as *spr.damp*.

After obtaining the OC3-Hywind dynamic model for its surge-heave-pitch motion in still water, parameter identification and validation should be performed to quantize the unknown parameters and verify the correctness of the proposed model. The parameter estimation is accomplished by minimizing the output

Table B.2: Term descriptions in the model of OC3-Hywind surge-heave-pitch motion

Terms	Descriptions
sg	DOF of platform surge motion
hv	DOF of platform have motion
p	DOF of platform pitch motion
tmd	DOF of TMD motion
t	DOF of tower fore-aft bending
θ_i	Rotation angle of DOF i
x_i	Displacement of DOF i
M_i^j	Generalized mass for DOF i with regard to DOF j
I_i^j	Generalized inertia tensor for DOF i with regard to DOF j
F_i^j	Generalized force for DOF i due to effect or DOF j
τ_i^j	Generalized torque for DOF i due to effect or DOF j
gr	Gravitational effect
hdr	Hydro effect
ctr	Centripetal effect
$moor$	Mooring lines effect
$spr.damp$	Spring and damping effect of TMD
A_i^j	Generalized added mass for DOF i with regard to DOF j
J_u^X	Inertia tensor for u with regard to point X
L_u	Length of part u
m_u	Mass of part u
$ptfm$	Platform
twr	Tower
rna	Rotor nacelle assembly (RNA)
d	Misalignment between RNA mass center and tower centerline
jot	Joint between platform and tower
D_i^j	Equivalent damping coefficient for DOF i with regard to DOF j
K_i^j	Equivalent spring coefficient for DOF i with regard to DOF j
g	Gravitational acceleration
CB	Center of buoyancy
CG_u	Gravity center of part u

difference between FAST-SC and the established model. Based on the estimation result, free decay response comparison for the OC3-Hywind surge-pitch-heave motion without TMD is illustrated in Figure B.3, where two results coincide well with each other. Then, in order to further validate the established model, free decay response comparisons are performed again with TMD

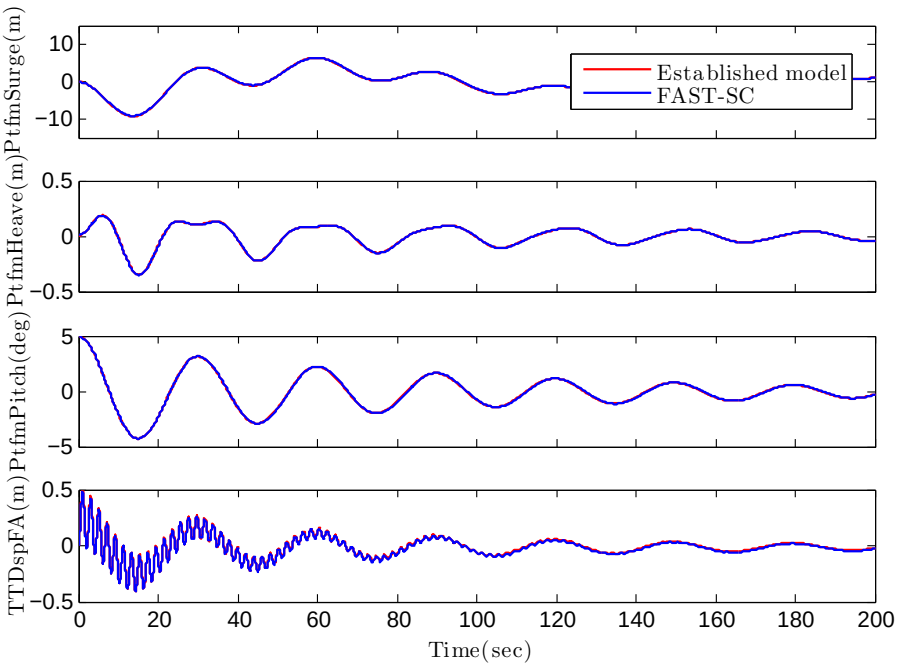

Figure B.3: Free decay response comparison between identified model and FAST-SC numerical simulation for surge-pitch-heave motion without TMD (5° initial platform pitch)

installed in nacelle. In practice, there exist space limitations for the nacelle, so the TMD displacement should be restricted into a certain range. According the nacelle dimensions defined in (Kooijman et al., 2003), the TMD displacement range is determined as ± 7m in this work. In FAST-SC, the TMD motion constraints were modelled as stops, where there would be spring stiffness and damping interaction between TMD and nacelle or platform when its displacement exceeds the user defined constraints. The stops effect in this work is characterized in the same way. Figure B.4 illustrates the free decay response comparison results with TMD stops. As expected, the established model still manages to capture the system dynamics including TMD stop interactions. It is worth mentioning that the stops with various spring and damping coefficients could have quite different impacts on system dynamics, but further analysis of stop parameters is not within the scope of this paper.

Based on the above analysis, the proposed model has captured most of the intrinsic dynamics for OC3-Hywind surge-heave-pitch motion, including hy-

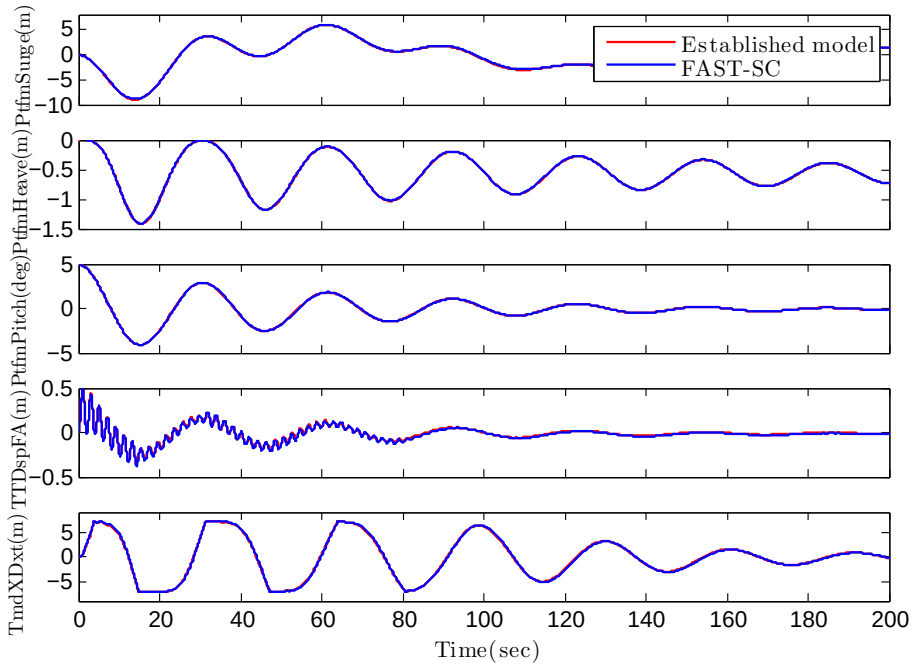

Figure B.4: Free decay response comparison with TMD and stops in nacelle

drodynamic and mooring loads, tower flexibility and TMD-nacelle interaction. Next step is to tune TMD parameters for effective system load reduction.

3 Parameter Tuning

Optimal parameter tuning of the vibration absorber is an important design consideration in passive structural control problems. The design aim in this work is to find the optimal TMD coefficients for wind turbine load reduction. The parameters to be determined include TMD spring and damping coefficients. TMD mass is not parametrically studied in this work since it is usually determined by cost and heavier mass will more likely produce better performance. Specifically, in order to be consistent with (Lackner and Rotea, 2011a), the mass is chosen to be 20,000kg, which takes about 3.33% of the weight for tower-RNA structure.

In fact, the most convincing solution here is to try all possible values of these parameters in FAST-SC. However, this global searching process will take tens of thousands of calls from FAST-SC, and it usually take minutes to run it for

only one time. Therefore, exhaustive search is almost impossible with ordinary computers, and appropriate optimization methods are needed. Based on the established model, in this section, three different methods are used for this parameter tuning problem.

3.1 Frequency and Damping Analysis

In engineering applications, the natural frequency of TMD is usually tuned to be near to that of the target system, thus it will effectively dissipate the undesirable system vibration energy. In order to systematically describe this phenomenon, Den Hartog (Den Hartog, 1985) analyzed the response of undamped main system with TMD subjected to harmonic external forces and derived an explicit expression to determine the optimal TMD natural frequency and damping ratio for vibration inhibition. The optimal solution is given by

$$f_{tmd} = \frac{f}{1+\mu}, \quad \xi_{tmd} = \sqrt{\frac{3\mu}{8(1+\mu)}}, \tag{B.7}$$

where μ denotes the mass ratio $\frac{m_{tmd}}{m}$, and f and ξ are the natural frequency and damping ratio of target system. f_{tmd} and ξ_{tmd} represent the optimal natural frequency and damping ratio of TMD.

In order to adopt this method, eigenanalysis based on model linearization result is performed first to obtain system natural frequencies and damping ratios for the modes of interest.

The eigenanalysis result has been presented in (Matha, 2010), where natural frequencies of two most critical modes, i.e. platform pitch mode and first tower fore-aft bending mode, are 0.4732Hz and 0.0342Hz, and there damping ratios are 0.0087 and 0.1418.

However, in this analysis process, the nonlinearity of TMD stops due to space constraints is not considered, which has been shown to have strong influence on TMD load reduction effectiveness according to the following nonlinear FAST-SC simulation results. Therefore, a more thorough method should be proposed to find the best combination of these TMD parameters.

3.2 Surface Plot

In previous section, we have obtained a mathematical model describing OC3-Hywind surge-heave-pitch motion, which manages to capture most of system structural dynamics, hydro and mooring effects. More importantly, the time for solving this dynamic equation is less than 1s, thus surface plotting, a global parameter searching method, becomes a possible solution to determine the optimal TMD parameters.

Next, we introduce the performance indices in Table B.3 which are used in the optimization process. The tower top fore-aft deflection is the best indicator of tower bottom bending moments, and the author in (Stewart, 2012) used standard deviation of tower top displacement as the performance index, which is also adopted in this work as the first performance index J_1. Secondly, we also care about load reduction effectiveness of the proposed method in extreme events, thus the range of tower top displacement in the free decay test is treated as another evaluation index J_2.

Table B.3: Performance indices

Index	Description
$J_1 = \sqrt{\frac{1}{T}\int_0^T (x_{tt} - \tilde{x}_{tt})^2 \mathrm{d}t}$	Standard deviation of tower top displacement under its equilibrium point
$J_2 = \max(x_{tt}) - \min(x_{tt})$	Range of tower top displacement

Based on these indices, exhaustive search is performed where TMD Spring and damping constants are regarded as two coefficients to be optimized. The parameter range and interval are chosen when both time consumption and accuracy are considered. The surface plots for different design criteria are illustrated in Figure B.5 and B.6, and the optimization results are listed in Table B.4.

Although surface plotting could be regarded as a global optimization method, which produces a relatively comprehensive evaluation of the performance index with possible parameters, it is still computationally expensive, which will take hours or days long to finish one optimization process. Also, there might exist

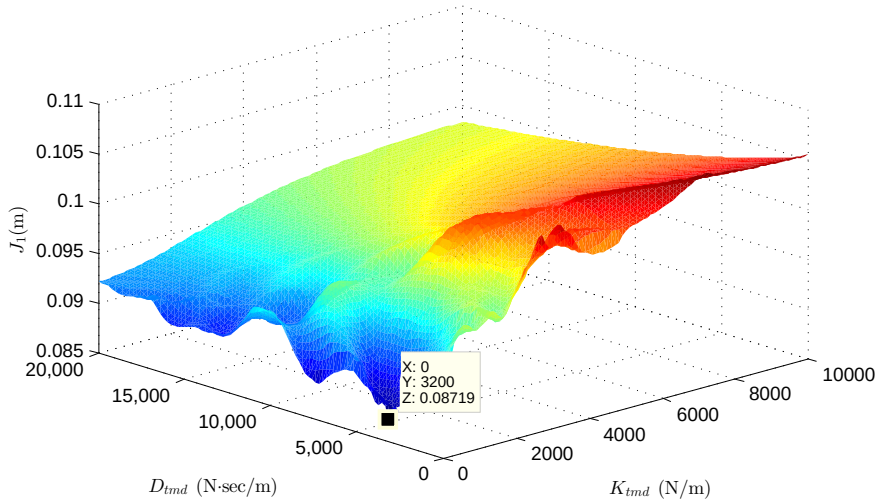

Figure B.5: Surface plot subjected to performance index J_1 with TMD installed in nacelle.

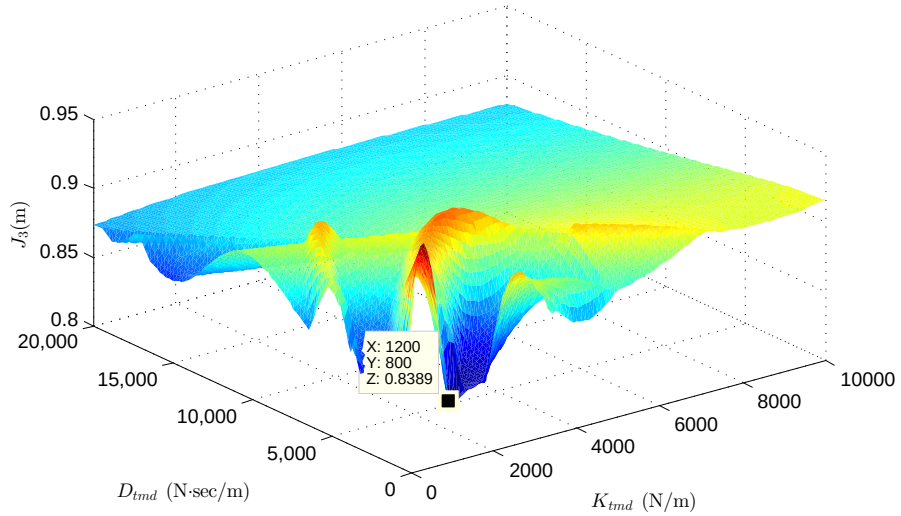

Figure B.6: Surface plot subjected to performance index J_2 with TMD installed in nacelle.

better solution if the parameter interval is not small enough. Therefore, more intelligent and efficient optimization algorithms are demanded.

3.3 Genetic Algorithm

In the past few years, genetic algorithm has been widely applied in a broad spectrum of real-world systems (Wang and Ohmori, 2013; Poirier et al., 2013;

Ramires et al., 2012). This approach starts with randomly generated population, and individuals with better fitness will be selected as the basis of next generation. The improved population will keep evolving after inheritance, mutation, selection, and crossover procedures until the it meets the final requirement. As a global optimization method, genetic algorithm is based on stochastic variables and does not require the derivatives of object function, which brings the advantages of global evaluation and objective tolerance when compared with other gradient based local optimization methods. It usually helps to obtain a better result in optimization problems with non-smooth objective functions, thus is suitable for the optimization problem in this work. When implementing the algorithm, probability of the roulette wheel uniform crossover is chosen as 0.6, and the mutation probability 0.01 is used. Minimum number of generations is set as 20. Optimization results are shown in Table B.4. It can be noticed that genetic algorithm gives a better result with respect to J_2 since the surface plotting has a limited searching range.

Table B.4: Parameter optimization result (m_{tmd}=20,000kg)

Method	Performance index	K_{tmd} (N/m)	D_{tmd} (N·s/m)
Den Hartog	Tower bending mode (Den1)	165571	12661
Den Hartog	Platform Pitch mode (Den2)	865	915
Surface plot	$J_1 = 0.0872$ m	0	3200
Surface plot	$J_2 = 0.8389$ m	1200	800
GA	$J_1 = 0.0871$ m	0	3130
GA	$J_2 = 0.7620$ m	164231	20889

4 Simulation and Analysis

In this section, based on the optimization result, fully nonlinear simulations are performed in FAST-SC with all wind turbine DOFs enabled. Each test runs 630 seconds, and the output data in first 30s are not recorded, waiting for generator torque and blade pitch motion arrive normal operation state. The modified generator torque and blade pitch controller from NREL is used in the

form of a dynamic link library for all tests (Jonkman, 2010).

The wind and wave conditions in the experiment are defined almost as same as that in (Lackner and Rotea, 2011b). For wind condition, both the above and below rated wind speeds are considered, and mean value of turbulent wind is defined as 18 m/s and 10 m/s separatively. The turbulent wind file is generated by TurbSim, where Kaimal spectra and the power law exponent of 0.14 are used according to the IEC61400-3 offshore wind turbine design standard. The normal turbulence intensity is set as 15% (18 m/s case) and 18%(10 m/s case). Random seed in this work is arbitrarily chosen as 231857312. In order to define the wave condition, JONSWAP spectrum is utilized to generate the stochastic wave inputs. The significant wave height is set as 2.3 m (10 m/s case) and 3.7 m (18 m/s case), and the peak spectral period is defined as 14s. Besides, the parked situation is also considered assuming the turbine suffers extreme 50-year storm, i.e. 37 m/s turbulent wind with power law exponent of 0.11 and 11% turbulence intensity. Wave height and period are defined as 13.8 m and 19 s.

Percentage of load reduction with different TMD parameter choice is shown in Table B.5. In order to measure the fatigue and extreme loading, damage equivalent load (DEL) and the 95th percentile of fore-aft and side-side tower base bending moments (TwrBsMyt abd TwrBsMxt) and flapwise bending moment at the first blade root (RootMyc1) are calculated, together with the 95th percentile of platform pitch and roll rotation angle. In above rated situation, the root mean square (RMS) of generated power is considered as another index.

It can be seen from results that the design of TMD with small spring and damping coefficients will achieve much load reduction in above rated condition, where one simulation result is shown in Figure B.7. However, it will deteriorate system performance when the turbine is working below rated or parked. In contrast, the design with large spring and damping constants will produce moderate load reduction in all working conditions.

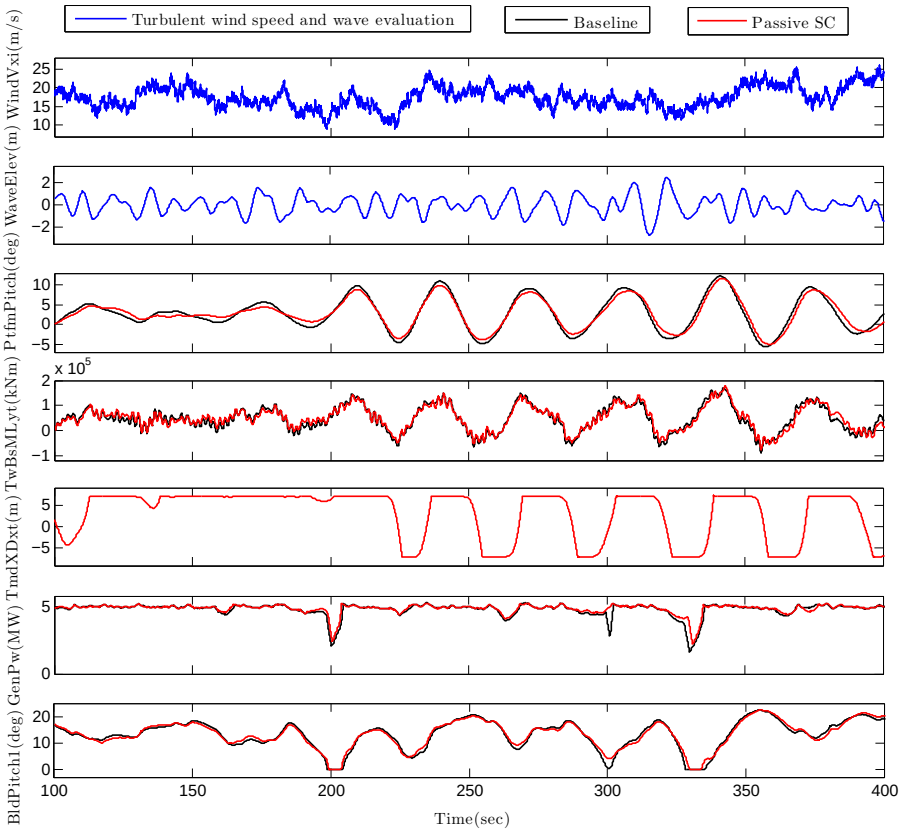

Figure B.7: FAST-SC simulation results with 18m/s turbulent wind and 3.7m wave height

Table B.5: Percentage of load reduction with different TMD tuning results compared with baseline

Case	Evaluation index	Den1	Den2	J_1	J_2
	DEL TwrBsMyt	6.35	0.66	0.52	6.00
	DEL TwrBsMxt	32.18	14.2	11.44	28.37
	DEL RootMyc1	1.07	-0.18	0.10	0.85
10m/s	DEL Anch1Ten	0.93	3.01	1.21	0.93
	95th TwrBsMyt	-2.00	-4.04	-3.89	-2.00
	95th TwrBsMxt	6.01	2.7	2.55	5.06
	95th PtfmPitch	-2.08	-1.96	-2.08	-2.08
	95th PtfmRoll	-1.67	0.21	0.13	-1.67
	DEL TwrBsMyt	3.61	7.77	8.78	3.35
	DEL TwrBsMxt	25.55	0.98	-3.94	21.24
	DEL RootMyc1	1.07	4.99	5.93	1.14
	DEL Anch1Ten	1.15	0.32	0.32	1.14
18m/s	95th TwrBsMyt	-3.15	5.02	6.48	-3.25
	95th TwrBsMxt	7.90	4.70	1.69	7.10
	95th PtfmPitch	-1.05	10.66	12.43	-1.04
	95th PtfmRoll	6.55	15.54	14.32	6.58
	RMS GenPwr	-5.46	21.09	29.22	-5.41
	DEL TwrBsMyt	1.47	-19.95	-16.25	1.22
	DEL TwrBsMxt	0.14	0.51	0.42	0.18
	DEL RootMyc1	1.80	-45.71	-28.34	2.03
37m/s	DEL Anch1Ten	1.33	1.83	0.96	0.78
	95th TwrBsMyt	-0.78	-4.88	-2.33	-0.77
	95th TwrBsMxt	0.41	0.40	0.25	0.47
	95th PtfmPitch	4.41	5.40	4.44	4.41
	95th PtfmRoll	-0.30	-0.63	-0.57	-0.30

5 Conclusion

This work focuses on the modelling and parameter tuning of a passive structural control design for the OC3-Hywind floating wind turbine. Firstly, the coupled surge-heave-pitch dynamic model with a TMD installed in nacelle is established based on the D'Alembert's principle. Parameter estimation is also performed for model validation. Then, different parameter tuning methods and performance indices are used for TMD parameter determination. FAST-SC is used for fully coupled nonlinear simulation with various wind and wave

conditions. The results show that the design of TMD with small spring and damping coefficients will achieve much load reduction in above rated condition, but it will deteriorate system performance when the turbine is working below rated or parked. In contrast, the design with large spring and damping constants will produce moderate load reduction in all working conditions. Therefore, inappropriate TMD design will not contribute to wind turbine load reduction. Besides, only enabling TMD in certain range of wind speed might be a possible solution for this design. Further real experiments need to be conducted to verify this idea. Future work will also consider the situation when TMD is installed in the spar itself or other types of platforms.

Appendix

$$
\begin{aligned}
M_{sg}^{sg} &= A_{sg}^{sg} + m_{ptfm} + m_{twr} + m_{rna} + m_{tmd} \\
I_{sg}^{p} &= A_{sg}^{p} + m_{twr}(L_{twr} + L_{jot})\cos\theta_p - m_{ptfm}L_{ptfm}\cos\theta_p \\
M_{sg}^{tmd} = M_{tmd}^{sg} &= m_{tmd}\cos(\theta_p + \sin(\theta_t - \theta_p)L_{rna}\dot{\Phi}_{rna}) \\
I_{sg}^{t} &= m_{rna}(L_{rna} + L_{jot})\cos\theta_t + m_{tmd}L_{rna}\cos\theta_t \\
M_{hv}^{hv} &= A_{hv}^{hv} + m_{ptfm} + m_{twr} + m_{rna} + m_{tmd} \\
I_{hv}^{p} &= -m_{twr}(L_{twr} + L_{jot})\sin\theta_p + m_{ptfm}L_{ptfm}\sin\theta_p \\
M_{hv}^{tmd} = M_{tmd}^{hv} &= -m_{tmd}\sin(\theta_p + \sin(\theta_t - \theta_p)L_{rna}\dot{\Phi}_{rna}) \\
I_{hv}^{t} &= -m_{rna}(L_{rna} + L_{jot})\sin\theta_t - m_{tmd}L_{rna}\sin\theta_t \\
M_{p}^{sg} &= A_{p}^{sg} + m_{rna}(L_{rna} + L_{jot})\cos\theta_t + m_{twr}(L_{twr} + L_{jot})\cos\theta_p \\
&\quad - m_{ptfm}L_{ptfm}\cos\theta_p + m_{tmd}(L_{rna} + L_{jot})\cos\theta_t \\
M_{p}^{hv} &= -m_{rna}(L_{rna} + L_{jot})\sin\theta_t - m_{twr}(L_{twr} + L_{jot})\sin\theta_p \\
&\quad + m_{ptfm}L_{ptfm}\sin\theta_p - m_{tmd}(L_{rna} + L_{jot})\sin\theta_t \\
I_{p}^{p} &= A_{p}^{p} + J_{ptfm}^{CG_{ptfm}} + m_{ptfm}{L_{ptfm}}^2 + J_{twr}^{CG_{twr}} \\
&\quad + m_{twr}(L_{twr} + L_{jot})^2 + m_{rna}(L_{rna} + L_{jot})^2 + m_{tmd}(L_{rna} + L_{jot})^2 \\
I_{tmd}^{p} &= 0 \\
M_{tmd}^{tmd} &= m_{tmd} \\
I_{tmd}^{t} = M_{t}^{tmd} &= m_{tmd}L_{rna}\cos(\sin(\theta_t - \theta_p)L_{rna}\dot{\Phi}_{rna}) \\
M_{t}^{sg} &= m_{rna}L_{rna}\cos\theta_t + m_{twr}L_{twr}\cos\theta_p + m_{tmd}L_{rna}\cos\theta_t \\
M_{t}^{hv} &= -m_{rna}L_{rna}\sin\theta_t - m_{twr}L_{twr}\sin\theta_p - m_{tmd}L_{rna}\sin\theta_t
\end{aligned}
$$

$$
\begin{aligned}
\dot{\Phi}_{rna} &= \left.\frac{\partial \Phi(h)}{\partial h}\right|_{h=L_{rna}} \\
F_{hv}^{gr} &= -(m_{ptfm} + m_{twr} + m_{rna} + m_{tmd})g \\
\tau_p^{gr} &= m_{rna}(L_{rna} + L_{jot})\sin\theta_t + m_{twr}g(L_{twr} + L_{jot})\sin\theta_p \\
&\quad - m_{ptfm}gL_{ptfm}\sin\theta_p - m_{rna}gL_d\cos\theta_t \\
&\quad + m_{tmd}gx_{tmd}\cos\theta_t + m_{tmd}g(L_{rna} + L_{jot})\sin\theta_t \\
F_{tmd}^{gr} &= m_{tmd}g\sin\left(\theta_p + \sin(\theta_t - \theta_p)L_{rna}\dot{\Phi}_{rna}\right) \\
\tau_t^{gr} &= m_{twr}gL_{twr}\sin\theta_p + m_{rna}gL_{rna}\sin\theta_t - m_{rna}gL_d\cos\theta_t \\
&\quad + m_{tmd}gx_{tmd}\cos\theta_t + m_{tmd}gL_{rna}\sin\theta_t \\
F_{sg}^{hdr.moor} &= -D_{sg}^{sg}\dot{x}_{sg} - \hat{D}_{sg}^{sg}\dot{x}_{sg}^2 - K_{sg}^{sg}x_{sg} - D_{sg}^{p}\dot{\theta}_p - K_{sg}^{p}\theta_p \\
F_{hv}^{hdr.moor} &= -D_{hv}^{hv}\dot{x}_{hv} - K_{hv}^{hv}x_{hv} - F_{moor} + F_{buoy} - K_{hv}^{p.sg}(x_{sg} - L_{moor}\sin\theta_p)^2 \\
\tau_p^{hdr.moor} &= -D_p^p\dot{\theta}_p - K_p^p\theta_p - D_p^{sg}\dot{x}_{sg} - \hat{D}_p^{sg}\dot{x}_{sg}^2 - K_p^{sg}x_{sg}
\end{aligned}
$$

$$
\begin{aligned}
F_{sg}^{ctr} &= m_{twr}\dot{\theta}_p^2(L_{twr} + L_{jot})\sin\theta_p + m_{rna}\dot{\theta}_t^2(L_{rna} + L_{jot})\sin\theta_t \\
&\quad - m_{ptfm}\dot{\theta}_p^2 L_{ptfm}\sin\theta_p + m_{tmd}\dot{\theta}_t(\dot{\theta}_t(L_{rna} + L_{jot}) - \dot{x}_{tmd})\sin\theta_t \\
F_{hv}^{ctr} &= m_{twr}\dot{\theta}_p^2(L_{twr} + L_{jot})\cos\theta_p + m_{rna}\dot{\theta}_t^2(L_{rna} + L_{jot})\cos\theta_t \\
&\quad - m_{ptfm}\dot{\theta}_p^2 L_{ptfm}\cos\theta_p + m_{tmd}\dot{\theta}_t(\dot{\theta}_t(L_{rna} + L_{jot}) - \dot{x}_{tmd})\cos\theta_t \\
\tau_p^{ctr} = \tau_t^{ctr} &= -m_{tmd}\dot{\theta}_t(\dot{\theta}_t(L_{rna} + L_{jot}) - \dot{x}_{tmd})x_{tmd} \\
F_{tmd}^{spr.damp} &= -D_{tmd}\dot{x}_{tmd} - K_{tmd}x_{tmd} \\
\tau_t^p &= D_t(\dot{\theta}_t - \dot{\theta}_p) + K_t(\theta_t - \theta_p)
\end{aligned}
$$

Acknowledgements

This work has been (partially) funded by Norwegian Centre for Offshore Wind Energy (NORCOWE) under grant 193821/S60 from Research Council of Norway (RCN). NORCOWE is a consortium with partners from industry and science, hosted by Christian Michelsen Research.

The authors would like to give sincere thanks to Dr. Lackner in University of Massachusetts Amherst for his generosity on the FAST-SC code sharing and

Dr. Jonkman from National Renewable Energy Laboratory for his enthusiastic help and support with the specifications of OC3-Hywind model.

REFERENCES

Butterfield, S., Musial, W., Jonkman, J., Sclavounos, P., and Wayman, L. (2005). Engineering challenges for floating offshore wind turbines. In *Copenhagen Offshore Wind 2005 Conference and Expedition Proceedings, 26–28 October 2005, Copenhagen, Denmark*.

Colwell, S. and Basu, B. (2009). Tuned liquid column dampers in offshore wind turbines for structural control. *Engineering Structures*, 31(2):358–368.

Den Hartog, J. P. (1985). *Mechanical vibrations*. Dover publications.

Jonkman, J. (2007). *Dynamics modeling and loads analysis of an offshore floating wind turbine*. PhD thesis, Department of Aerospace Engineering Sciences, University of Colorado.

Jonkman, J. (2009). Dynamics of offshore floating wind turbines - model development and verification. *Wind Energy*, 12(5):459–492.

Jonkman, J. (2010). Definition of the floating system for phase iv of oc3. *NREL/TP-500-38060. Golden, Colorado: National Renewable Energy Laboratory*.

Jonkman, J. and Buhl Jr, M. (2005). Fast users guide. Technical report, NREL/EL-500-29798. Golden, Colorado: National Renewable Energy Laboratory.

Jonkman, J., Butterfield, S., Musial, W., and Scott, G. (2009). Definition of a 5-mw reference wind turbine for offshore system development. Technical report, NREL/TP-500-47535. Golden, Colorado: National Renewable Energy Laboratory.

Jonkman, J. and Matha, D. (2009). A quantitative comparison of the responses of three floating platform concepts. In *European Offshore Wind 2009 Conference & Exhibition*, pages 14–16.

Kooijman, H., Lindenbug, C., Winkelaar, D., and Van der Hooft, E. (2003). Dowec 6 mw pre-design: Aeroelastic modeling of the dowec 6 mw pre-design in phatas. *Energy research Centre of the Netherlands, NL*.

Korkmaz, S. (2011). A review of active structural control: challenges for engineering informatics. *Computers & Structures*, 89:2113 – 2132.

Lackner, M. A. and Rotea, M. A. (2011a). Passive structural control of offshore wind turbines. *Wind Energy*, 14(3):373–388.

Lackner, M. A. and Rotea, M. A. (2011b). Structural control of floating wind turbines. *Mechatronics*, 21(4):704 – 719.

Larsen, T. J. and Hanson, T. D. (2007). A method to avoid negative damped low frequent tower vibrations for a floating, pitch controlled wind turbine. *Journal of Physics: Conference Series*, 75(1).

Li, J., Zhang, Z., and Chen, J. (2012). Experimental study on vibration control of offshore wind turbines using a ball vibration absorber. *Energy and Power Engineering*, 4(3):153–157.

Matha, D. (2010). Model development and loads analysis of an offshore wind turbine on a tension leg platform with a comparison to other floating turbine concepts. Technical report, NREL/SR-500-45891. National Renewable Energy Laboratory (NREL), Golden, CO.

Murtagh, P. J., Ghosh, A., Basu, B., and Broderick, B. M. (2008). Passive control of wind turbine vibrations including blade/tower interaction and rotationally sampled turbulence. *Wind Energy*, 11(4):305–317.

Namik, H. and Stol, K. (2011). Performance analysis of individual blade pitch control of offshore wind turbines on two floating platforms. *Mechatronics*, 21(4):691 – 703.

Newman, J. (1977). *Marine hydrodynamics*. MIT press.

Poirier, J. D., Vel, S. S., and Caccese, V. (2013). Multi-objective optimization of laser-welded steel sandwich panels for static loads using a genetic algorithm. *Engineering Structures*, 49:508–524.

Ramires, F. B., Andrade, S. A. L. d., Vellasco, P. C. G. d. S., and Lima, L. R. O. d. (2012). Genetic algorithm optimization of composite and steel endplate semi-rigid joints. *Engineering Structures*, 45:177–191.

Rao, S. and Durgaiah, R. (2005). *Engineering Mechanics*. Universities Press,India.

Stewart, G. (2012). *Load reduction of floating wind turbines using tuned mass dampers*. PhD thesis, University of Massachusetts Amherst.

Stewart, G. and Lackner, M. A. (2012). Optimization of a passive tuned mass damper for reducing loads in offshore wind turbines. *IEEE Transactions on Control Systems Technology: Special Issue on Wind Energy*.

Stewart, G. M. and Lackner, M. A. (2011). The effect of actuator dynamics on active structural control of offshore wind turbines. *Engineering Structures*, 33(5):1807 – 1816.

Wang, H. and Ohmori, H. (2013). Elasto-plastic analysis based truss optimization using genetic algorithm. *Engineering Structures*, 50:1–12.

PAPER C

LOAD REDUCTION FOR FLOATING OFFSHORE WIND TURBINES USING TUNED LIQUID COLUMN DAMPERS

Yulin Si, Hamid Reza Karimi

This paper has been published as:

Y. Si, H. R. Karimi, "Load reduction for floating offshore wind turbines using tuned liquid column dampers", *Proceedings of the 12th German Wind Energy Conference*, Bremen, Germany, 19-20 May, 2015.

Load Reduction for Floating Offshore Wind Turbines Using Tuned Liquid Column Dampers

Yulin Si, Hamid Reza Karimi
Department of Engineering
Faculty of Engineering and Science, University of Agder
Jon Lilletunsvei 9, 4879 Grimstad, Norway.

Abstract — **This work investigates the idea of installing TLCD in floating wind turbines for load reduction. Dynamic model is established, and design optimization is performed for TLCD parameters by using genetic algorithm. Fully coupled simulation is conducted with the developed code FAST-SC-TLCD. Results show that it is promising to use TLCD for offshore turbine load reduction considering its cost and performance.**

1 Introduction

Strong potentials for offshore wind energy have been found in the deep sea areas. According to extensive experiences in offshore industry, floating foundation for wind turbines are considered as an economical and applicable solution. So far, plenty of numerical investigations (Jonkman and Matha, 2009; Jonkman, 2007) have been conducted by world-wide research institutions, and different kinds of prototype programs have also been launched, including OC3-Hywind, MIT/NREL TLP, ITI Barge, and Principle Power WindFloat, etc.
Different from fixed-bottom wind turbines, one big challenge (Butterfield et al., 2005) for floating windmills is the platform motion, which will heavily increase the load on the nacelle and tower due to high inertial and gravitational forces. This might cause severe fatigue and ultimate damage on the blades, tower

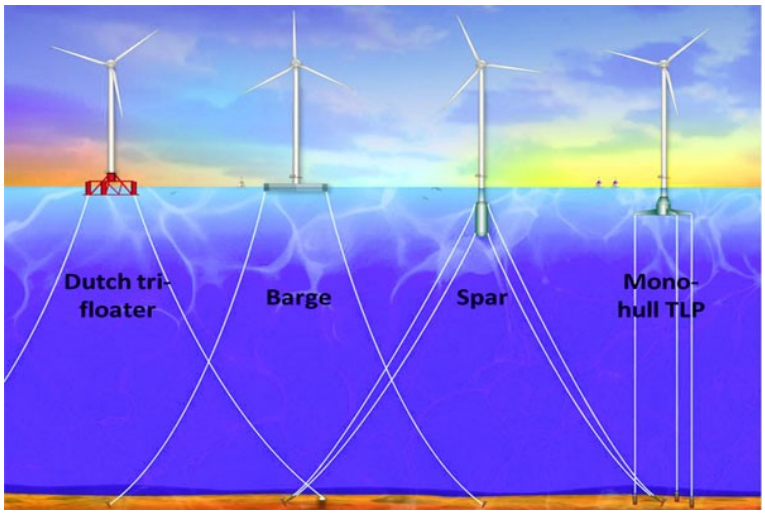

Figure C.1: Different floating wind turbine concepts.

base, nacelle-tower bearing. Therefore, further load reduction strategy should be considered during the design process of floating wind turbines.

Blade pitch control system plays an important role in not only power regulation, but also load mitigation. It is thus reasonable to tackle with the floating wind turbine load problem by improving the blade pitch strategy. Existing research works (Jonkman, 2007; Skaare et al., 2007) have shown that detuning the control gains would avoid negative damping and extend the fatigue life of turbine structures. If analyzed in the frequency-domain, this is, essentially, to keeping the desired natural frequency of control system lower than the lowest critical frequency of the floating structure. Besides, advanced control schemes were also designed for either collective or individual blade pitch control (Lackner, 2012; Namik and Stol, 2010).

A more direct approach for wind turbine load reduction is to adopt structural control devices, such as tuned mass dampers. These resonance absorbers have been widely used in large civil structures, e.g. skyscrapers and bridges, thus are also seen promising to deal with wind turbine load problem, especially for offshore types. For high-fidelity simulation, the state-of-the-art numerical wind turbine simulator FAST was modified by Lackner (Lackner and Rotea, 2011a), in order to characterize the dynamic influence of passive and active structural control. With this so-called code FAST-SC, different parameter optimization

methods were used to find the optimal parameters of passive structural control devices (Si et al., 2014; Stewart and Lackner, 2012). However, passive tuned mass damper has to bring a huge mass into the system, usually made of concrete or steel, which is unfavorable to the system cost. It was also shown that more load reduction could be achieved when introducing active structural control (Lackner and Rotea, 2011b), but the improvement is at the expenses of more power consumption and longer mass stroke. Besides, active mass damper highly depends on the actuation control strategy, which might bring instability to the system. Regarding these issues, semi-active structural control device, such as tuned-liquid column damper (TLCD), shows a compromise due to its low cost and decent performance. In (Colwell and Basu, 2009), Colwell et al. explored the structural responses of a fixed-bottom offshore wind turbine with a TLCD installed in nacelle. However, this work didnt use the state-of-the-art wind turbine simulator, and its load reduction effectiveness on floating wind turbines was not considered.

Motivated by the above mentioned problems and research potentials, we further modified FAST-SC into FAST-SC-TLCD, which is capable of simulating dynamics of wind turbines equipped with TLCD. For parameter optimization, a mathematical model for a spar-type floating wind turbine in longitudinal motion is established based on the first principle. Simulation results and performance comparison are also given to show the effectiveness of the proposed idea.

2 FAST-SC-TLCD

Semi-active structural control method, i.e. installing tuned column liquid dampers (TLCD) in either nacelle or foundation of a floating wind turbine, can be used for load reduction (Figure C.2). Only nacelle installation is discussed here due to the length of this paper.

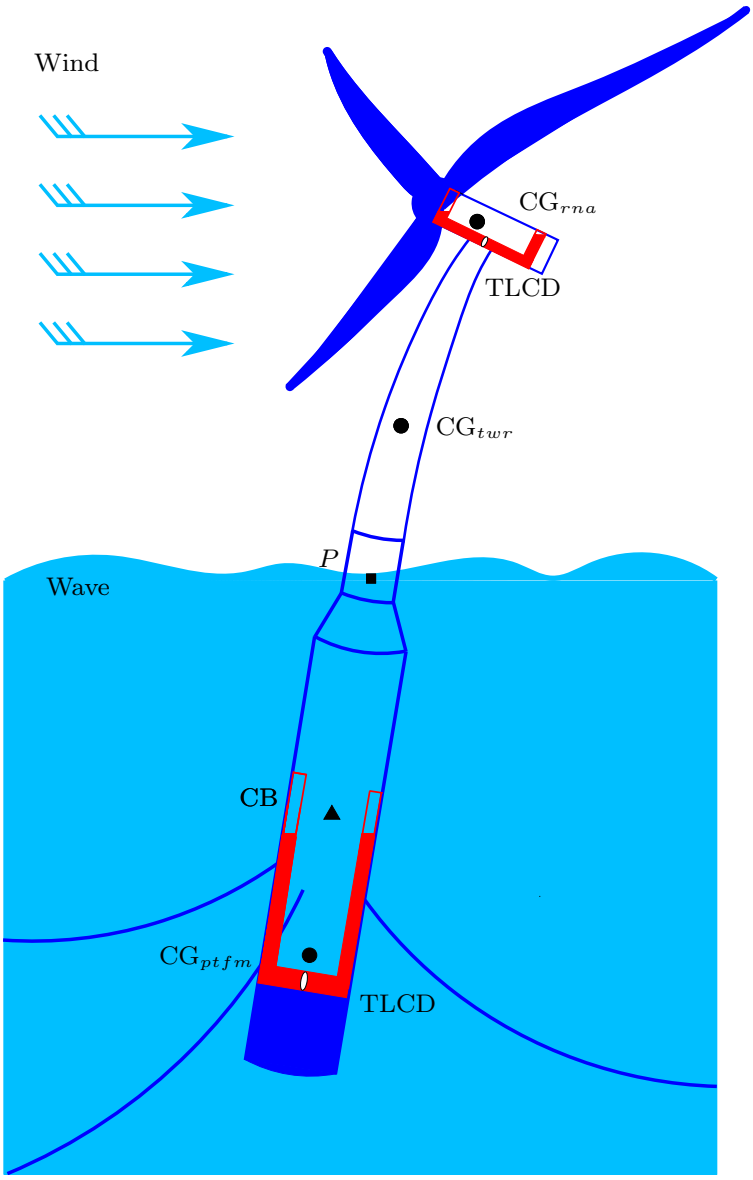

Figure C.2: TLCDs installed in a spar-type floating wind turbine.

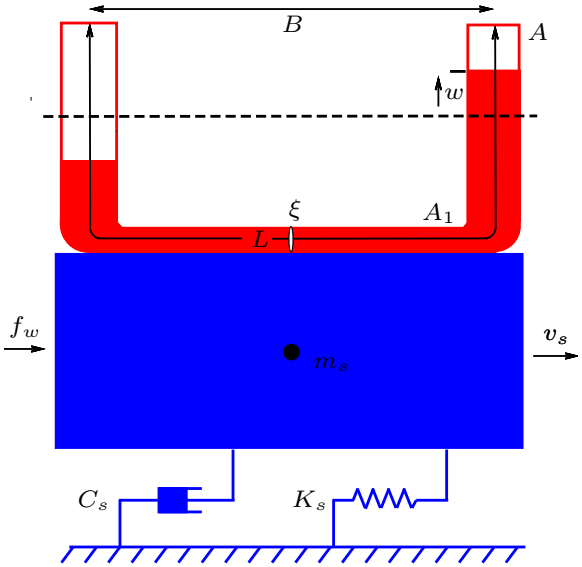

Figure C.3: Tuned liquid column damper under horizontal excitation.

2.1 TLCD Dynamics

Figure C.3 is the illustration of a TLCD under horizontal excitation. Here we only take the surge motion as an example, since similar model derivation process can be obtained for other degrees of freedom, e.g. pitch and heave.

The dynamic model of this TLCD was developed by Gao et al. (Gao et al., 1997), which can be established as

$$\rho A L_{ee} \ddot{w} + 0.5\rho A \xi |\dot{w}| \dot{w} + 2\rho A g w = -\rho A B \ddot{v}_s,$$
$$|w| < \frac{L - B}{2},$$

where w represents the liquid relative displacement. A and A_1 denote cross-sectional area of liquid column vertical and horizontal sections, respectively. B is the horizontal length, and L is the total length of the liquid. $\alpha = A/A_1$ is the area ratio, and $L_{ee} = L - B + \alpha B$. ρ is the liquid density. ξ is coefficient of head loss of liquid column. $\ddot{v}_s$ is the structure horizontal acceleration, and

the motion equation of the structure can be written as

$$m_s\ddot{v}_s + C_s\dot{v}_s + K_s v_s = f_w - \rho AB\ddot{w} - \rho AL_{em}\ddot{v}_s,$$
$$|w| < \frac{L-B}{2},$$

where m_s, C_s, K_s denote structural mass, damping coefficient and stiffness, respectively. f_w is the external force, and $L_{em} = B/\alpha + (L-B)$ is the length of an equivalent uniform crosssectional area liquid column with area A which has the same mass as the TLCD.

2.2 Code Implementation

FAST-SC (Lackner and Rotea, 2011a) manages to incorporate passive or active spring mass dampers into wind turbine simulation, but it has not yet included the option of TLCD. Following similar coding procedure and style, we developed FAST-SC-TLCD for fully coupled high-fidelity wind turbine simulation with semi-active structural control channel. More details, including the source code, can be found here [1].

The equations of motion of FAST are based on Kanes dynamics (Jonkman and Buhl Jr, 2005), which is also used to characterize the numerical model of TLCD and its interaction with the wind turbine. For a simple holonomic system with P generalized coordinate, system dynamic equation can be expressed via the following equation,

$$F_i + F_i^* = 0 (i = 1, 2, ..., P)$$

For a set of W rigid bodies, and reference frame N_r, mass m_r and center of mass (CM) location X_r the generalized active forces, F_i, and the generalized inertial forces, F_i^*, are expressed using the following equations.

$$F_i = \sum_{r=1}^{W} {}^E v_i^{X_r} \cdot F^{X_r} + {}^E\omega_i^{N_r} \cdot M^{N_r},$$
$$F_i^* = \sum_{r=1}^{W} {}^E v_i^{X_r} \cdot (-m_r {}^E a^{X_r}) + {}^E\omega_i^{N_r} \cdot (-{}^E\dot{H}^{N_r}).$$

[1] https://github.com/yulins/FAST-SC-TLCD-DLL-OC3Hywind

F^{X_r} and M^{N_r} are the active force and moment vectors applied at the mass center. ${}^{E}a^{X_r}$ is the acceleration of point X_r in the inertial frame E, ${}^{E}\dot{H}^{N_r}$ is the first time derivative of the angular momentum of rigid body N_r about point X_r in the inertial frame E, ${}^{E}v_i^{X_r}$ is the partial linear velocity of point X_r in the inertial frame E, and ${}^{E}\omega_i^{N_r}$ is the partial angular velocity of rigid body N_r in the inertial frame E.

Note that four independent single DOF TLCDs are modeled in FAST-SC-TLCD. Two TLCDs are located in the nacelle of the turbine, and other two are positioned in the foundation. TLCDx translates in the fore-aft direction (the x-axis in the nacelle frame of reference), while TLCDy translates in the side-side direction. Same as FAST-SC, each TLCD also has two stops, which are spring dampers that only engage when the fluid exceeds the column stop position.

3 Design Optimization

Optimal parameter tuning of the vibration absorber is an important design consideration in structural control problems. The design aim in this part is to find the optimal TLCD coefficients for wind turbine load reduction. The parameters to be determined include its dimension and location. The head loss is also a parameter to be optimized, since it is regarded as a constant in this part.

In fact, the most convincing solution here is to try all possible values of these parameters in FAST-SC-TLCD. However, this global searching process will take tens of thousands of calls of the code, and it usually take minutes to run it for only one time. Therefore, exhaustive search is almost impossible with ordinary computers, and appropriate optimization methods are needed. In this part, a limited DOF model is established in order to perform the design optimization. Based on the D'Alembert's principle of inertial forces, the following longitudinal model can be established as follows, see (Si et al., 2014),

$$\mathbf{M}(\mathbf{q})\ddot{\mathbf{q}} + \mathbf{L}(\mathbf{q}, \dot{\mathbf{q}}) = \mathbf{F}, \tag{C.1}$$

where

$$\mathbf{q} = \begin{bmatrix} x_{sg} \\ x_{hv} \\ \theta_p \\ x_{tlcd} \\ \theta_t \end{bmatrix}, \ \mathbf{M}(\mathbf{q}) = \begin{bmatrix} M_{sg}^{sg} & 0 & I_{sg}^{p} & M_{sg}^{tlcd} & 0 \\ 0 & M_{hv}^{hv} & I_{hv}^{p} & M_{hv}^{tlcd} & 0 \\ M_{p}^{sg} & M_{p}^{hv} & I_{p}^{p} & M_{p}^{tlcd} & 0 \\ M_{tlcd}^{sg} & M_{tlcd}^{hv} & I_{tlcd}^{p} & M_{tlcd}^{tlcd} & 0 \\ M_{t}^{sg} & M_{t}^{hv} & 0 & M_{t}^{tlcd} & I_{t}^{t} \end{bmatrix},$$

$$\mathbf{L}(\mathbf{q}, \dot{\mathbf{q}}) = \begin{bmatrix} F_{sg}^{hdr} + F_{sg}^{moor} + F_{sg}^{ctr} + F_{sg}^{wnd} \\ F_{hv}^{gr} + F_{hv}^{hdr} + F_{hv}^{moor} + F_{hv}^{ctr} + F_{hv}^{wnd} \\ \tau_{p}^{gr} + \tau_{p}^{hdr} + \tau_{p}^{moor} + \tau_{p}^{ctr} + \tau_{p}^{wnd} \\ F_{tlcd}^{gr} + F_{tlcd}^{tlcd} \\ \tau_{t}^{gr} + \tau_{t}^{p} + \tau_{t}^{ctr} + \tau_{t}^{wnd} \end{bmatrix}, \mathbf{F} = \begin{bmatrix} 0 \\ 0 \\ 0 \\ F \\ 0 \end{bmatrix}.$$

In this model, $\mathbf{q}$ is the state vector, and sg, hv, p, $tlcd$, t represent, respectively, the enabled 5 DOFs, i.e. platform surge, heave, pitch motion about P, TLCD liquid displacement, and tower deflection. $\mathbf{M}(\mathbf{q})$ is the system inertial matrix, which is positive definite.M_i^j and I_i^j denote generalized mass and generalized inertial tensor for DOF i with regard to DOF j. $\mathbf{L}(\mathbf{q}, \dot{\mathbf{q}})$ represents external loads, and gr, hdr, $moor$, ctr, wnd describe, respectively, gravitational, hydro, mooring, centripetal, aerodynamic loads in forces or moments. As shown in Table C.1 and Figure C.4, the correctness of the established model is verified by comparing the simulation results from FAST-SC-TLCD.

Table C.1: TLCD parameters for model verification

Term	Value
Liquid density	1,225 kg/m^3
Horizontal length	14 m
Vertical length	4 m
Horizontal area	1 m^2
Vertical area	2 m^2
Head loss	1
Stop damping coefficient	1,000,000 Ns/m
Stop stiffness coefficient	1,000,000 N/m

In the past few years, genetic algorithm has been widely applied in a broad spectrum of real-world systems. As a global optimization method, genetic

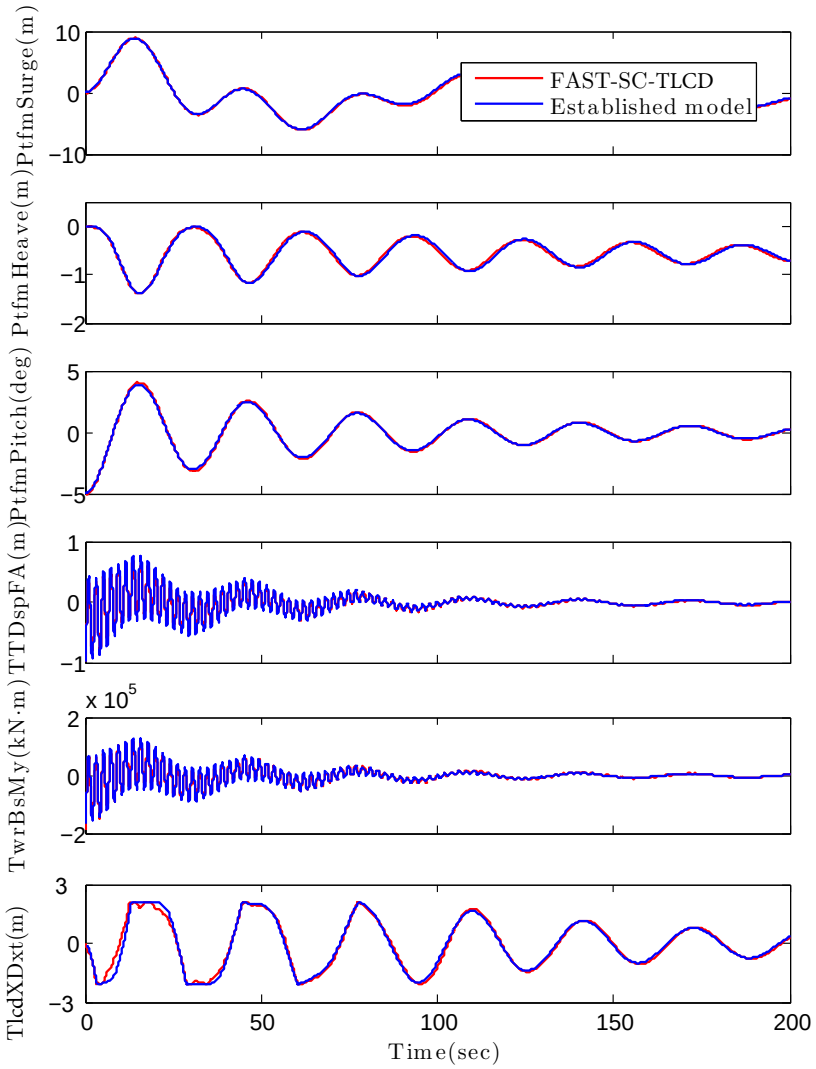

Figure C.4: Dynamic response comparison with TLCD installed in nacelle.

algorithm does not require the derivatives of object function, which brings the advantages of global evaluation and objective tolerance when compared with other gradient based local optimization methods. Therefore, we use generic algorithm is used here for design optimization of TLCD (Si et al., 2014). Based on the same evaluation indices in Table C.2, the optimization results are shown in Table C.3.

Table C.2: Performance indices

Index	Description
$J_1 = \sqrt{\frac{1}{T}\int_0^T (x_{tt} - \tilde{x}_{tt})^2 \mathrm{d}t}$	Standard deviation of tower top displacement under its equilibrium point
$J_2 = \max(x_{tt}) - \min(x_{tt})$	Maximum range of tower top displacement

Table C.3: Parameter optimization result with TLCD in nacelle

Performance index	A (m^2)	A_1 (m^2)	ξ
J_1	2.74	1.21	2.15
J_2	4.12	0.87	0.92

4 Simulation results

In this section, based on the optimization result, fully nonlinear simulations are performed in FAST-SC-TLCD with all wind turbine DOFs enabled. Each test runs 630 seconds. The modified generator torque and blade pitch controller from NREL is used in the form of a dynamic link library for all tests.

We consider two different simulation scenarios (Lackner and Rotea, 2011b). For wind condition, the mean value of the turbulent wind is defined as 10 m/s and 18 m/s, respectively. The turbulent wind file is generated by TurbSim, where Kaimal spectra and the power law exponent of 0.14 are used according to the IEC61400-3 offshore wind turbine design standard. The normal turbulence intensity is set as level B, i.e. 18% (10 m/s case) and 15%(18 m/s case). For

wave condition, JONSWAP spectrum is utilized to generate the stochastic wave inputs. The significant wave height is set as 2.3 m (10 m/s case) and 3.7 m (18 m/s case), and the peak spectral period is defined as 14s. For each case, at least two sets of random variables are used to generate wind and wave data. Percentage of load reduction for tower fore-aft motion is shown below, and a simulation example is given in Figure C.5. Simulation results shown that TLCD with appropriate size and installation can potentially reduce the wind turbine loads.

Table C.4: Percentage of load reduction (%)

Case	Term	J_1	J_2
10m/s	DEL tower fore-aft bending	3.43	10.41
	95th tower fore-aft bending	2.21	-3.45
18m/s	DEL tower fore-aft bending	8.23	6.12
	95th tower fore-aft bending	0.23	2.23

5 Conclusions

This work proposed to install TLCD in floating wind turbines for load reduction. Optimal parameters were located by using genetic algorithm based on the established model. Fully coupled simulation was performed with the developed code FAST-SC-TLCD. Results show the promises of TLCD for offshore turbine load reduction. Further study can be focused on the feedback control of head loss coefficient.

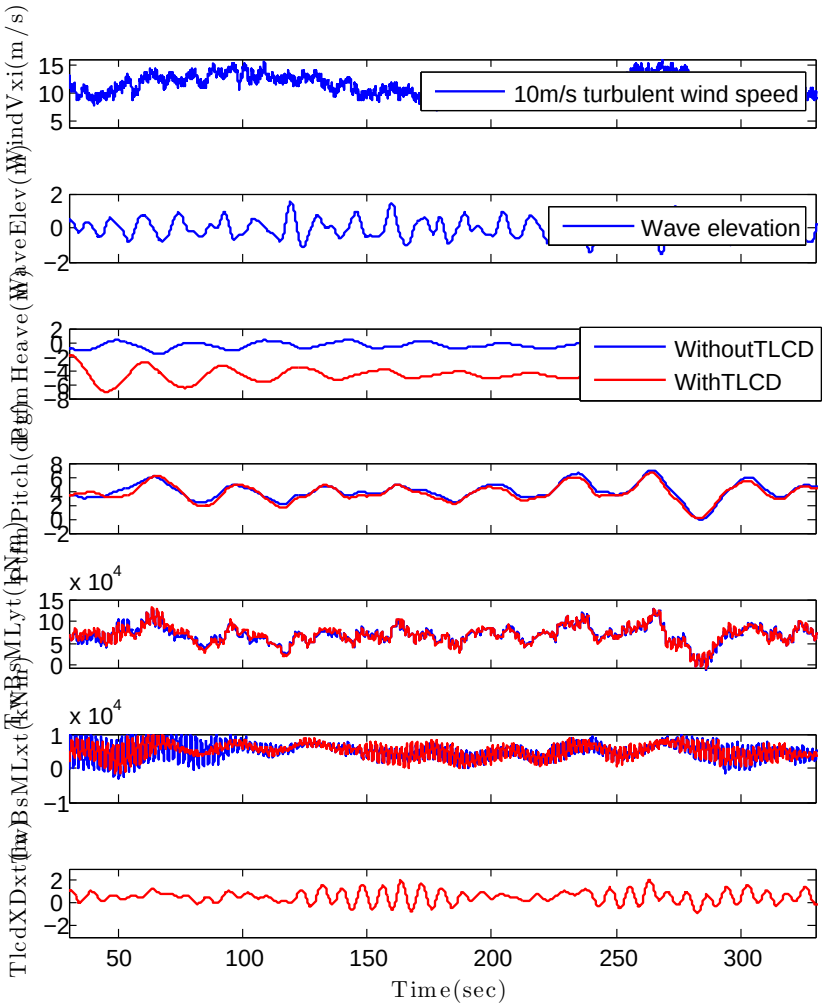

Figure C.5: Nonlinear simulation comparison under 10m/s turbulent wind and 2.3m wave.

REFERENCES

Butterfield, S., Musial, W., Jonkman, J., Sclavounos, P., and Wayman, L. (2005). Engineering challenges for floating offshore wind turbines. In *Copenhagen Offshore Wind 2005 Conference and Expedition Proceedings, 26–28 October 2005, Copenhagen, Denmark*.

Colwell, S. and Basu, B. (2009). Tuned liquid column dampers in offshore wind turbines for structural control. *Engineering Structures*, 31(2):358–368.

Gao, H., Kwok, K., and Samali, B. (1997). Optimization of tuned liquid column dampers. *Engineering structures*, 19(6):476–486.

Jonkman, J. (2007). *Dynamics modeling and loads analysis of an offshore floating wind turbine*. PhD thesis, Department of Aerospace Engineering Sciences, University of Colorado.

Jonkman, J. and Buhl Jr, M. (2005). Fast users guide. Technical report, NREL/EL-500-29798. Golden, Colorado: National Renewable Energy Laboratory.

Jonkman, J. and Matha, D. (2009). A quantitative comparison of the responses of three floating platform concepts. In *European Offshore Wind 2009 Conference & Exhibition*, pages 14–16.

Lackner, M. A. (2012). An investigation of variable power collective pitch control for load mitigation of floating offshore wind turbines. *Wind Energy*, 16(3):435 – 444.

Lackner, M. A. and Rotea, M. A. (2011a). Passive structural control of offshore wind turbines. *Wind Energy*, 14(3):373–388.

Lackner, M. A. and Rotea, M. A. (2011b). Structural control of floating wind turbines. *Mechatronics*, 21(4):704 – 719.

Namik, H. and Stol, K. (2010). Individual blade pitch control of floating offshore wind turbines. *Wind Energy*, 13(1):74–85.

Si, Y., Karimi, H. R., and Gao, H. (2014). Modelling and optimization of a passive structural control design for a spar-type floating wind turbine. *Engineering Structures, to appear.*

Skaare, B., Hanson, T., and Nielsen, F. (2007). Importance of control strategies on fatigue life of floating wind turbines. In *Proceedings of the 26th International Conference on Offshore Mechanics and Arctic Engineering.* ASME.

Stewart, G. and Lackner, M. A. (2012). Optimization of a passive tuned mass damper for reducing loads in offshore wind turbines. *IEEE Transactions on Control Systems Technology: Special Issue on Wind Energy.*

PAPER D

GAIN SCHEDULING H_2/H_∞ STRUCTURAL CONTROL OF A FLOATING WIND TURBINE

Yulin Si, Hamid Reza Karimi

This paper has been published as:

Y. Si, H. R. Karimi, "Gain scheduling H_2/H_∞ structural control of a floating wind turbine", *Proceedings of the 19th World Congress of the International Federation of Automatic Control*, Cape Town, South Africa, 24-29 August, 2014.

Gain Scheduling H_2/H_∞ Structural Control of a Floating Wind Turbine

Yulin Si, Hamid Reza Karimi
Department of Engineering
Faculty of Engineering and Science, University of Agder
Jon Lilletunsvei 9, 4879 Grimstad, Norway.

Abstract — **For wind turbine load mitigation, this paper proposes an active structural control deign of a hybrid mass damper installed at the tower top of a spar-type floating wind turbine. System dynamic model is established based on first principles and the polynomial curve fitting approach, while different steady-state points are derived. Then, a gain scheduling H_2/H_∞ state feedback controller is designed by solving linear matrix inequalities, which aims to reduce the loading. At last, nonlinear simulations are performed under different wind and wave conditions, and the results demonstrate that more load reduction could be achieved at the expense of more energy consumption in mass damper actuator.**

Keywords — Floating wind turbine, dynamic modelling, structural control, hybrid mass damper (HMD), H_2/H_∞ control design, gain scheduling, linear matrix inequality (LMI)

1 Introduction

Floating offshore wind turbine has been a hot topic in wind energy exploration during the past few years. It provides the opportunities of cheap and clean power supply for those highly populated places near to deep offshore, such as coastal cities in the US, Spain, Japan, Korea, and Norway, see (Breton and Moe, 2009).

There are many engineering challenges in developing floating windmills, see (Butterfield et al., 2005), among which the key difficulty lies in the additional loads caused by extra degrees of freedom (DOFs) of floating platforms. Different methods have been proposed to mitigate the fatigue and ultimate loading of tower and blades for floating wind turbines. One idea is to improve the blade pitch control strategy in order to avoid negative damping or even provide active damping of platform tilt motion, such as the works in (Larsen and Hanson, 2007; Namik and Stol, 2010; Lackner, 2012). In contrast, this work focuses on another approach, which proposes to install structural vibration control devices either in the nacelle or platform of floating wind turbines for direct load reduction. This method has been successfully used in civil engineering applications, such as vibration inhibition of buildings and bridges, see (Korkmaz, 2011).

In 2008, the authors in (Murtagh et al., 2008) investigated the use of a tuned mass damper (TMD) placed at the tower top of a simplified wind turbine model for vibration mitigation. Following the same installation idea, Colwell et al. explored the structural responses of a fixed-bottom offshore wind turbine with a tuned liquid column damper (TLCD), see (Colwell and Basu, 2009). However, these discussions are only about fixed-bottom wind turbines, while their intrinsic dynamics are quite different from that of floating types. Besides, these works are not based on the cutting edge high-fidelity codes, which may not capture the comprehensive coupled nonlinear dynamics of wind turbines. Later, based on the aero-hydro-servo-elastic wind turbine numerical simulator FAST (fatigue, aerodynamics, structures, and turbulence), see (Jonkman and Buhl Jr, 2005), Lackner et al. implemented a new simulation tool, called FAST-SC, for passive, semi-active, and active structural control design of wind turbines, see (Lackner and Rotea, 2011a). The code incorporates extra DOFs of structural control devices which are installed either in wind turbine nacelle or platform (if floating) into the state-of-the-art wind turbine simulator FAST. Utilizing this code, Lackner et al. presented more realistic simulation results by installing a TMD in the nacelle of both a barge-type and a monopile supported wind turbines, see (Lackner and Rotea, 2011a). For more compre-

hensive parametric study, they also established a 3-DOF dynamic model for different types of floating wind turbines based on first principles, see (Stewart and Lackner, 2013), and TMD parameters are determined under different optimization methods. However, the coupling between platform surge and pitch motion was not captured in their model. This effect can be ignored for the barge model but might be a strong mode for other platforms (Namik and Stol, 2011; Jonkman, 2010). Si et al. then improved the model by incorporating platform surge and heave modes when considering a spar-type floating wind turbine, see (Si et al., 2013, 2014), but still aerodynamic load has not been considered yet, which is necessary to determine different steady states. Compared with passive design, recent research results showed that more load reduction could be achieved when introducing active structural control. In (Lackner and Rotea, 2011b), H_∞ multi-variable loop shaping technique was utilized for active feedback structural control design of a barge-type floating wind turbine. The actuator dynamics and control-structure interaction in active control were also considered in (Stewart and Lackner, 2011). Nevertheless, the 3-DOF model in these works still did not include either platform surge mode or wind loads. Therefore, better modelling and control techniques are in demand to improve and verify this design.

This work will discuss the modelling and control design for load mitigation of a spar-type floating wind turbine, where a hybrid mass damper (HMD) is installed in the nacelle. Section 2 presents the modelling improvement by introducing aerodynamic thrust and approximating the nonlinearities in hydrodynamic and mooring loads. After linearization, a gain scheduling state-feedback H_2/H_∞ structural controller is designed in Section 3. Then, FAST-SC simulation results based on the proposed design is given in Section 4. Conclusions are drawn in the last section.

2 Dynamic Modelling

In 2009, one Norwegian company Statoil developed the world first full scale experimental floating wind turbine “Hywind”. In cooperation with Statoil,

Jonkman from the National Renewable Energy Laboratory (NREL) specified a detailed model for OC3-Hywind spar, which combines the data of the 5MW baseline wind turbine from NREL and the Hywind spar from Statoil, see Table D.1.

Table D.1: Properties of the 5MW OC3-Hywind model according to (Jonkman, 2010; Jonkman et al., 2009).

Item	Value
Rating	5 MW
Rotor configuration	Upwind, 3 blades
Cut-in, rated, cut-out wind speed	3 m/s, 11.4 m/s, 25 m/s
Total draft below sea water level (SWL)	120 m
Tower base above SWL	10m
Hub height above SWL	90m
Nacelle dimension (length, width, height)	14.2m, 2.3m, 3.5m
Platform diameter above taper	6.5m
Platform diameter below taper	9.4m
Rotor nacelle assembly (RNA) mass	350,000kg
Tower mass	249,718 kg
Platform mass	7,466,000 kg
Number of mooring lines	3
Depth to fairleads below SWL	70m
Baseline control in Region 3	GSPI and constant torque

The structural control idea in this work is illustrated in Figure D.1, where an HMD is installed in the nacelle of OC3-Hywind. The HMD consists of a TMD with mass M, spring and damping constants K and D, and an actuator acting force F on the mass. Since FAST-SC does not support model linearization yet, establishing the dynamic model is considered as a good option to facilitate parameter tuning and control design.

2.1 Overall Longitudinal Dynamics

Based on the D'Alembert's principle of inertial forces, the following longitudinal model can be established as follows, see (Si et al., 2013).

$$\mathbf{M}(\mathbf{q})\ddot{\mathbf{q}} + \mathbf{L}(\mathbf{q}, \dot{\mathbf{q}}) = \mathbf{F}, \tag{D.1}$$

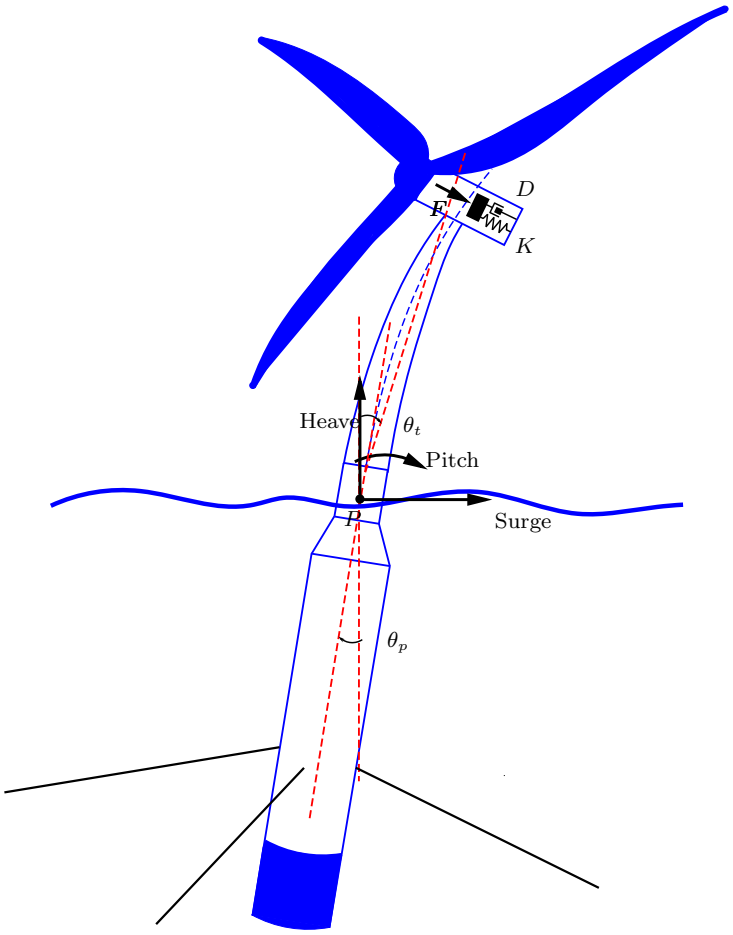

Figure D.1: Illustration of the active structural control of OC3-Hywind.

where

$$\mathbf{q} = \begin{bmatrix} x_{sg} \\ x_{hv} \\ \theta_p \\ x_{hmd} \\ \theta_t \end{bmatrix}, \ \mathbf{M}(\mathbf{q}) = \begin{bmatrix} M_{sg}^{sg} & 0 & I_{sg}^{p} & M_{sg}^{hmd} & 0 \\ 0 & M_{hv}^{hv} & I_{hv}^{p} & M_{hv}^{hmd} & 0 \\ M_{p}^{sg} & M_{p}^{hv} & I_{p}^{p} & M_{p}^{hmd} & 0 \\ M_{hmd}^{sg} & M_{hmd}^{hv} & I_{hmd}^{p} & M_{hmd}^{hmd} & 0 \\ M_{t}^{sg} & M_{t}^{hv} & 0 & M_{t}^{hmd} & I_{t}^{t} \end{bmatrix},$$

$$\mathbf{L}(\mathbf{q}, \dot{\mathbf{q}}) = \begin{bmatrix} F_{sg}^{hdr} + F_{sg}^{moor} + F_{sg}^{ctr} + F_{sg}^{wnd} \\ F_{hv}^{gr} + F_{hv}^{hdr} + F_{hv}^{moor} + F_{hv}^{ctr} + F_{hv}^{wnd} \\ \tau_{p}^{gr} + \tau_{p}^{hdr} + \tau_{p}^{moor} + \tau_{p}^{ctr} + \tau_{p}^{wnd} \\ F_{hmd}^{gr} + F_{hmd}^{hmd} \\ \tau_{t}^{gr} + \tau_{t}^{p} + \tau_{t}^{ctr} + \tau_{t}^{wnd} \end{bmatrix}, \mathbf{F} = \begin{bmatrix} 0 \\ 0 \\ 0 \\ F \\ 0 \end{bmatrix}.$$

In this model, $\mathbf{q}$ is the state vector, and sg, hv, p, hmd, t represent, respectively, the enabled 5 DOFs, i.e. platform surge, heave, pitch motion about P, HMD translation, and tower deflection. $\mathbf{M}(\mathbf{q})$ is the system inertial matrix, which is positive definite.M_i^j and I_i^j denote generalized mass and generalized inertial tensor for DOF i with regard to DOF j. $\mathbf{L}(\mathbf{q}, \dot{\mathbf{q}})$ represents external loads, and gr, hdr, $moor$, ctr, wnd describe, respectively, gravitational, hydro, mooring, centripetal, aerodynamic loads in forces or moments.

However, the aerodynamic load was not characterized in (Si et al., 2013, 2014), where hydrodynamic and mooring loads were approximated by linear or quadratic terms around zero-displacement position. It is shown in (Jonkman, 2010) that there will exist strong hydrodynamic and mooring nonlinearities if the wind turbine is blown far away from its initial position, thus better representation of these loads is needed.

2.2 Hydrodynamic Loads

The nonlinearity of hydrodynamic loads mainly come from platform viscous drag, and it was approximated by linear and quadratic terms in (Si et al., 2013, 2014) as shown in Figure D.2. However, in later model verification process,

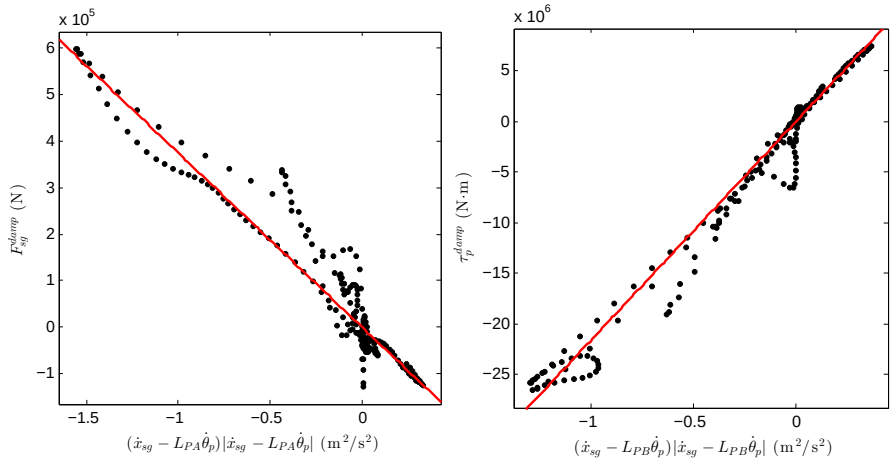

Figure D.2: Quadratic curve fitting result of drag force and its induced torque around P

it is found that this hydro damping approximation is not accurate enough to

govern system dynamics. The inaccuracy is also noticeable as the fitting errors in the above figure. In this work, 3-order polynomials are used to approximate this nonlinear behaviour, which are given by

$$\begin{aligned} F_{sg}^{damp} &= a_1\dot{x}_{sg} + a_2\dot{x}_{sg}^2 + a_3\dot{x}_{sg}^3 + a_4\dot{\theta}_p, \\ \tau_p^{damp} &= b_1\dot{x}_{sg} + b_2\dot{x}_{sg}^2 + b_3\dot{x}_{sg}^3 + b_4\dot{\theta}_p. \end{aligned} \tag{D.2}$$

The fitting results are shown in Figure D.3, which are surprisingly much better than previous guess.

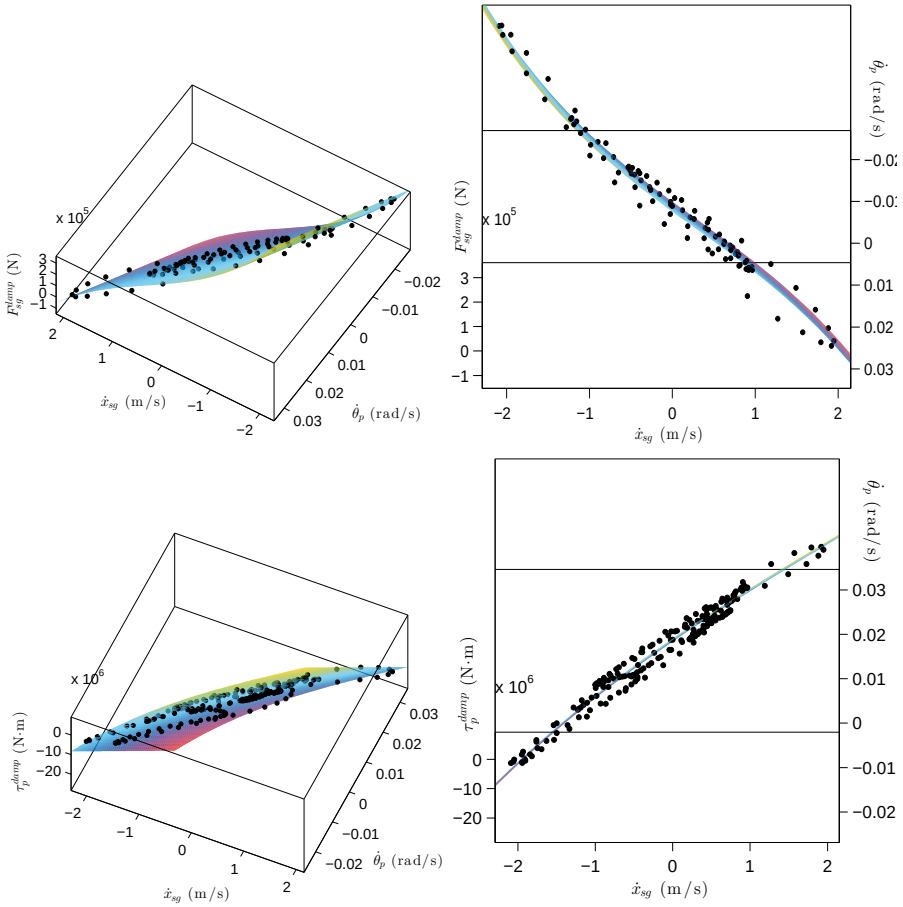

Figure D.3: Polynomial approximation result of viscous drag force and its induced torque around P.

2.3 Mooring Loads

FAST simulator uses a quasi-static model to calculate the load of an individual mooring line, which exhibits nonlinear behaviors due to both mooring dynamics and asymmetry of the three-point mooring system. The nonlinear relationship between mooring loads and platform motion are meshed in Figure D.4.

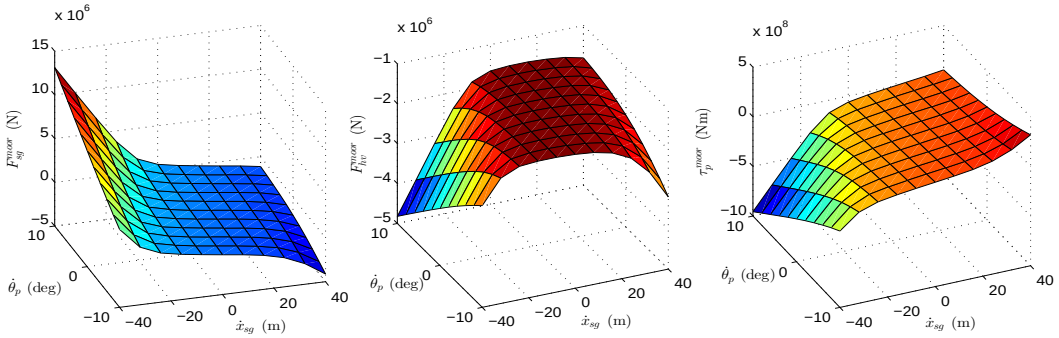

Figure D.4: Load-displacement relationships for the OC3-Hywind mooring system (Jonkman, 2010).

Regarding mooring system, one idea easily comes to mind that the variation of mooring loads could be determined by the surge displacement of fairleads,

$$x_{sg}^{fair} = x_{sg} - L_{moor}\theta_p. \tag{D.3}$$

In order to verify this idea, mooring loads for different displacement of platform surge, heave, pitch are extracted from FAST, and the relationship between fairlead displacement in surge direction and mooring loads are demonstrated in Figure D.5. Obviously, they are almost smooth curves, thus it is possible to use polynomials to approximate this functional relationship. It needs noting that the three-line mooring system also brings asymmetry to the load-displacement relationship, so that it is more proper to use two separate polynomials in the curve fitting process. Considering fitting accuracy, the separation point is located at -20m of fairlead surge displacement. As also shown in Figure D.5, perfect curve fitting results can be achieved , and the polynomials for F_{sg}^{moor}

and F_{hv}^{moor} are expressed as

$$\begin{aligned} F_{sg}^{moor} &= c_1(x_{sg}^{fair}) + c_2(x_{sg}^{fair})^2 + c_3(x_{sg}^{fair})^3, \\ F_{hv}^{moor} &= d_1(x_{hv}^{fair})^2 + d_2(x_{sg}^{fair})^3 + d_3(x_{sg}^{fair})^4. \end{aligned} \tag{D.4}$$

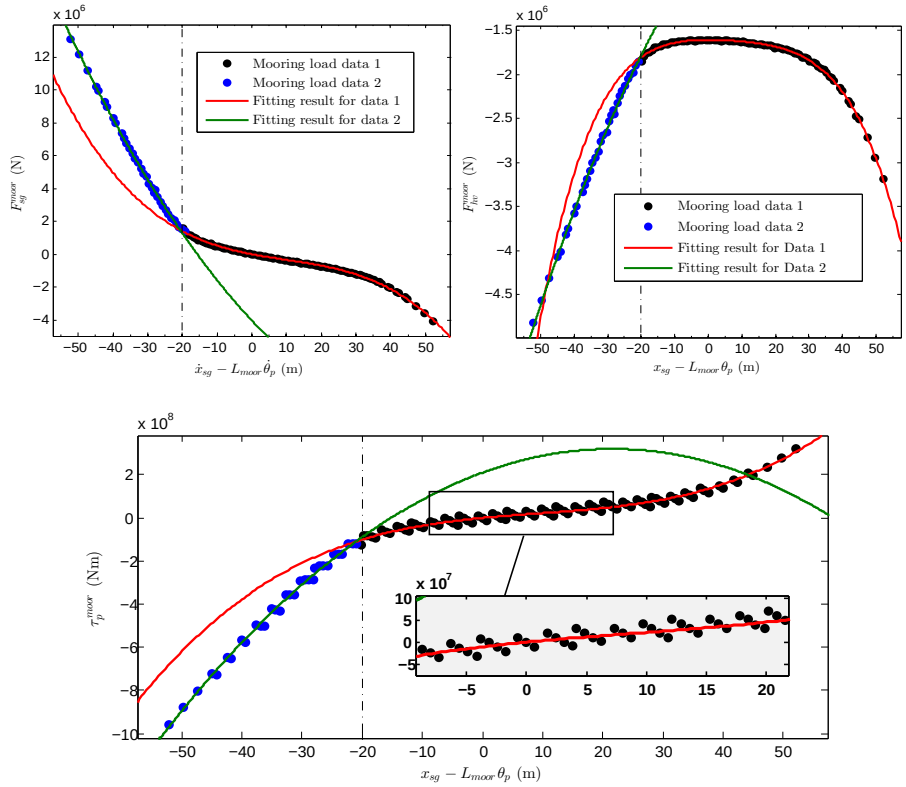

Figure D.5: Relationship approximation between mooring loads for system surge/heave/pitch modes and fairlead surge displacement.

However, when it comes to mooring torque for platform pitch motion, the assumed functional relationship is not valid, which has been amplified in Figure D.5. This is because not only fairlead surge, but also platform pitch will affect the mooring torque. Therefore, θ_p needs to be considered in the curve fitting process for τ_p^{moor}. The proposed approximation is described as

$$\tau_p^{moor} = e_1(x_{sg}^{fair}) + e_2(x_{sg}^{fair})^2 + e_3(x_{sg}^{fair})^3 + e_4\theta_p, \tag{D.5}$$

and the effectiveness could then be seen in Figure D.6.

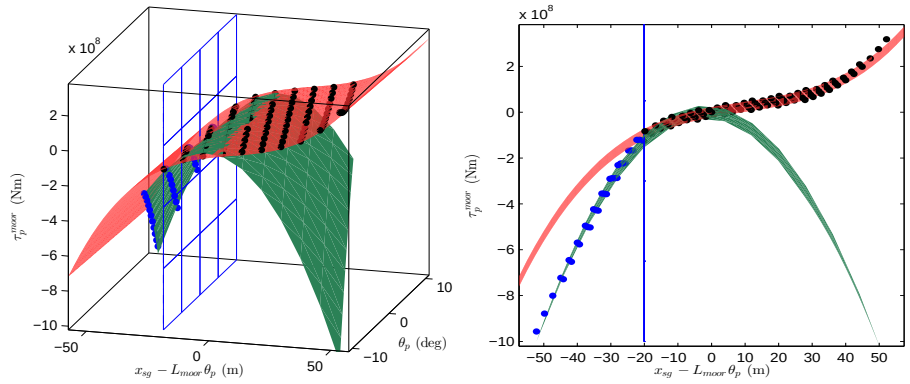

Figure D.6: Relationship among mooring torque around P, fairlead surge displacement, and platform pitch angle.

2.4 Aerodynamic Loads

According to (Jonkman, 2007), the dominant component of wind turbine aerodynamic loads is the aerodynamic rotor thrust T, which can be represented as the sum of a constant rotor thrust and the aerodynamic damping. After the first-order Taylor series expansion, the expression of T will be expressed as

$$T = T_0 - \left.\frac{\partial T}{\partial \theta_t}\right|_V \dot{\theta}_t, \tag{D.6}$$

where T_0 is the aerodynamic rotor thrust at a steady state point. V is the rotor-disk-averaged wind speed, and θ_t denotes the tower tilt angle.

It needs noting that either steady-state aerodynamic thrust T_0 or thrust sensitivity to wind speed $\frac{\partial T}{\partial \theta_t}$ depends on hub-height wind speed, rotor rotation speed, and blade pitch angle, thus listing the relationships among these factors at different steady states is necessary. Table D.2 gives different steady states with varying wind speeds, where T_0 and $\left.\frac{\partial T}{\partial \theta_t}\right|_V$ need to be estimated.

2.5 Model Verification

In the verification process, generator torque and blade pitch control are both disabled, and the rotor speed and blade pitch angle are set as constant for each equilibrium point. T_0 and $\left.\frac{\partial T}{\partial \theta_t}\right|_V$ are estimated for each equilibrium point. The identification results with previous load approximation are satisfactory, e.g.,

the 8m/s case is shown in Figure D.7.

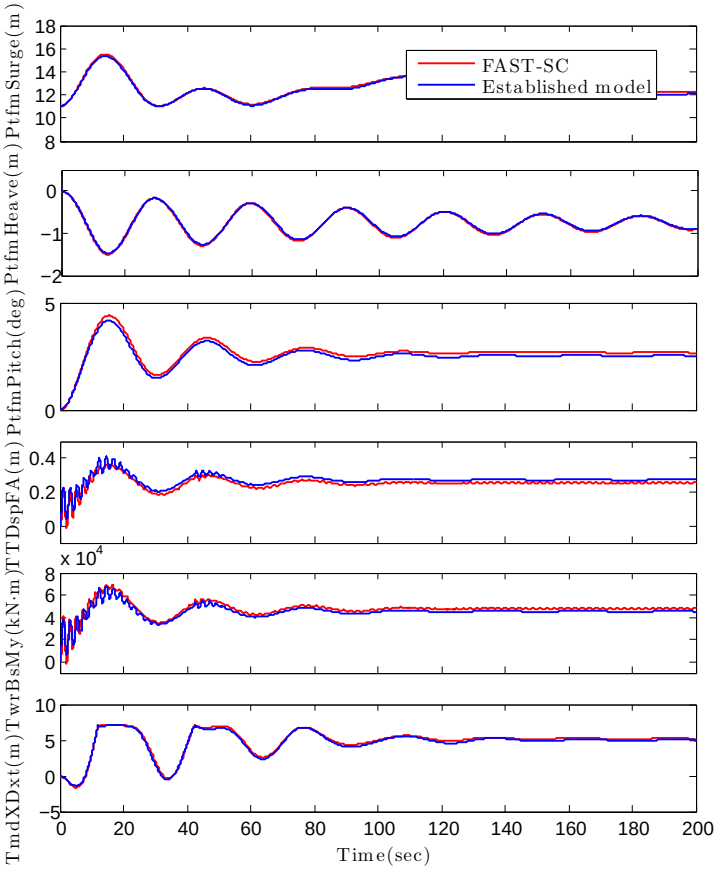

Figure D.7: Dynamic response comparison with wind load approximation.

3 Gain Scheduling H_2/H_∞ Control Design

3.1 Model Linearization

Based on small deviation approximation, the model around each equilibrium point can be linearized into the following state-space representation,

$$\begin{cases} \dot{x} = Ax + Bu \\ z = Cx \end{cases}, \tag{D.7}$$

Table D.2: OC3-Hywind 5MW turbine steady-state points under different wind speeds.

V (m/s)	ω (RPM)	θ_b (°)	x_{sg} (m)	x_{hv} (m)	θ_p (°)	T_0 (10^5 N)	$\frac{\partial T}{\partial V}$ (10^6 N·s)
3.0	6.97	0.00	2.44	-0.02	0.47	0.7414	2.9428
4.0	7.18	0.00	3.90	-0.04	0.79	1.1733	3.1436
5.0	7.50	0.00	5.67	-0.07	1.15	1.6817	3.4245
6.0	7.92	0.00	7.72	-0.10	1.58	2.2563	3.8583
7.0	8.43	0.00	10.02	-0.14	2.05	2.8900	4.5637
8.0	9.07	0.00	12.67	-0.20	2.59	3.6172	5.3733
9.0	10.17	0.00	16.09	-0.29	3.28	4.5504	5.9377
10.0	11.27	0.00	19.85	-0.41	4.03	5.5921	6.5443
11.0	11.84	0.00	23.28	-0.53	4.73	6.5711	7.1261
12.0	12.10	2.96	21.31	-0.44	4.33	6.0740	8.0656
13.0	12.10	6.19	17.89	-0.35	3.66	5.1049	8.9981
14.0	12.10	8.34	16.04	-0.29	3.29	4.5911	9.5531
15.0	12.10	10.21	14.67	-0.25	3.01	4.1898	9.9529
16.0	12.10	11.84	13.60	-0.22	2.80	3.8990	10.2480
17.0	12.10	13.34	12.75	-0.20	2.64	3.6610	10.4610
18.0	12.10	14.73	12.05	-0.18	2.50	3.4804	10.4800
19.0	12.10	16.05	11.47	-0.16	2.39	3.3292	10.3800
20.0	12.10	17.34	10.95	-0.14	2.29	3.1847	10.2720
21.0	12.10	18.60	10.51	-0.12	2.20	3.0691	10.0460
22.0	12.10	19.83	10.13	-0.11	2.13	2.9717	9.7724
23.0	12.10	21.02	9.79	-0.10	2.06	2.8791	9.5400
24.0	12.10	22.19	9.49	-0.08	2.01	2.7977	9.4149
25.0	12.10	23.31	9.23	-0.07	1.96	2.7326	9.4154

where $x = \left[\dot{x}_{sg}, \dot{x}_{hv}, \dot{\theta}_p, \dot{x}_{hmd}, \dot{\theta}_t, x_{sg}, x_{hv}, \theta_p, x_{hmd}, \theta_t \right]^T$ is the state vector. It includes the velocity and displacement of platform surge, heave, pitch, HMD mass translation, as well as tower pitch motion. $u = F$ is the control input, and $z = \theta_p - \theta_t$ is the controlled output.

3.2 H_2/H_∞ Control Design

Similar to (D.7), consider the linear system around a certain setpoint

$$\begin{cases} \dot{x} = Ax + Bu + B_w w \\ z = Cx \end{cases}, \tag{D.8}$$

where w is the aerodynamic disturbance acting on the rotor. We would like to design a state feedback controller $u = Kx$ that keeps the closed-loop system

$$\begin{cases} \dot{x} = (A + BK)x + B_w w \\ z = Cx \end{cases} \tag{D.9}$$

asymptotically stable and improves the dynamic performance of the closed-loop system simultaneously. More specifically, regarding performance improvement, the controller should keep the closed-loop system robust to disturbance w, i.e. the H_∞ norm of the transfer function T_{wz} in the closed-loop system does not exceed a given upper bound γ_1. More importantly, the H_2 norm of T_{wz} should be as small as possible (e.g. less than γ_2) so that the vibration energy of tower top deflection will be reduced.

Therefore, this problem is equivalent to a mixed H_2/H_∞ control design, see (Scherer, 1995; Doyle et al., 1994), and the design objective is to determine a desired state feedback gain K such that the closed-loop system is asymptotically stable and γ_2 is minimal for the controllers such that

$$\|T_{wz}\|_\infty < \gamma_1, \|T_{wz}\|_2 < \gamma_2.$$

The following theorem helps to convert the H_2/H_∞ control design problem into an optimization process for several linear matrix inequalities (LMIs). It is then more convenient to solve by using well developed LMI toolbox.

Theorem 1. *For the closed-loop system (D.9), if there exists a given* $\gamma_1 > 0$

and the following LMIs have an optimal solution,

$$\begin{aligned} & & & & \min \gamma_2 \\ s.t. & \begin{bmatrix} AX+BW+(AX+BW)^T & B_w & (CX)^T \\ B_w^T & -\gamma_1 I & 0 \\ CX & 0 & -\gamma_1 I \end{bmatrix} < 0 \\ & AX+BW+(AX+BW)^T + B_w B_w^T < 0 \\ & \begin{bmatrix} -Z & CX \\ (CX)^T & -X \end{bmatrix} < 0 \\ & Trace(Z) < \gamma_2 \end{aligned} \quad , \tag{D.10}$$

where $X = X^T > 0$, $Z = Z^T > 0$ and W are matrices of appropriate dimensions, then the state feedback H_2/H_∞ control design is feasible, and the control law is

$$u = WX^{-1}x. \tag{D.11}$$

3.3 Gain Scheduling

It is possible to design a controller for each steady-state point, but controller switching will be frequent and when to switch becomes a problem. Therefore, these setpoints are categorized in 7 intervals, which are determined by rotor speed and blade pitch angle, which are possible to obtain from a wind turbine.

3.4 Low Pass Filter

The control force has to pass a second order low pass filter,

$$G(s) = \frac{\omega^2}{s^2 + 2\zeta\omega s + \omega^2},$$

which represents the actuator dynamics. Here $\omega = 10$ rad/s and ζ=0.5.

4 Simulation Analysis

In this section, based on the control design, fully nonlinear simulations are performed in FAST-SC with all wind turbine DOFs enabled. Each test runs 630 seconds, and the output data in first 30s are not recorded, waiting for generator torque and blade pitch motion arriving normal operation state. The modified generator torque and blade pitch controller from NREL is used in the form of a dynamic link library for all tests (Jonkman, 2010).

In total, we consider two different simulation scenarios. The wind and wave conditions in (Lackner and Rotea, 2011b) are adopted as two cases in this experiment. For wind condition, the mean value of the turbulent wind is defined as 10 m/s and 18 m/s respectively. The turbulent wind file is generated by TurbSim, where Kaimal spectra and the power law exponent of 0.14 are used according to the IEC61400-3 offshore wind turbine design standard. The normal turbulence intensity is set as level B, i.e. 18% (10 m/s case) and 15%(18 m/s case). For wave condition, JONSWAP spectrum is utilized to generate the stochastic wave inputs. The significant wave height is set as 2.3 m (10 m/s case) and 3.7 m (18 m/s case), and the peak spectral period is defined as 14s. For each case, at least two sets of random variables are used to generate wind and wave data.

According to the parameter study in (Si et al., 2013; Stewart and Lackner, 2013), the property of the hybrid mass damper on tower top is chosen as follows, which matches first tower fore-aft vibration mode.

Table D.3: Property of the hybrid mass damper in simulation.

Mass m	Spring constant K	Damping constant D
$20,000$ kg	$120,000$ N/m	$16,000$ N/(m/s)

Nonlinear simulation results for tower bottom load reduction can be seen in Table D.4. Compared with the passive case, more load reduction can be achieved with the designed controller. One simulation comparison is illustrated in Figure D.8. $TwrBsMxt$ and $TwrBsMyt$ denote side-side and fore-aft tower base

bending moment, respectively. TmdXDxt is the HMD displacement, and TmdXFext is the actuating force. However, this load reduction improvement is based on more energy consumption in HMD, and it could also be risky for instability.

Table D.4: Percentage of load reduction for passive and active structural control (%)

Case	Term	Passive	Active
10m/s	DEL tower fore-aft bending	9.7	12.7
	DEL tower side-side bending	35.1	40.3
	95th tower fore-aft bending	4.1	2.57
	95th tower side-side bending	11.7	11.4
18m/s	DEL tower fore-aft bending	4.1	6.5
	DEL tower side-side bending	32.4	42.25
	95th tower fore-aft bending	0.3	0.2
	95th tower side-side bending	14.9	19.3

5 Conclusion

This paper dealt with a gain scheduling H_2/H_∞ active structural control deign for a hybrid mass damper installed at the tower top of the OC3-Hywind floating wind turbine. Firstly, system dynamic model was improved based on polynomial curve fitting approach, and different steady-state points were derived. Then, a gain scheduling H_2/H_∞ state feedback controller was designed by solving linear matrix inequalities, which aimed to reduce the tower bottom loads. At last, nonlinear simulations were performed under different wind and wave conditions, and the results demonstrated that more load reduction could be achieved at the expense of more energy consumption.

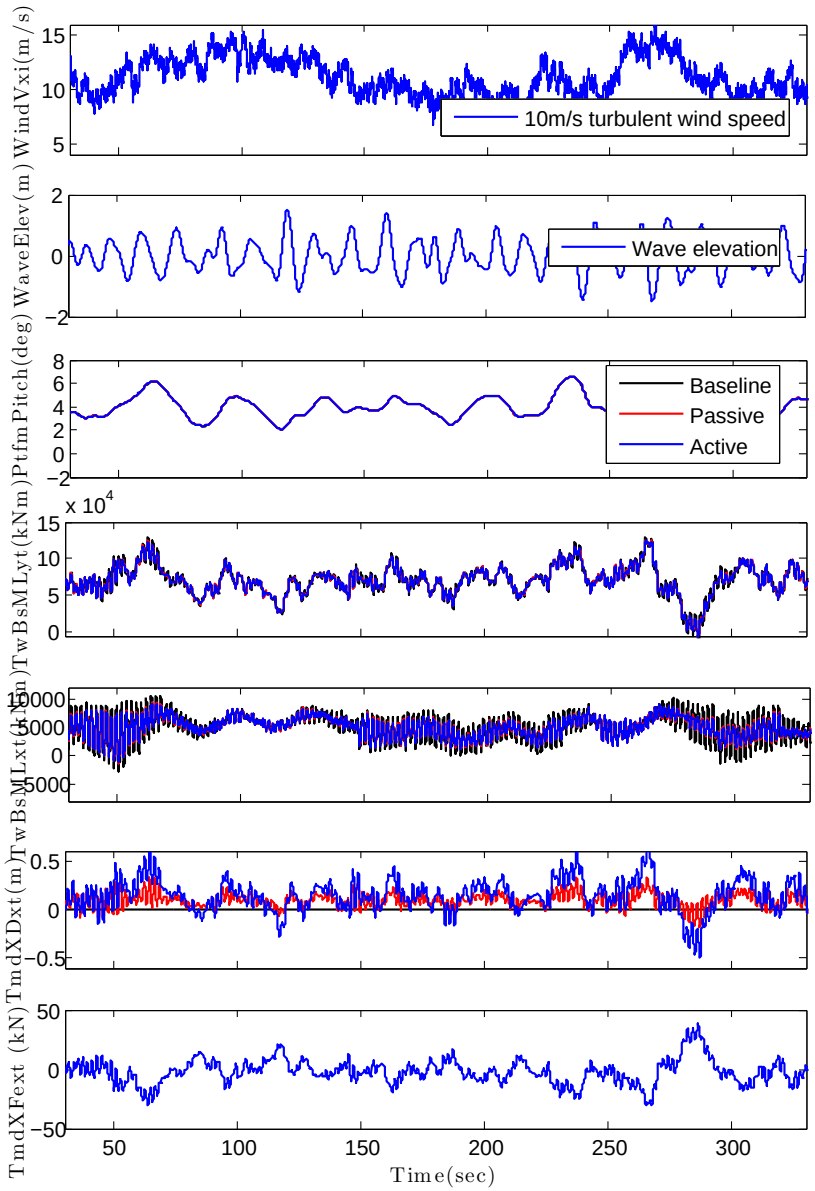

Figure D.8: Nonlinear simulation comparison under 10m/s turbulent wind and 2.3m wave.

REFERENCES

Breton, S. P. and Moe, G. (2009). Status, plans and technologies for offshore wind turbines in europe and north america. *Renewable Energy*, 34(3):646 – 654.

Butterfield, S., Musial, W., Jonkman, J., Sclavounos, P., and Wayman, L. (2005). Engineering challenges for floating offshore wind turbines. In *Copenhagen Offshore Wind 2005 Conference and Expedition Proceedings, 26–28 October 2005, Copenhagen, Denmark*.

Colwell, S. and Basu, B. (2009). Tuned liquid column dampers in offshore wind turbines for structural control. *Engineering Structures*, 31(2):358–368.

Jonkman, J. (2007). *Dynamics modeling and loads analysis of an offshore floating wind turbine*. PhD thesis, Department of Aerospace Engineering Sciences, University of Colorado.

Jonkman, J. (2010). Definition of the floating system for phase iv of oc3. *NREL/TP-500-38060. Golden, Colorado: National Renewable Energy Laboratory*.

Jonkman, J. and Buhl Jr, M. (2005). Fast users guide. Technical report, NREL/EL-500-29798. Golden, Colorado: National Renewable Energy Laboratory.

Jonkman, J., Butterfield, S., Musial, W., and Scott, G. (2009). Definition of a 5-mw reference wind turbine for offshore system development. Technical report, NREL/TP-500-47535. Golden, Colorado: National Renewable Energy Laboratory.

Korkmaz, S. (2011). A review of active structural control: challenges for engineering informatics. *Computers & Structures*, 89:2113 – 2132.

Lackner, M. A. (2012). An investigation of variable power collective pitch control for load mitigation of floating offshore wind turbines. *Wind Energy*, 16(3):435 – 444.

Lackner, M. A. and Rotea, M. A. (2011a). Passive structural control of offshore wind turbines. *Wind Energy*, 14(3):373–388.

Lackner, M. A. and Rotea, M. A. (2011b). Structural control of floating wind turbines. *Mechatronics*, 21(4):704 – 719.

Larsen, T. J. and Hanson, T. D. (2007). A method to avoid negative damped low frequent tower vibrations for a floating, pitch controlled wind turbine. *Journal of Physics: Conference Series*, 75(1).

Murtagh, P. J., Ghosh, A., Basu, B., and Broderick, B. M. (2008). Passive control of wind turbine vibrations including blade/tower interaction and rotationally sampled turbulence. *Wind Energy*, 11(4):305–317.

Namik, H. and Stol, K. (2010). Individual blade pitch control of floating offshore wind turbines. *Wind Energy*, 13(1):74–85.

Namik, H. and Stol, K. (2011). Performance analysis of individual blade pitch control of offshore wind turbines on two floating platforms. *Mechatronics*, 21(4):691 – 703.

Si, Y., Karimi, H. R., and Gao, H. (2013). Modeling and parameter analysis of the oc3-hywind floating wind turbine with a tuned mass damper in nacelle. *Journal of Applied Mathematics*, page 679071.

Si, Y., Karimi, H. R., and Gao, H. (2014). Modelling and optimization of a passive structural control design for a spar-type floating wind turbine. *Engineering Structures, to appear*.

Stewart, G. M. and Lackner, M. A. (2011). The effect of actuator dynamics on active structural control of offshore wind turbines. *Engineering Structures*, 33(5):1807 – 1816.

PAPER E

OBSERVER-BASED GUARANTEED COST STRUCTURAL CONTROL FOR AN OFFSHORE FLOATING WIND TURBINE

Yulin Si, Hamid Reza Karimi

This paper has been published as:

Y. Si, H. R. Karimi, "Observer-based guaranteed cost structural control for an offshore floating wind turbine", *Proceedings of the 6th World Conference on Structural Control and Monitoring*, Barcelona, Spain, 15–17 July, 2014.

Observer-based Guaranteed Cost Structural Control for an Offshore Floating Wind Turbine

Yulin Si, Hamid Reza Karimi
Department of Engineering
Faculty of Engineering and Science, University of Agder
Jon Lilletunsvei 9, 4879 Grimstad, Norway.

Abstract — **Deep water floating wind turbine has to suffer from severe structural loads due to extra degrees of freedom, while the commonly used structural control methods in civil engineering could provide a solution for load reduction. Due to the limited sensor data from wind turbines, this paper deals with an observer-based guaranteed cost structural control design for a spar-type floating wind turbine, where an hybrid mass damper (HMD) is assumed to be installed on top of the turbine tower. Firstly, the 5-DOF mathematical model for wind turbine surge-heave-pitch motion is presented, and the linear state-space expressions are also obtained for different equilibrium points. Secondly, an observer is designed based on the sensor data for platform pitch angle, tower top and HMD displacement. Then, an observer-based guaranteed cost structural control strategy is developed aiming for load reduction. Finally, high fidelity nonlinear simulations with the proposed design are conducted under different wind and wave conditions. Simulation results demonstrate the designed observer manages to estimate the system states and the designed guaranteed cost controller will help to achieve more load reduction than the passive case.**

1 Introduction

Offshore wind energy has attracted great worldwide attention in recent years (Musial et al., 2006), while strong potentials have been found in deep sea areas in many places, such as the coastal lines of the United States, north Europe, and east Asia. In deep sea areas, floating foundations are considered to be an economical and applicable choice to support the turbines, but the big challenge for floating windmills compared with fixed bottom installations is the extra platform motion, which will heavily increase the load on turbine structure due to the high inertial and gravitational forces or even cause the failure of turbine control strategy (Jonkman, 2007). According to (Jonkman and Matha, 2009), when comparing a spar-type floating wind turbine with an onshore design, the sea-to-land ratio of fatigue damage equivalent loads (DEL) with respect to fore-aft tower base bending moments is 2.5, and the number has reached 7 for the barge-type, thus special mechanical design or advanced control technique is required to improve wind turbine reliability. Therefore, effective load reduction methods are needed for the design of floating wind turbines. Among different approaches for load mitigation, structural control (Korkmaz, 2011) has offered a direct solution to dynamically compensate the vibrations of turbine structures and reduce their loads.

In (Murtagh et al., 2008), Murtagh et al. investigated the use of a tuned mass damper (TMD) placed at the tower top of a simplified wind turbine model for vibration mitigation. Following the same installation idea, Colwell et al. explored the structural responses of a fixed bottom offshore wind turbine with a tuned liquid column damper (TLCD) (Colwell and Basu, 2009). Later, Mensah et al. assessed the reliability of this idea (Mensah and Dueñas-Osorio, 2012). Moreover, Li et al. performed an experimental study on an offshore wind turbine with a ball vibration absorber fixed on top of the nacelle (Li et al., 2012). However, these discussions are about vibration mitigation of fixed-bottom wind turbines, while their motion dynamics are quite different from that of floating wind turbines. Besides, these works are not based on the cutting edge high-fidelity codes for wind turbine models, which may not capture the comprehensive coupled nonlinear dynamics of wind turbines.

Based on the aero-hydro-servo-elastic wind turbine numerical simulator FAST (fatigue, aerodynamics, structures, and turbulence) (Jonkman and Buhl Jr, 2005), Lackner et al. implemented a new simulation tool, called FAST-SC, for passive, semi-active, and active structural control design of wind turbines (Lackner and Rotea, 2011a), which has incorporated TMDs into the nacelle or platform of wind turbines for load mitigation. Utilizing this code, Lackner et al. presented more realistic simulation results by installing a TMD in the nacelle of both a barge-type and a monopile supported wind turbines, and a simple parametric study was also performed to determine the TMD parameters (Lackner and Rotea, 2011a). It was shown more load reduction could be achieved when introducing active structural control, such as the multi-variable H_∞ control with a loop-shaping technique (Lackner and Rotea, 2011b). The actuator dynamics and control-structure interaction were also considered in (Stewart and Lackner, 2011). Furthermore, in order to perform a more comprehensive parametric study, the authors in (Stewart and Lackner, 2012) established a 3-DOF dynamic model for different types of floating wind turbines based on first principles, and TMD parameters are designed under different optimization methods. This limited-DOF model has greatly facilitated parametric analysis and active control design, but the coupling between platform surge and pitch motion was not captured. This effect can be ignored for the barge model, but might be a strong mode for other platforms (Jonkman, 2010). Regarding this problem, we developed a more comprehensive 5-DOF floating wind turbine dynamic model for passive structural control optimization, where the platform surge and heave motion were also considered (Si et al., 2014). Besides, this model could be used as the basis for model-based active structural control design. However, the sensors installed in commercial wind turbines are very limited, thus the full-state feedback controller is technically impossible to implement, while the observer-based control design approach could be a possible solution (Skaare et al., 2007).

2 Dynamic Modelling

Based on decades of experience from offshore oil and gas industry, several different traditional floating platforms have been proposed to support large wind turbines in deep sea regions, including the spar-buoy, tension-leg, barge, and semi-submersible (Jonkman, 2009). Among these designs, in 2009 one Norwegian company Statoil developed the world first full scale experimental floating wind turbine "Hywind". In cooperation with Statoil, Jonkman from the National Renewable Energy Laboratory (NREL) specified a detailed model for OC3-Hywind spar, which combines the data of the 5MW baseline wind turbine from NREL and the Hywind spar from Statoil. Its 3-D illustration and the critical parameters are shown in Figure E.1 and Table E.1.

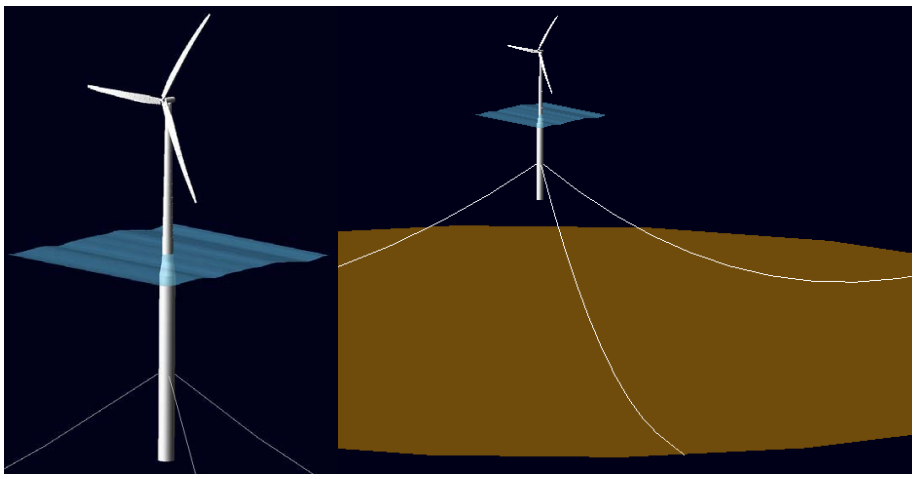

Figure E.1: Illustrations of the NREL 5-MW wind turbine on the OC3-Hywind spar (Jonkman, 2010).

The structural control idea in this work is demonstrated in Figure E.2, where an HMD is installed in the nacelle of OC3-Hywind. The HMD consists of a TMD with mass M, spring and damping constants K and D, and an actuator acting force F on the mass. The control force from the actuator is usually designed based on the linearized model at certain equilibrium points. However, FAST-SC does not support the model linearization yet, so that establishing the dynamic model from first principles is beneficial for the control synthesis.

Table E.1: Properties of the 5MW OC3-Hywind model (Jonkman, 2010)

Item	Value
Rating	5 MW
Rotor configuration	Upwind, 3 blades
Cut-in, rated, cut-out wind speed	3 m/s, 11.4 m/s, 25 m/s
Total draft below sea water level (SWL)	120 m
Tower base above SWL	10m
Hub height above SWL	90m
Nacelle dimension (length, width, height)	14.2m, 2.3m, 3.5m
Platform diameter above taper	6.5m
Platform diameter below taper	9.4m
Rotor nacelle assembly (RNA) mass	350,000kg
Tower mass	249,718 kg
Platform mass	7,466,000 kg
Number of mooring lines	3
Depth to fairleads below SWL	70m
Baseline control in Region 3	GSPI and constant torque

2.1 Longitudinal Dynamics

According to our previous works (Si et al., 2014), the following longitudinal dynamic model for the floating wind turbine can be established based on the D'Alembert's principle of inertial forces,

$$\mathbf{M}(\mathbf{q})\ddot{\mathbf{q}} + \mathbf{L}(\mathbf{q}, \dot{\mathbf{q}}) = \mathbf{F}, \tag{E.1}$$

where

$$\mathbf{q} = \begin{bmatrix} x_{sg} \\ x_{hv} \\ \theta_p \\ x_{hmd} \\ \theta_t \end{bmatrix}, \ \mathbf{M}(\mathbf{q}) = \begin{bmatrix} M_{sg}^{sg} & 0 & I_{sg}^{p} & M_{sg}^{hmd} & 0 \\ 0 & M_{hv}^{hv} & I_{hv}^{p} & M_{hv}^{hmd} & 0 \\ M_{p}^{sg} & M_{p}^{hv} & I_{p}^{p} & M_{p}^{hmd} & 0 \\ M_{hmd}^{sg} & M_{hmd}^{hv} & I_{hmd}^{p} & M_{hmd}^{hmd} & 0 \\ M_{t}^{sg} & M_{t}^{hv} & 0 & M_{t}^{hmd} & I_{t}^{t} \end{bmatrix},$$

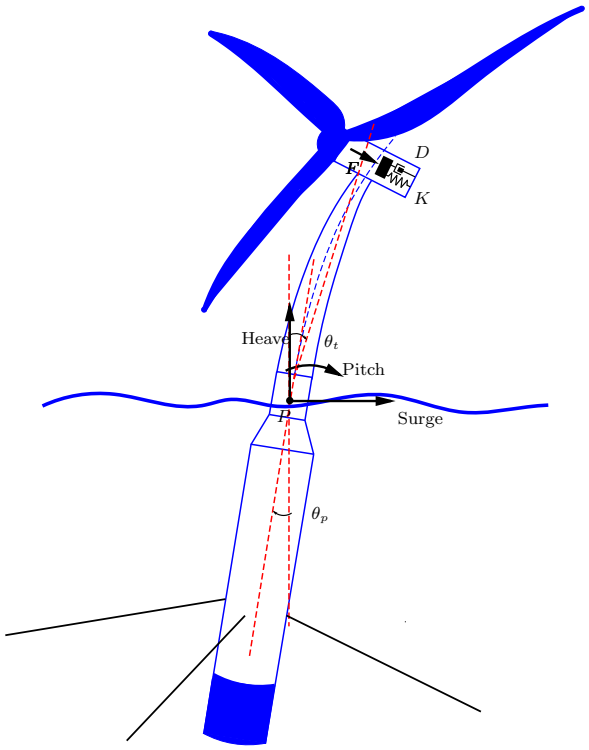

Figure E.2: Illustration of the active structural control of OC3-Hywind.

$$\mathbf{L}(\mathbf{q},\dot{\mathbf{q}}) = \begin{bmatrix} F_{sg}^{hdr} + F_{sg}^{moor} + F_{sg}^{ctr} + F_{sg}^{wnd} \\ F_{hv}^{gr} + F_{hv}^{hdr} + F_{hv}^{moor} + F_{hv}^{ctr} + F_{hv}^{wnd} \\ \tau_p^{gr} + \tau_p^{hdr} + \tau_p^{moor} + \tau_p^{ctr} + \tau_p^{wnd} \\ F_{hmd}^{gr} + F_{hmd}^{hmd} \\ \tau_t^{gr} + \tau_t^{p} + \tau_t^{ctr} + \tau_t^{wnd} \end{bmatrix}, \mathbf{F} = \begin{bmatrix} 0 \\ 0 \\ 0 \\ F \\ 0 \end{bmatrix}.$$

In this model, $\mathbf{q}$ is the state vector, and sg, hv, p, hmd, t represent, respectively, the enabled 5 DOFs, i.e. platform surge, heave, pitch motion about P, HMD translation, and tower deflection. $\mathbf{M}(\mathbf{q})$ is the system inertial matrix, which is positive definite. M_i^j and I_i^j denote generalized mass and generalized inertial tensor for DOF i with regard to DOF j. $\mathbf{L}(\mathbf{q},\dot{\mathbf{q}})$ represents external loads, and gr, hdr, $moor$, ctr, wnd describe, respectively, gravitational, hydro, mooring, centripetal, aerodynamic loads in forces or moments. Our recent results (Si and Karimi, 2014) show that better representations of the aerodynamic, hydrodynamic and mooring loads can be found with the curve fitting technique.

In order to verify the established model, the generator torque and blade pitch control are both disabled in FAST-SC, and the rotor speed and blade pitch angle are set as constant for each equilibrium point. Then, free decay response comparison is performed between FAST-SC and the established model, e.g., the 8 m/s case is shown in Figure E.3. Here, PtfmSurge, PtfmHeave, PtfmPitch, represent platform surge, heave, and pitch displacement, respectively. TTDspFA is the tower top displacement, and TwrBsMy denotes the tower bottom bending moment. TmdXDxt represents the mass damper displacement. It can be seen from the figure that these two responses agree well with each other.

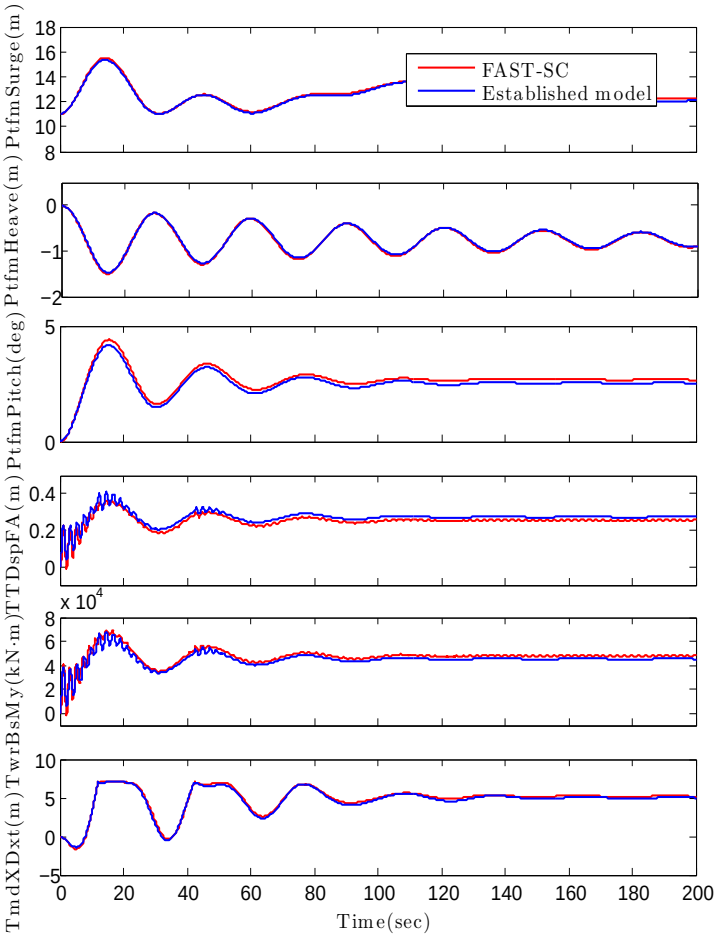

Figure E.3: Dynamic response comparison between FAST-SC and the established model.

Table E.2: OC3-Hywind 5MW turbine steady-state points under different wind speeds.

V (m/s)	ω (RPM)	θ_b (°)	x_{sg} (m)	x_{hv} (m)	θ_p (°)	T_0 (10^5 N)	$\frac{\partial T}{\partial V}$ (10^6 N·s)
3.0	6.97	0.00	2.44	-0.02	0.47	0.7414	2.9428
4.0	7.18	0.00	3.90	-0.04	0.79	1.1733	3.1436
5.0	7.50	0.00	5.67	-0.07	1.15	1.6817	3.4245
6.0	7.92	0.00	7.72	-0.10	1.58	2.2563	3.8583
7.0	8.43	0.00	10.02	-0.14	2.05	2.8900	4.5637
8.0	9.07	0.00	12.67	-0.20	2.59	3.6172	5.3733
9.0	10.17	0.00	16.09	-0.29	3.28	4.5504	5.9377
10.0	11.27	0.00	19.85	-0.41	4.03	5.5921	6.5443
11.0	11.84	0.00	23.28	-0.53	4.73	6.5711	7.1261
12.0	12.10	2.96	21.31	-0.44	4.33	6.0740	8.0656
13.0	12.10	6.19	17.89	-0.35	3.66	5.1049	8.9981
14.0	12.10	8.34	16.04	-0.29	3.29	4.5911	9.5531
15.0	12.10	10.21	14.67	-0.25	3.01	4.1898	9.9529
16.0	12.10	11.84	13.60	-0.22	2.80	3.8990	10.2480
17.0	12.10	13.34	12.75	-0.20	2.64	3.6610	10.4610
18.0	12.10	14.73	12.05	-0.18	2.50	3.4804	10.4800
19.0	12.10	16.05	11.47	-0.16	2.39	3.3292	10.3800
20.0	12.10	17.34	10.95	-0.14	2.29	3.1847	10.2720
21.0	12.10	18.60	10.51	-0.12	2.20	3.0691	10.0460
22.0	12.10	19.83	10.13	-0.11	2.13	2.9717	9.7724
23.0	12.10	21.02	9.79	-0.10	2.06	2.8791	9.5400
24.0	12.10	22.19	9.49	-0.08	2.01	2.7977	9.4149
25.0	12.10	23.31	9.23	-0.07	1.96	2.7326	9.4154

2.2 Model Linearization

In this work, the linear expression of the above established model for each equilibrium point needs to be derived to design the controller. Table E.2 gives the system steady states for different equilibrium points. In this table, V represents the wind speed, ω and θ_b represent the rotor speed and blade pitch angle. x_{sg}, x_{hv} and θ_p are the platform surge, heave and pitch displacement, respectively. T_0 is the aerodynamic rotor thrust at a steady state point. $\frac{\partial T}{\partial \theta_t}$ is the thrust sensitivity to wind speed.

Based on small deviation approximation, the model around each equilibrium point can be linearized into the following state-space representation,

$$\begin{aligned} \dot{x}(t) &= Ax(t) + Bu(t), \\ z(t) &= C_1 x(t), \\ y(t) &= C_2 x(t), \end{aligned} \tag{E.2}$$

where $x = \left[\dot{x}_{sg}, \dot{x}_{hv}, \dot{\theta}_p, \dot{x}_{hmd}, \dot{\theta}_t, x_{sg}, x_{hv}, \theta_p, x_{hmd}, \theta_t \right]^T$ is the state vector. $u = F$ is the control input, $z = \theta_p - \theta_t$ is the controlled output, and $y = [x_{sg} + (\theta_p - \theta_t) l_{twr}, \theta_p, x_{hmd}]^T$ is the measured output.

3 Control Design

Since the number of sensors in wind turbines is limited, implementing a full-state feedback controller is almost impossible in this case, thus the observer-based control design is needed to estimate the system states. Also, guaranteed cost control could be used to improve the concerned system performance, which is appropriate for the load reduction problem.

3.1 Observer Design

Consider the observer for (E.2)

$$\begin{aligned} \dot{\hat{x}}(t) &= A\hat{x}(t) + Bu(t) - L(y(t) - \hat{y}(t)), \\ \hat{y}(t) &= C_2 \hat{x}(t), \end{aligned} \tag{E.3}$$

where L is the observer gain. If the state estimation error is defined as $e(t) = x(t) - \hat{x}(t)$, then

$$\begin{aligned} \dot{\hat{e}}(t) &= \dot{x}(t) - \dot{\hat{x}}(t), \\ &= Ax(t) + Bu(t) - A\hat{x}(t) - Bu(t) + L(y(t) - \hat{y}(t)), \\ &= (A + LC_2)e(t). \end{aligned} \tag{E.4}$$

In order to keep the the estimation error asymptotically stable, we need to design L such that all the eigenvalues of $A + LC$ have negative real parts. Here we use the pole placement technique for the observer design, and the following lemma is introduced (Chilali and Gahinet, 1996).

Let $\mho(\eta, r)$ denotes any disk region centered in η with radius r in the complex plane (η, $r \in \mathbb{R}$ and $r > 0$). Then, all the eigenvalues of $A + LC$ in (E.4) lie in the region $\mho(\eta, r)$ if and only if there exists a symmetric matrix $P_1 > 0$ satisfying

$$\begin{bmatrix} -P_1 & P_1 (A + LC_2 - \eta I) \\ * & -r^2 P_1 \end{bmatrix} < 0. \tag{E.5}$$

Then, the desired observer gain can be obtained by simply solving this linear matrix inequality (LMI).

3.2 Guaranteed Cost Control Design

Regarding load reduction, the guaranteed cost control design could offer a solution to keep the closed-loop system stable and improve system performance simultaneously. The design objective can be converted to find a desired control law $u(t) = K\hat{x}(t)$ such that the closed-loop system

$$\begin{aligned} \dot{x}(t) &= Ax(t) + BK\hat{x}(t) \\ &= (A + BK)x(t) - BKe(t) \\ &\approx (A + BK)x(t), \\ z(t) &= C_1 x(t), \end{aligned} \tag{E.6}$$

is asymptotically stable and the cost function

$$\begin{aligned} J &= \int_0^\infty \left[u^T(\tau) R u(\tau) + x^T(\tau) Q x(\tau)\right] \mathrm{d}\tau \\ &= \int_0^\infty x^T(\tau) \left[K^T R K + Q\right] x(\tau) \mathrm{d}\tau, \end{aligned} \tag{E.7}$$

satisfies $J \leq \bar{J}$. Here R and Q are given positive-definite symmetric matrices, and note that the term $BKe(t)$ could be ignored in (E.6) since the designed

observer has governed the convergence rate of $e(t)$. Next, the guaranteed control design approach is presented.

For a given K, the closed-loop system in (E.6) is asymptotically stable and the performance index in (E.7) has an upper bound $\bar{J} = x^T(0)P_2x(0)$, if there exists a matrix $P_2 > 0$ satisfying

$$[P_2(A + BK)]_s + Q + K^T RK < 0. \tag{E.8}$$

Proof. For $Q = Q^T \geq 0$ and $R = R^T \geq 0$, from (E.8) we have

$$P_2(A + BK) + (A + BK)^T P_2 < 0.$$

According to Lyapunov theory, the closed-loop system in (E.6) is asymptotically stable. Next, we consider the performance index J:

$$\begin{aligned} J &= \int_0^\infty x^T(\tau) \left[K^T RK + Q\right] x(\tau)\mathrm{d}\tau \\ &< -\int_0^\infty x^T(\tau) \left[P_2(A + BK) + (A + BK)^T P_2\right] x(\tau)\mathrm{d}\tau \\ &= -\int_0^\infty \frac{\mathrm{d}}{\mathrm{d}\tau} \left[x^T(\tau)P_2x(\tau)\right] \mathrm{d}\tau \\ &\leq x^T(0)P_2x(0). \end{aligned}$$

The proof is completed. Notice that (E.8) can be transformed into an LMI for easier numerical solution. Consider the closed-loop system in (E.6), if there exist matrices $X > 0$ and Y with appropriate dimensions such that the LMI

$$\begin{bmatrix} [AX + BY]_s & X & Y^T \\ * & -Q^{-1} & 0 \\ * & * & -R^{-1} \end{bmatrix} < 0, \tag{E.9}$$

holds, then there will exist a proper controller such that the closed-loop system is asymptotically stable and the performance index in (E.7) has an upper bound as follows

$$J \leq \bar{J} = \mathit{Trace}(X^{-1}). \tag{E.10}$$

The desired state-feedback control gain will be given by

$$K = YX^{-1}. \tag{E.11}$$

4 Simulation Study

In this section, based on the control design, fully nonlinear simulations are performed in FAST-SC with all wind turbine DOFs enabled. Each test runs 630 seconds, and the output data in first 30s are not recorded, waiting for generator torque and blade pitch motion arriving normal operation state. The modified generator torque and blade pitch controller from NREL is used in the form of a dynamic link library for all tests (Jonkman, 2010).

Here we consider two different simulation scenarios. The wind and wave conditions in (Lackner and Rotea, 2011b) are adopted as two cases in this experiment. For wind condition, the mean value of the turbulent wind is defined as 10 m/s and 18 m/s, respectively. The turbulent wind file is generated by TurbSim, where Kaimal spectra and the power law exponent of 0.14 are used according to the IEC61400-3 offshore wind turbine design standard. The normal turbulence intensity is set as level B, i.e. 18% (10 m/s case) and 15%(18 m/s case). For wave condition, JONSWAP spectrum is utilized to generate the stochastic wave inputs. The significant wave height is set as 2.3 m (10 m/s case) and 3.7 m (18 m/s case), and the peak spectral period is defined as 14s. For each case, at least two sets of random variables are used to generate wind and wave data.

According to the parameter study in (Si et al., 2014), the property of the hybrid mass damper on tower top is chosen as follows, which matches the first tower fore-aft vibration mode.

Table E.3: Property of the hybrid mass damper in simulation.

Mass m	Spring constant K	Damping constant D
$20,000$ kg	$120,000$ N/m	$16,000$ N/(m/s)

Besides, The control force needs to pass a second order low pass filter to characterize the actuator dynamics,

$$G(s) = \frac{\omega^2}{s^2 + 2\zeta\omega s + \omega^2},$$

where $\omega = 10$ rad/s and ζ=0.5.

Then, the observer-based controller is designed for different setpoints, and the gain scheduling technique is used to switch among the family of designed controllers. In the guaranteed cost control design, the maximum value of the performance bound is 237. Nonlinear simulation results for tower bottom load reduction can be seen in Table E.4. Compared with the passive case, more load reduction can be achieved with the designed controller. One simulation comparison is illustrated in Figure E.4. TwrBsMxt and TwrBsMyt denote side-side and fore-aft tower base bending moment, respectively. TmdXDxt is the HMD displacement, and TmdXFext is the actuating force. However, this load reduction improvement is based on more energy consumption in the actuator, and it could also be risky for instability.

Table E.4: Percentage of load reduction for passive and active structural control (%)

Case	Term	Passive	Active
10m/s	DEL tower fore-aft bending	9.7	13.2
	DEL tower side-side bending	35.1	36.3
	95th tower fore-aft bending	4.1	1.57
	95th tower side-side bending	11.7	17.2
18m/s	DEL tower fore-aft bending	4.1	8.4
	DEL tower side-side bending	32.4	48.37
	95th tower fore-aft bending	0.3	0.1
	95th tower side-side bending	14.9	23.3

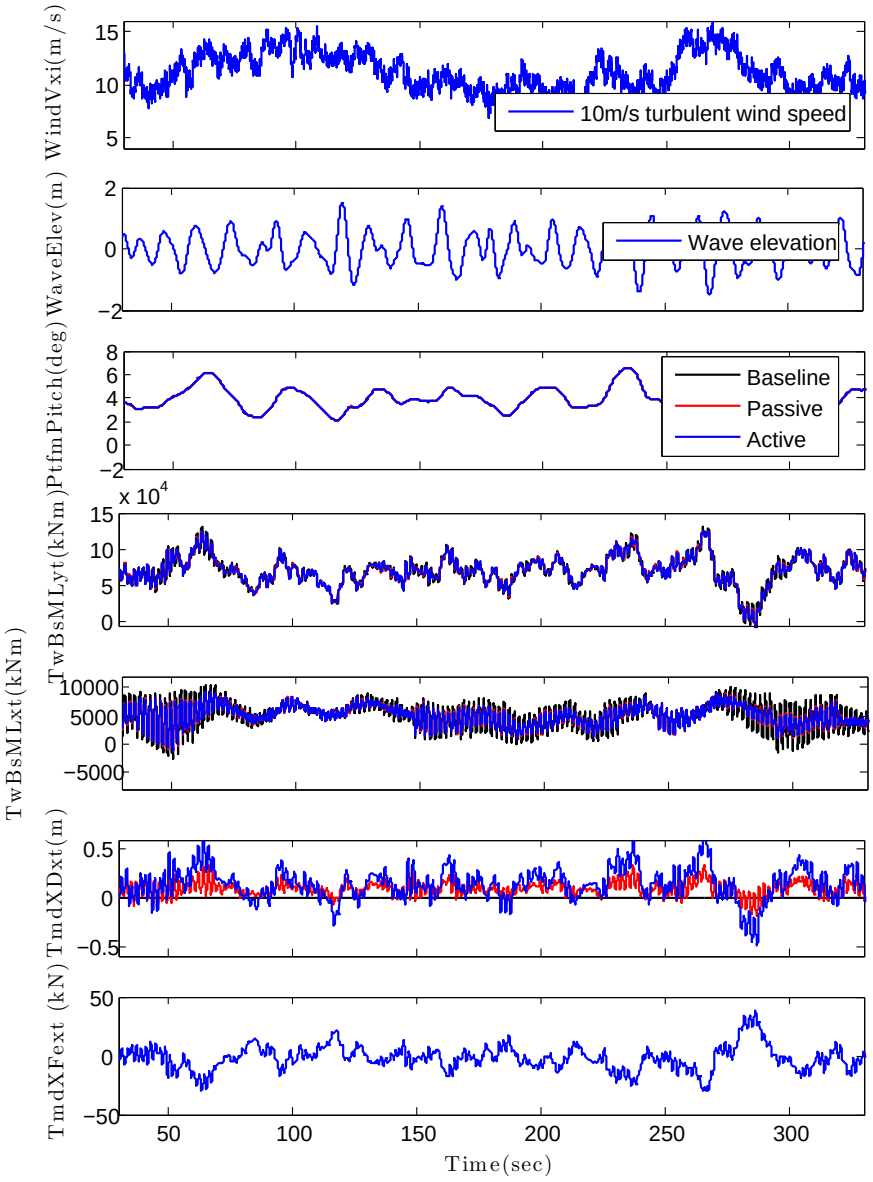

Figure E.4: Nonlinear simulation comparison under 10m/s turbulent wind speed and 2.3m wave height.

5 Conclusions

In this work, an hybrid mass damper is assumed to be installed on top of the tower for a spar-type floating wind turbine, and an observer-based guaranteed cost structural controller is designed for load reduction. The 5-DOF mathematical model for wind turbine surge-heave-pitch motion is presented, and the

linear state-space expressions for different equilibrium points are also obtained as the control design basis. Then, an observer is designed based on the sensor data for platform pitch angle, tower top and HMD displacement, and an observer-based guaranteed cost structural control strategy is developed. Finally, high fidelity nonlinear simulations with the proposed design are conducted under different wind and wave conditions. Simulation results demonstrate the designed observer manages to estimate the system states and the designed guaranteed cost controller will help to achieve more load reduction than the passive case.

REFERENCES

Chilali, M. and Gahinet, P. (1996). h_∞ design with pole placement constraints: an lmi approach. *IEEE Transactions on Automatic Control*, 41(3):358–367.

Colwell, S. and Basu, B. (2009). Tuned liquid column dampers in offshore wind turbines for structural control. *Engineering Structures*, 31(2):358–368.

Jonkman, J. (2007). *Dynamics modeling and loads analysis of an offshore floating wind turbine*. PhD thesis, Department of Aerospace Engineering Sciences, University of Colorado.

Jonkman, J. (2009). Dynamics of offshore floating wind turbines - model development and verification. *Wind Energy*, 12(5):459–492.

Jonkman, J. (2010). Definition of the floating system for phase iv of oc3. *NREL/TP-500-38060. Golden, Colorado: National Renewable Energy Laboratory*.

Jonkman, J. and Buhl Jr, M. (2005). Fast users guide. Technical report, NREL/EL-500-29798. Golden, Colorado: National Renewable Energy Laboratory.

Jonkman, J. and Matha, D. (2009). A quantitative comparison of the responses of three floating platform concepts. In *European Offshore Wind 2009 Conference & Exhibition*, pages 14–16.

Korkmaz, S. (2011). A review of active structural control: challenges for engineering informatics. *Computers & Structures*, 89:2113 – 2132.

Lackner, M. A. and Rotea, M. A. (2011a). Passive structural control of offshore wind turbines. *Wind Energy*, 14(3):373–388.

Lackner, M. A. and Rotea, M. A. (2011b). Structural control of floating wind turbines. *Mechatronics*, 21(4):704 – 719.

Li, J., Zhang, Z., and Chen, J. (2012). Experimental study on vibration control of offshore wind turbines using a ball vibration absorber. *Energy and Power Engineering*, 4(3):153–157.

Mensah, A. and Dueñas-Osorio, L. (2012). Reliability analysis of wind turbines equipped with tuned liquid column dampers (tlcd). In *Structures Congress*, pages 1190–1200.

Murtagh, P. J., Ghosh, A., Basu, B., and Broderick, B. M. (2008). Passive control of wind turbine vibrations including blade/tower interaction and rotationally sampled turbulence. *Wind Energy*, 11(4):305–317.

Musial, W., Butterfield, S., and Ram, B. (2006). Energy from offshore wind. In *Offshore Technology Conference*, pages 1888–1898.

Si, Y. and Karimi, H. R. (2014). Gain scheduling h_2/h_∞ structural control of a floating wind turbine. In *Proceedings of the 19th World Congress of the International Federation of Automatic Control. Cape Town, South Africa, 24-29 August.*

Si, Y., Karimi, H. R., and Gao, H. (2014). Modelling and optimization of a passive structural control design for a spar-type floating wind turbine. *Engineering Structures, to appear.*

Skaare, B., Hanson, T., and Nielsen, F. (2007). Importance of control strategies on fatigue life of floating wind turbines. In *Proceedings of the 26th International Conference on Offshore Mechanics and Arctic Engineering.* ASME.

Stewart, G. and Lackner, M. A. (2012). Optimization of a passive tuned mass damper for reducing loads in offshore wind turbines. *IEEE Transactions on Control Systems Technology: Special Issue on Wind Energy.*

Stewart, G. M. and Lackner, M. A. (2011). The effect of actuator dynamics on active structural control of offshore wind turbines. *Engineering Structures*, 33(5):1807 – 1816.